# SEISMIC RESPONSE AND DEFORMATION ANALYSES OF EARTHEN DAMS

by

LEILA MOSADEGH

Presented to the Faculty of the Graduate School of
The University of Texas at Arlington in Partial Fulfillment of the
Requirements for the Degree of

DOCTOR OF PHILOSOPHY

THE UNIVERSITY OF TEXAS AT ARLINGTON

December 2019

*To my parents and their endless love that keeps guiding me in life.*

# Acknowledgments

I would like to express my deepest gratitude toward my advisor Dr. Anand J. Puppala, for his support and for giving me the chance to work with him and learn from him, this research could not be done without his guidance.

I would like to thank Dr. Laureano R. Hoyos and Dr. Xinbao Yu for their support and for sharing their knowledge during my course work. I have learned a lot from them. Also, I would like to thank Dr. Erick Jones for his time and valuable comments. I would like to thank Dr. Sayantan Chakraborty for always making time to help me during the past four years. I would like to thank Mr. Louie Verreault, Ms. Dorota Koterba and Mr. Jason Gehrig of Tarrant Regional Water District, Fort Worth, Texas for their insightful comments. I would also like to thank my colleagues at geotechnical research group at UTA.

I am forever grateful to my parents, Hassan and Zohreh Mosadegh, for their love, support and encouragement. I would like to thank my dearest Maryam, my lovely family and friends for their continuous encouragement.

# Abstract


## SEISMIC RESPONSE AND DEFORMATION ANALYSES OF EARTHEN DAMS

by

Leila Mosadegh

The University of Texas at Arlington, 2019

Supervising Professor: Anand J. Puppala

Assessment of the response of earthen structures, such as dams and levees, during earthquake events, is crucially important to geotechnical engineers. It is imperative to perform seismic response analysis to assess the stability and serviceability of these structures during probable seismic events. Before performing a seismic response analysis, an engineer or a researcher needs to select between two-dimensional (2D) plane strain analysis and a computationally intensive three dimensional (3D) analysis of an infrastructure. The 3D analysis should closely capture the behavior of infrastructure seismic response than a simplistic 2D analysis. Furthermore, a dilemma remains regarding the choice of a suitable method to incorporate the effect of the non-linear behavior of geomaterials at different induced strain levels. The non-linear behavior can be incorporated into the analysis using a fully-coupled non-linear method that can capture the soil behavior more accurately as compared to the simple equivalent linear method. However, the calibration of the non-linear models requires extensive high-quality test data, which is seldom available for most projects.

A comprehensive study was planned and formulated to identify the conditions/scenarios which warrant a 3D analysis over a 2D analysis and would require a fully-coupled analysis instead of an equivalent linear type of non-linear analysis. Real and hypothetical earthen dams with widely different geometric configurations and material variabilities were exposed to a broad spectrum of earthquake excitations, and the behavior of the structures was studied using the aforementioned analyses methods. Different parameters such as natural frequency, earthquake-induced accelerations, shear stresses, excess pore water pressure, and post-earthquake deformations are used to evaluate the conditions where the comparatively simple analyses methods can be considered sufficient without incurring appreciable errors.

The estimation of liquefaction-induced lateral deformation of the foundation layers of dams and levees plays a vital role in evaluating the post-earthquake performance of these structures. Post-earthquake deformations are estimated by numerical modeling or using well-known semi-empirical equations that were developed based on real case-history data. A comparative study was performed by estimating the lateral displacements of the downstream foundation of an earthen dam in north Texas. The lateral displacements were computed using both numerical analyses and semi-empirical equations for earthquakes of different magnitudes and peak ground accelerations. The scenarios where both the analyses methods yield similar results were identified, and the post-earthquake performance of the dam was evaluated based on the lateral displacement values.

The findings of this research are expected to facilitate researchers and the geotechnical earthquake engineering fraternity in selecting the appropriate analysis method depending on the characteristics of the site and earthquake scenarios to be used for the analyses. Results suggest that when extensive information is available at the site 3D analysis should be performed and the 2D analysis may overlook potential stability issues of an earthen dam. Also, for dams with dense sand

shells experiencing earthquakes with low intensity of excitation, without chances of near-resonance condition, equivalent linear analysis was recognized to show similar results as non-linear method. Furthermore, estimated lateral displacement in the foundation of studied dam was measured to be small and no concern about the stability of this dam was observed.

# Table of Contents

# List of Tables

List of Illustrations

# Chapter 1:

# Introduction and Background

## 1.1 Earthen dams

The stability of earthen structures is crucially important to geotechnical engineers (Seed et al. 1978, Chowdhury et al. 2009, FEMA 2017). Induced forces during seismic events may affect the structure and have a detrimental impact on their stability and serviceability (Seed and Martin 1966, Seed 1981, Fell et al. 2005, Hack et al. 2007, Choudhury et al. 2007, Meehan and Vahedifard 2013, Chatterjee and Choudhury 2014). Therefore, it is of utmost importance to analyze the response of earthen structures such as dams and levees during probable seismic events.

Earthen dams can be primarily classified into three major categories: homogeneous earth-fill dams, rock-fill dams (zoned earth) and hydraulic-fill dams (Council 1983, Pelecanos 2013, MacGregor et al. 2014a) (Figures 1.1, 1.2 and 1.3). Homogeneous earth-fill dams have the same material throughout and they have the simplest type of construction (Pelecanos 2013, Chakraborty 2018). Rock-fill dams have zones of rock-fill which each zone has a specific effect on the stability of the structure (Pelecanos 2013, MacGregor et al. 2014b, Chakraborty 2018). Hydraulic-fill dams are constructed by discharging the mixture of excavated soil and water along the edges of the embankment (Heinz 1976, Küpper 1991, Vick 1996, Wiltshire 2002, Nazarian et al. 2015). In this method of construction, the coarse-grained particles get deposited at first to form the shell and fine-grained particles eventually settle to form the impermeable core of the dam (Vick 1996) (Figure 1.3).

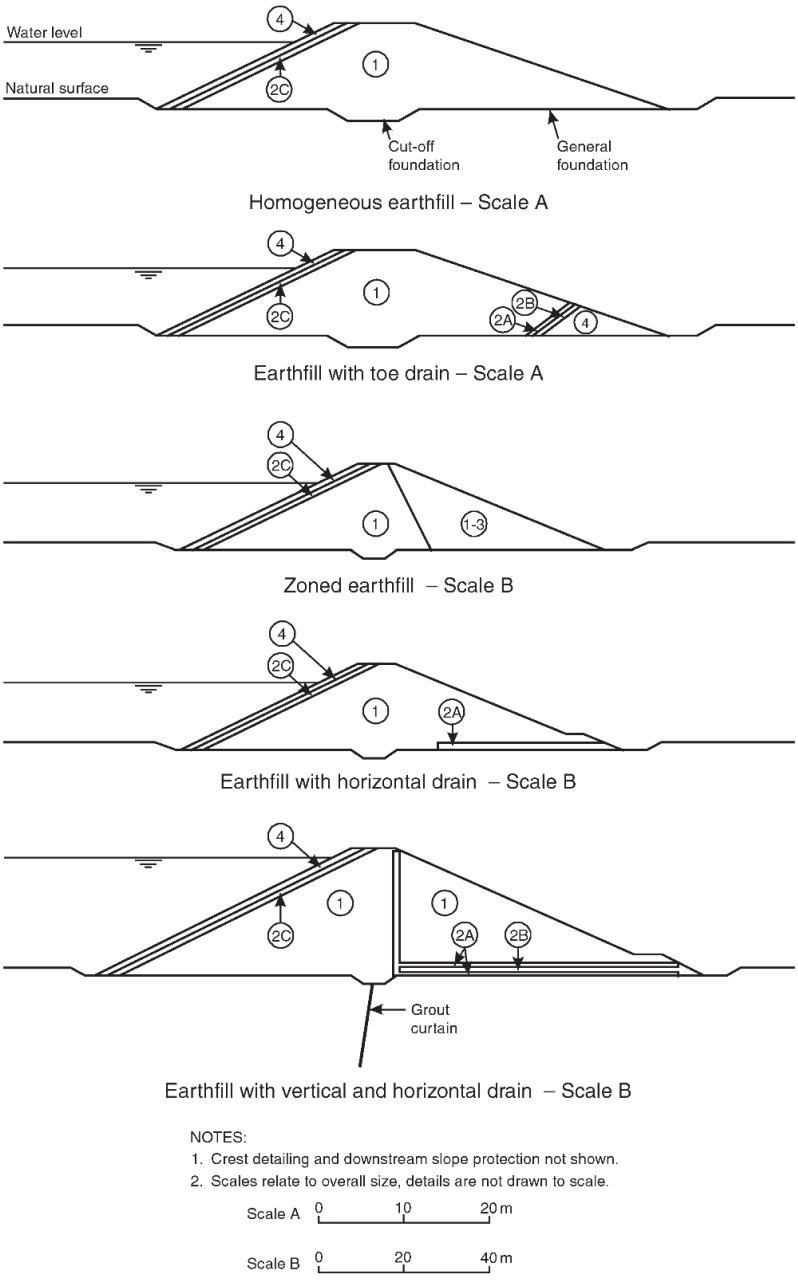


Figure 1.1: Cross-sections of earth-fill dams
(after Fell at al. 2005)

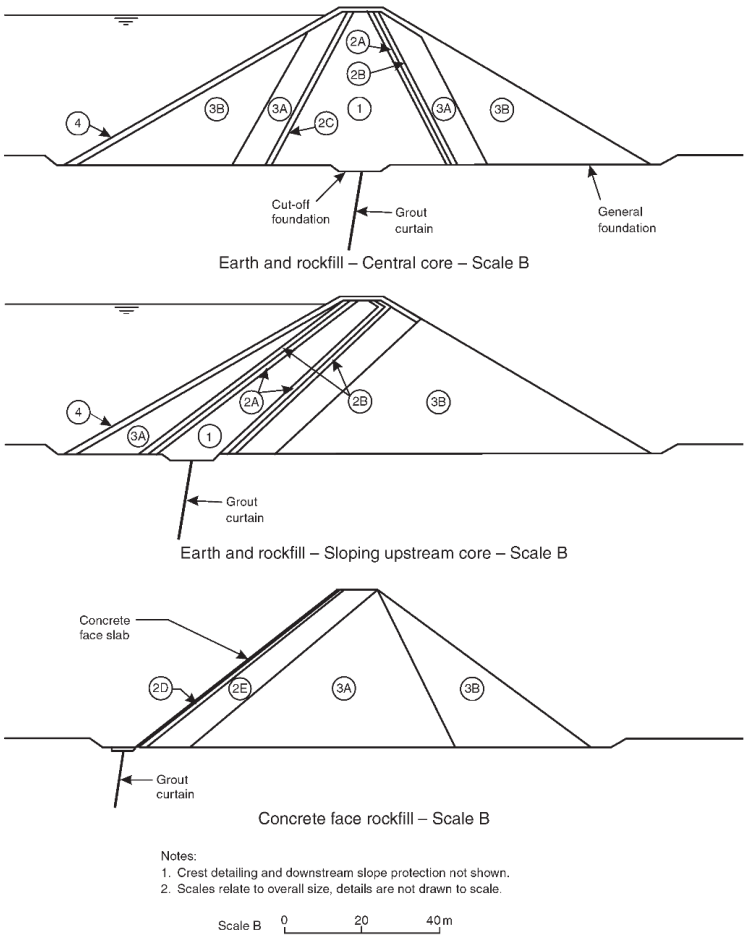


Figure 1.2: Cross-sections of earth-fill and rock-fill dams
(after Fell at al. 2005)

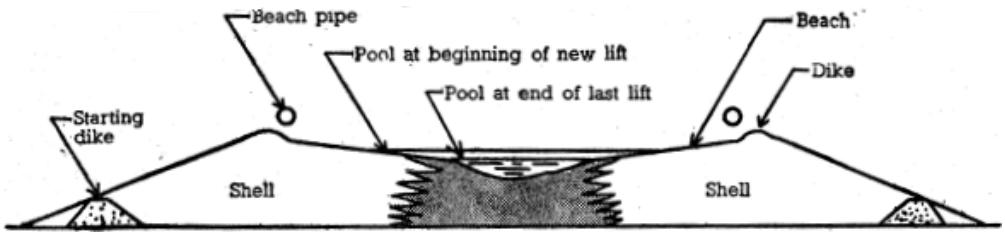


Figure 1.3: Formation of shell and core of a hydraulic-fill dam
(Source: http://community.dur.ac.uk/~des0www4/cal/dams/cons/conss4.htm )

Several dams such as the Fujinuma and the lower and upper San Fernando dams have experienced extensive damage because of earthquakes (Seed et al. 1975a, 1975b, 1978, Heinz 1976, Seed 1979b, 1981, Castro et al. 1985, 1992, Gu et al. 1993, Puppala et al. 2004, 2014). Due to the catastrophic consequence of an earthen dam failure, seismic response, stability and post-earthquake deformation analyses of these water-retaining structures remain as one of the most important field of research in the domain of geotechnical earthquake engineering. The first step in any seismic analysis of a dam is characterization of the geomaterial properties that can be used as input parameters required for the analysis (Seed 1979a). In the next section, important parameters for seismic response analysis are introduced.

## 1.2 Material properties for dynamic analysis

Small strain shear modulus ($G_{max}$) and damping ratio ($D$) are two important parameters required for analyzing any geotechnical earthquake engineering problem (Mayne and Rix 1995, Chaney et al. 1996, Kayen et al. 2013, Correia et al. 2016). Small strain shear modulus is defined as the shear modulus of soil at strain levels less than 0.001%. At such small strain levels, the soil exhibits maximum shear modulus and is therefore denoted by $G_{max}$ (Robertson et al. 1986, Stokoe et al. 1991, Mayne and Rix 1995). The $G_{max}$ values of subsurface layers can be determined from the shear wave velocity profile is available using equation 2.1. $G_{max} = \rho V_s^2$ where $\rho$ is the mass density and $V_s$ is shear wave velocity. Different methods are available to estimate the shear wave velocity of subsurface soil layers such as laboratory tests, in-situ tests and empirical/semi-empirical equations. Since providing undisturbed samples for laboratory tests is difficult, empirical/semi-empirical equations developed based on in-situ tests are mostly used for shear wave velocity determination (Anderson et al. 1978, Hryciw 1990, Mayne and Rix 1995, Hoyos et al. 2004, Saride et al. 2010).

Another important parameter is dynamic response analysis is damping ratio. Loss of energy in soil bodies subjected to excitation is called damping (Richart et al. 1970). The damping ratio which often is used in geotechnical earthquake engineering is the ratio of coefficient of damping to the critical damping of a system (Richart et al. 1970). Tests like torsional shear, resonant column and cyclic triaxial can be used for damping determination (Ashmawy et al. 1995, Lentini and Castelli 2017). Performing "half-power method" on the response of the soil on resonant column test data can also be used to determine damping (Kramer 1996, Wu 2015). Figure 1.4 presents the area that can be used for the estimation of the hysteretic damping ratio after performing laboratory tests (Teachavorasinskun et al. 1991, Ashmawy et al. 1995, Chittoori et al. 2013).

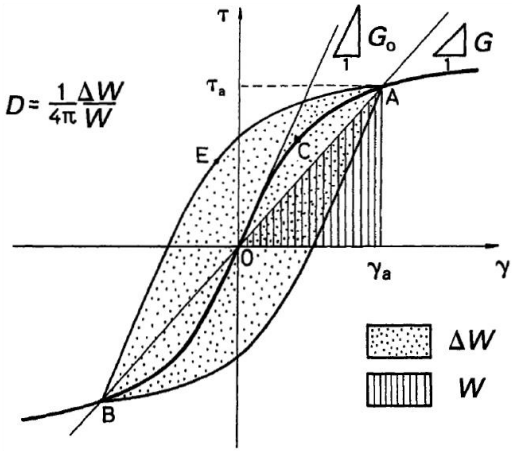


Figure 1.4: Relationship between shear stress-strain and hysteresis loop
(after Ishihara 1996)

The damping ratio for natural soils is reported to have the range of 0.5-5% (Vucetic and Dobry 1991, Kallioglou et al. 2008). Another way of damping ratio determination is based on Rayleigh damping which depends on frequency, as presented in Figure 1.5 (Gazetas 1987, Woodward and Griffiths 1996, Amorosi et al. 2008, Parish et al. 2009, Song and Su 2017). After seismic parameters determination, seismic response analysis can be performed and earthquake induced deformation can be measured which are mentioned in the next section.

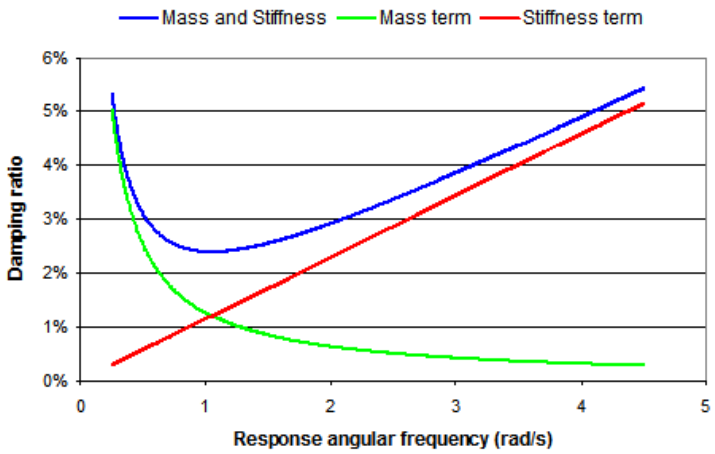


Figure 1.5: Mass and stiffness term in Rayleigh damping

(Source:https://www.orcina.com/SoftwareProducts/OrcaFlex/Documentation/Help/Content/html/RayleighDamping,Guidance.htm)

1.3 Seismic response and earthquake induced deformation of earthen dams

Numerical analyses techniques such as finite element/finite difference methods of analyses are frequently used to perform seismic response analysis where the variations of material properties, geometric configurations and diverse loading conditions can be included (Chopra 1967, Gazetas 1987). Although these numerical methods have the capability of predicting accurate behavior of the structure, the accuracy of the results depends on the accuracy of the modeled structure. Several researchers have performed seismic response of dams by modeling the dams in 2D or 3D (Mejia and Seed 1983, Woodward and Griffiths 1993, Mejia and Dawson 2010, Ozel and Arici 2012, Tahar Berrabah et al. 2012, Dulinska 2013, Mahesh et al. 2015, Bybordiani and Arıcı 2017). The geometric configurations of the dam, canyon geometry, properties of the material and nature of input motions have been reported to be the major reasons that affect the dynamic response of an earthen (Mejia and Seed 1983). The response of different dams during seismic events is usually studied by estimating the natural frequencies of the structure and evaluating the stresses and

accelerations induced at different pre-defined locations of the dam (Chopra 1967, Makdisi 1976, Mejia and Seed 1983, Cetin et al. 2005, Parish et al. 2009, Albano et al. 2015).

Natural frequency obtained by 2D and 3D analyses has been reported to be similar in long earthen dams in rectangular canyons, with the length of the dam being greater than six times the height of the dam (L/H >6) (Mejia and Seed 1983) (Figure 1.6). More comprehensive studies were done by considering different canyon geometries and the effect of width of canyon on natural frequency, amplification and acceleration response of the crest of the dam (Dakoulas and Gazetas 1986, 1987, Woodward and Griffiths 1993). The stiffening effect of the canyon, which can be only incorporated in a 3D analysis, significantly affects the natural frequency and response of a dam, especially in very narrow canyons (Mejia and Seed 1983). Hence the current state of practice is to perform a 3D analysis for dams build in narrow canyons and perform a 2D analysis for long earthen dams in rectangular canyons (Mejia and Seed 1983, Mejia and Dawson 2010). However, all these studies considered the same distribution of material properties along the length of the dam. This assumption is frequently adopted in practice and may be considered as an acceptable approximation for wetted and rolled dams.

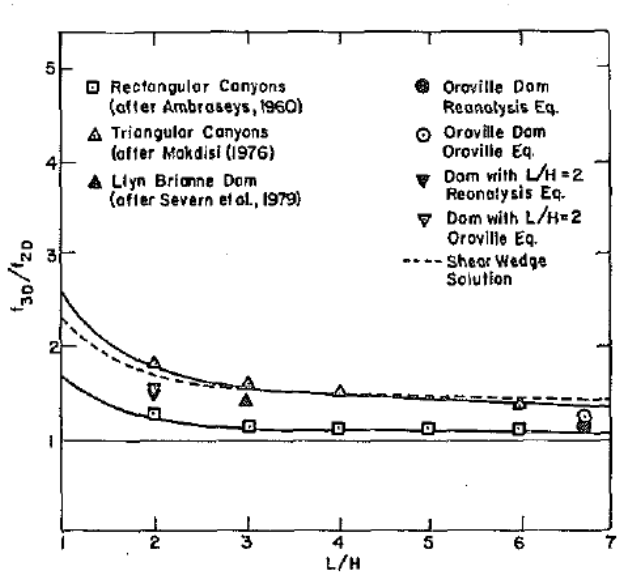


Figure 1.6: Comparison of obtained frequencies in 3D and 2D modeling (after Mejia and Seed 1983)

In addition to deciding the suitability of performing a 2D or 3D analyses, it is also required to select between an equivalent-linear method and non-linear method to incorporate the effect of non-linear behavior of soils at different induced strain levels. The equivalent linear analysis tries to present the non-linear behavior of the soil by performing an iterative analysis (Gazetas 1987, Jibson 2011b) (Figure 1.7). Shear modulus and damping ratio variations with strain depend primarily on the mean effective confining pressure, plasticity index and type of soil (Seed and Idriss 1970, Vucetic and Dobry 1991, Ishibashi and Zhang 1993, Puppala 2016). The procedure outlined by Lee and Albaisa (1974) and De Alba et al. (1976) is widely used in practice to estimate the earthquake-induced excess pore water pressure in conjunction with the equivalent linear method of analysis (Krahn 2004, Dash and Sitharam 2009). Several studies have confirmed that predictions obtained from the equivalent linear method are satisfactorily (Abdel-Ghaffar and Scott 1979, Mejia and Seed 1983, Rathje and Bray 2000). However, the equivalent

linear method of analysis is effectively a linear-elastic method of analysis and may not accurately capture the actual behavior of the soil layers during seismic shaking (Seed et al. 1986).

Nonetheless, this method has been found to provide acceptable results for most practical purposes, other than for very strong seismic excitations (Rathje and Bray 2000).

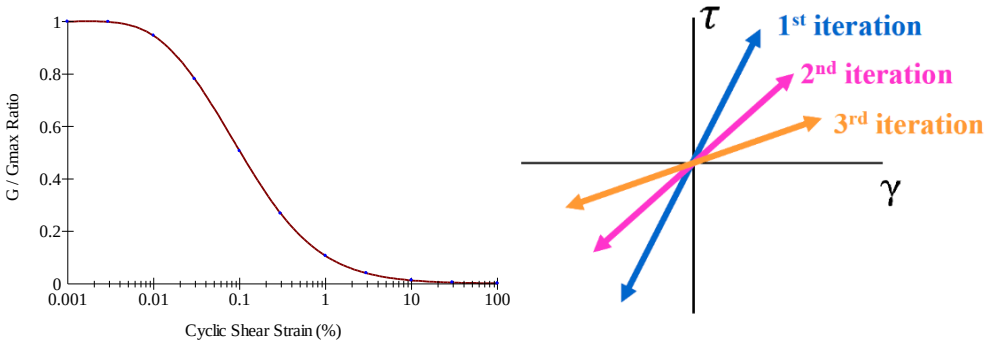


(a) (b)

Figure 1.7: (a) Typical modulus degradation curve, and (b) change in shear modulus with each iteration (after Krahn 2004a)

In the fully non-linear analysis, the changes in pore water pressure and strain are computed at every time-step of the earthquake loading and the subsequent changes in shear modulus is also computed at every time-step (Prevost et al. 1985, Abouseeda and Dakoulas 1998, Krahn 2004). Hence, the non-linear analysis is expected to capture the actual behavior of the soil layers during earthquake shaking. However, suitable pore-pressure models along with non-linear constitutive relations are required to compute the increase in pore water pressure and associated changes in shear modulus due to different strain levels induced at every time-step of the earthquake (Martin et al. 1975, Beaty and Byrne 1998, Boulanger and Ziotopoulou 2015). These models need to be calibrated based on extensive laboratory tests on undisturbed samples collected from the site (Boulanger and Montgomery 2016). However, using advanced constitutive models with assumed

values of the different input parameters does not guarantee the accuracy of the estimated excess pore water pressure and associated deformation results.

One of the common post-earthquake consequences is lateral displacement. Lateral displacement occurs on gently sloping ground as a result of liquefaction of soil layers during an earthquake event (Figure 1.8). Empirical/semi-empirical equations and numerical analysis can be used to predict lateral displacement and the extent of possible movements can be judged based on criteria developed by previous researchers (Youd and Perkins 1987, Bartlett and Youd 1992, Youd et al. 2002, Zhang et al. 2004). Empirical/semi-empirical are developed based on past earthquake events (Youd and Perkins 1987, Bartlett and Youd 1992, Youd et al. 2002, Zhang et al. 2004). These equations are frequently used around the world to predict the lateral displacements which can be compared with numerical lateral displacement predictions.

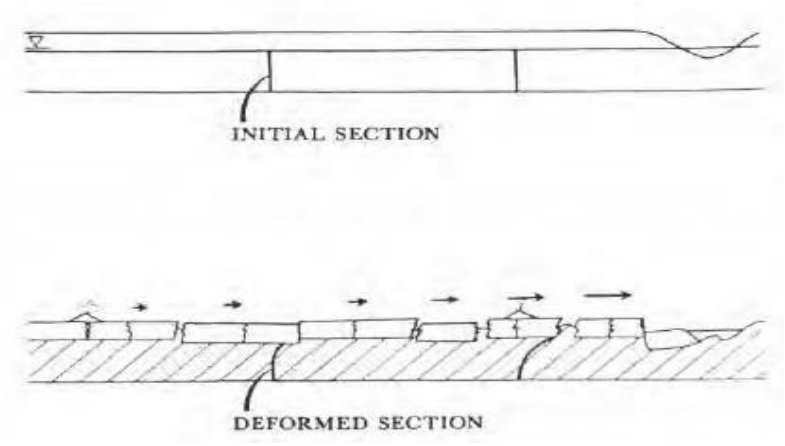


Figure 1.8: Lateral displacement caused by liquefaction-induced softening of soils (after Youd 1993)

## 1.4 Problem statement and research objective

The availability and use of commercially available finite element/finite difference method-based software packages have provided engineers with powerful tools to model and analyze the seismic response of earthen dams with different geometric configurations, material variability, and diverse loading conditions. However, very often an engineer needs to decide on the type of analysis that is suitable to obtain acceptable results. The analysis may be performed by modeling the dam as a 2D plane strain model or by creating a more complex and computationally intensive 3D model of the dam. Furthermore, a dilemma remains regarding the choice of using an equivalent linear method or a non-linear method of analysis to present the behavior of the geomaterials at different earthquake-induced strain levels. The decision of the type of analysis primarily depends on the importance of the project, site details and data available to capture the field conditions, available technical knowledge and computational capability of the software package. Even though the final objective of any numerical analysis is to try to model the problem close to reality, different constraints such as inadequate quality of field or laboratory test data and computational capability of the software package make it difficult to accurately analyze the problem (Gazetas and Uddin 1994, Baker et al. 2006, Shukha and Baker 2008, Jibson 2011a). In this research the suitability of performing a 2D analysis according to the current state of practice and the need of performing a 3D analysis for a long hydraulic fill dam (L/H = 80) to incorporate the effect of material variability existing in similar heterogeneous dams is studied. Furthermore, comparative study between selecting the suitable approach for seismic analysis and post-earthquake deformation measurements are studied for different scenarios using equivalent linear method, non-linear method and semi-empirical equations.

## 1.5 Dissertation organization

This dissertation consists of three manuscripts one of which is accepted in Geocongress 2020 and the other two are ready for submission. This dissertation starts with an overall introduction of the topic in chapter 1. In chapter 2 seismic response analysis of an earthen dam, Eagle Mountain (EM), located at Fort Worth, Texas, USA is performed. 2D and 3D modeling of EM, including its extensive material variability is considered to observe and interpret different seismic parameters such as natural frequency, max crest acceleration and shear stresses in scenarios where low-level earthquakes occur. In chapter 3 the effect of different methods of analysis in the case of high-level earthquake occurrence is studied. A hypothetical typical zoned earthen dam was modeled and the effect of using the equivalent linear method and the non-linear method in the excess pore water pressure and associated deformations estimations were compared. Since extensive CPTu data was available for EM dam, in chapter 4 the study on this dam was further continued considering higher magnitude earthquakes in 2D numerical modeling to recognize liquefiable areas at this site and the horizontal movements which can occur due to liquefaction were measured and compared with predictions from semi-empirical equations. And finally, in chapter 5 conclusion and recommendations for future studies are provided. This comparative study considering different scenarios can help researchers who need to select the appropriate method of seismic response analysis based on available data in specific projects.

# References


Abdel-Ghaffar, A.M., and Scott, R.F. 1979. Analysis of earth dam response to earthquakes. Available from http://resolver.caltech.edu/CaltechAUTHORS:20151104-154157041.

Abouseeda, H., and Dakoulas, P. 1998. Non-linear dynamic earth dam-foundation interaction using a BE-FE method. Earthquake Engineering & Structural Dynamics, **27**(9): 917–936. doi:10.1002/(SICI)1096-9845(199809)27:9<917::AID-EQE763>3.0.CO;2-A.

De Alba, P., Chan, C.K., and Seed, H.B. 1976. Determination of soil liquefaction characteristics by large-scale laboratory tests. Shannon & Wilson.

Albano, M., Modoni, G., Croce, P., and Russo, G. 2015. Assessment of the seismic performance of a bituminous faced rockfill dam. Soil Dynamics and Earthquake Engineering, **75**: 183–198. Elsevier. doi:10.1016/j.soildyn.2015.04.005.

Amorosi, A., Elia, G., Chan, A.C.H., and Kavvadas, M. 2008. Fully coupled dynamic analysis of a real earth dam overlaying a stiff natural clayey deposit using an advanced constitutive model. *In* Proc. 12th Int. Conf. of IACMAG, Goa. pp. 2750–2757.

Anderson, D.G., Espana, C., and Mclamore, V.R. 1978. Estimating in situ shear moduli at competent sites. *In* Proceedings of the ASCE Geotechnical Engineering Division Specialty Conference.

Ashmawy, A.K., Salgado, R., Guha, S., and Drnevich, V.P. 1995. Soil damping and its use in dynamic analyses. University of Missouri--Rolla.

Baker, R., Shukha, R., Operstein, V., and Frydman, S. 2006. Stability charts for pseudo-static slope stability analysis. Soil Dynamics and Earthquake Engineering, **26**(9): 813–823. doi:10.1016/j.soildyn.2006.01.023.

Bartlett, S.F., and Youd, T.L. 1992. Empirical analysis of horizontal ground displacement generated by liquefaction-induced lateral spreads.

Beaty, M., and Byrne, P.M. 1998. An Effective Stress Model for Pedicting Liquefaction Behaviour of Sand. *In* Geotechnical Earthquake Engineering and Soil Dynamics III. pp. 766–777.

Boulanger, R.W., and Montgomery, J. 2016. Nonlinear deformation analyses of an embankment dam on a spatially variable liquefiable deposit. Soil Dynamics and Earthquake Engineering, **91**: 222–233. doi:10.1016/j.soildyn.2016.07.027.

Boulanger, R.W., and Ziotopoulou, K. 2015. Pm4Sand (Version 3): a Sand Plasticity Model for Earthquake Engineering.

Bybordiani, M., and Arıcı, Y. 2017. The use of 3D modeling for the prediction of the seismic demands on the gravity dams. Earthquake Engng Struct.

Castro, G., Poulos, S.J., And, and Leathers, F.D. 1985. Re-examination of slide of lower San Fernando Dam. **I**(9): 1093–1107. Available from https://doi.org/10.1061/(ASCE)0733-

9410(1985)111:9(1093).

Castro, G., Seed, R.B., Keller, T.O., and Seed, H.B. 1992. Steady State Strength Analysis of Lower San Fernando Dam Slide. Journal of Geotechnical Engineering, **118**(3): 406–427. doi:10.1061/(ASCE)0733-9410(1992)118:3(406).

Cetin, K., Isik, N.S., Batmaz, S., and Karabiber, S. 2005. A comparative study on the actual and estimated seismic response of kiralkizi dam in turkey. Journal of Earthquake Engineering, **9**(4): 445–460. doi:10.1080/13632460509350550.

Chakraborty, S. 2018. A comprehensive seismic response and slope stability analysis framework for evaluating the stability of hydraulic-fill dams.

Chaney, R., Demars, K., Brignoli, E., Gotti, M., and Stokoe, K. 1996. Measurement of Shear Waves in Laboratory Specimens by Means of Piezoelectric Transducers. Geotechnical Testing Journal, **19**(4): 384–397. doi:10.1520/GTJ10716J.

Chatterjee, K., and Choudhury, D. 2014. Seismic Analysis of Soil Slopes Using FLAC2D and Modified Newmark Approach. *In* Geo-Congress 2014 Technical Papers. American Society of Civil Engineers, Reston, VA. pp. 1196–1205. doi:10.1061/9780784413272.116.

Chittoori, B.C., Puppala, A.J., Wejrungsikul, T. and Hoyos, L.R., 2013. Experimental studies on stabilized clays at various leaching cycles. Journal of Geotechnical and Geoenvironmental Engineering, 139(10): 1665-1675.

Chopra, A.K. 1967. Earthquake Response of Earth Dams.

Choudhury, D., Basu, S., and Bray, J.D. 2007. Behaviour of Slopes under Static and Seismic Conditions by Limit Equilibrium Method. *In* Embankments, Dams, and Slopes. American Society of Civil Engineers, Reston, VA. pp. 1–10. doi:10.1061/40905(224)6.

Chowdhury, R., Flentje, P., and Bhattacharya, G. 2009. Geotechnical slope analysis. Crc Press.

Correia, A.G., Winter, M.G. and Puppala, A.J., 2016. A review of sustainable approaches in transport infrastructure geotechnics. Transportation Geotechnics, 7: 21-28.

Council, N.R. 1983. Safety of Existing Dams. National Academies Press, Washington, D.C. doi:10.17226/289.

Dakoulas, P., and Gazetas, G. 1986. Seismic lateral vibration of embankment dams in semi-cylindrical valleys. Earthquake Engineering and Struc- tural Dynamics,.

Dakoulas, P., and Gazetas, G. 1987. Vibration characteristics of dams in narrow canyons. Journal of Geotechnical Engineering,.

Dash, H.K., and Sitharam, T.G. 2009. Undrained Cyclic Pore Pressure Response of Sand–Silt Mixtures: Effect of Nonplastic Fines and Other Parameters. Geotechnical and Geological Engineering, **27**(4): 501–517. doi:10.1007/s10706-009-9252-5.

Dulinska, J.M. 2013. 3D Vs. 2D Modeling of Concrete Gravity Dam Subjected to Mining Tremor. Applied Mechanics and Materials, **405**–**408**: 2015–2019. doi:10.4028/www.scientific.net/amm.405-408.2015.

Fell, R., MacGregor, P., Stapledon, D., and Bell, G. 2005. Geotechnical engineering of dams. *In* 2nd editio. CRC press.

FEMA. 2017. Information Needs for Dam Safety.

Gazetas, G. 1987. Seismic response of earth dams : some recent developments. **6**(1).

Gazetas, G., and Uddin, N. 1994. Permanent Deformation on Preexisting Sliding Surfaces in Dams. Journal of Geotechnical Engineering,.

Hack, R., Alkema, D., Kruse, G.A.M., Leenders, N., and Luzi, L. 2007. Influence of earthquakes on the stability of slopes. Engineering Geology, **91**(1): 4–15. doi:10.1016/j.enggeo.2006.12.016.

Heinz, R.A. 1976. Hydraulic Fill Dams/Earthquake Stability. Civil Engineering—ASCE, **46**(5): 55–60. ASCE.

Hoyos, L. R., Puppala, A. J., & Chainuwat, P. 2004. Dynamic properties of chemically stabilized sulfate rich clay. Journal of Geotechnical and Geoenvironmental Engineering, 130(2), 153-162.

Hryciw, R.D. 1990. Small Strain Shear Modulus of Soil by Dilatometer. Journal of Geotechnical Engineering, **116**(11): 1700–1716. doi:10.1061/(ASCE)0733-9410(1990)116:11(1700).

Ishibashi, I., and Zhang, X. 1993. Unified dynamic shear moduli and damping ratios of sand and clay. Soils and Foundations, **33**(1): 182–191. doi:10.3208/sandf1972.33.182.

Ishihara, K. 1996. Soil behaviour in earthquake geotechnics. Clarendon Press Oxford.

Jibson, R.W. 2011a. Methods for assessing the stability of slopes during earthquakes—A retrospective. Engineering Geology,.

Jibson, R.W. 2011b. Methods for assessing the stability of slopes during earthquakes—A retrospective. Engineering Geology, **122**(1–2): 43–50. Elsevier B.V. doi:10.1016/j.enggeo.2010.09.017.

Kallioglou, P., Tika, T., and Pitilakis, K. 2008. Shear Modulus and Damping Ratio of Cohesive Soils. Journal of Earthquake Engineering,.

Kayen, R., Moss, R.E.S., Thompson, E.M., Seed, R.B., Cetin, K.O., Kiureghian, A. Der, Tanaka, Y., and Tokimatsu, K. 2013. Shear-Wave Velocity–Based Probabilistic and Deterministic Assessment of Seismic Soil Liquefaction Potential. Journal of Geotechnical and Geoenvironmental Engineering, **139**(3): 407–419. doi:10.1061/(ASCE)GT.1943-5606.0000743.

Krahn, J. 2004. Dynamic modeling with QUAKE/W: an engineering methodology. GEO-SLOPE.

Kramer, S.L. 1996. Geotechnical earthquake engineering. *Edited By*W.J. Hall. Prentice-Hall Civil Engineering and Engineering Mechanics Series, Upper Saddle River, NJ.

Küpper, A.M.A.G. 1991. Design of hydraulic fill. University of Alerta.

Lee, K.L., and Albaisa, A. 1974. Earthquake Induced Settlements in Saturated Sands. Journal of

the Geotechnical Engineering Division, **100**(4): 387–406. ASCE.

Lentini, V., and Castelli, F. 2017. Resonant column and torsional shear tests for the evaluation of the shear modulus and damping ratio of soil. p. 190003. doi:10.1063/1.5012466.

MacGregor, P., Fell, R., Stapledon, D., Bell, G., and Foster, M. 2014a. Geotechnical engineering of dams. CRC press.

MacGregor, P., Fell, R., Stapledon, D., Bell, G., and Foster, M. 2014b. Geotechnical engineering of dams.

Mahesh, M.J., Pandey, A.D., Das, R., Anvesh, S., and Saini, P. 2015. Comparison of 2D and 3D Finite Element Analysis of Dams with Foundation- Structure Interaction Comparison of 2D and 3D Finite Element Analysis of Dams with Foundation-Structure Interaction. (August).

Makdisi, F.L. 1976. Performance and Analysis of Earth Dams During Strong Earthquakes.

Martin, G.R., Finn, W.D.L., and Seed, H.B. 1975. Fundementals of liquefaction under cyclic loading. Journal of Geotechnical and Geoenvironmental Engineering, **101**(ASCE# 11231 Proceeding).

Mayne, P.W., and Rix, G.J. 1995. Correlations between Shear Wave Velocity and Cone Tip Resistance in Natural Clays. Soils and Foundations, **35**(2): 107–110. doi:10.3208/sandf1972.35.2_107.

Meehan, C.L., and Vahedifard, F. 2013. Evaluation of simplified methods for predicting earthquake-induced slope displacements in earth dams and embankments. Engineering Geology, **152**(1): 180–193. doi:10.1016/j.enggeo.2012.10.016.

Mejia, L., and Dawson, E. 2010. 3D Analysis of the Seismic Response of Seven Oaks Dam. *In* 3D ANALYSIS OF THE SEISMIC RESPONSE OF SEVEN OAKS DAM. pp. 1–13.

Mejia, L.H., and Seed, H.B. 1983. Comparison of 2D and 3D Dynamic Analyses of Earth Dams. Journal of Geotechnical Engineering, **109**(11): 1383–1398. doi:10.1061/(ASCE)0733-9410(1983)109:11(1383).

Nazarian, S., Mazari, M., Abdallah, I.N., Puppala, A.J., Mohammad, L.N. and Abu-Farsakh, M.Y., 2015. Modulus-based construction specification for compaction of earthwork and unbound aggregate. Washington, DC: Transportation Research Board.

Ozel, H.F., and Arici, Y. 2012. Comparison of 2D vs. 3D Modeling Approaches for the Analyses of Concrete Faced Rockfill Dams. 15th World Conference on Earthquake Engineering (15WCEE),.

Parish, Y., Sadek, M., and Shahrour, I. 2009. Review article: Numerical analysis of the seismic behaviour of earth dam. Natural Hazards and Earth System Science, **9**(2): 451–458. doi:10.5194/nhess-9-451-2009.

Pelecanos, L. 2013. Seismic response and analysis of earth dams. (September).

Prevost, J.H., Abdel-Ghaffar, A.M., and Lacy, S.J. 1985. Nonlinear Dynamic Analyses of an Earth Dam. Journal of Geotechnical Engineering, **111**(7): 882–897. doi:10.1061/(ASCE)0733-9410(1985)111:7(882).

Puppala, A.J., 2016. Advances in ground modification with chemical additives: From theory to practice. Transportation Geotechnics, 9: 123-138.

Puppala, A.J., Manosuthikij, T. and Chittoori, B.C., 2014. Swell and shrinkage strain prediction models for expansive clays. Engineering Geology, 168: 1-8.

Puppala, A. J., Griffin, J. A., Hoyos, L. R., & Chomtid, S. 2004. Studies on sulfate-resistant cement stabilization methods to address sulfate-induced soil heave. Journal of geotechnical and geoenvironmental engineering, 130(4), 391-402.

Rathje, E.M., and Bray, J.D. 2000. Nonlinear Coupled Seismic Sliding Analysis of Earth Structures. Journal of Geotechnical and Geoenvironmental Engineering, **126**(11): 1002–1014. doi:10.1061/(ASCE)1090-0241(2000)126:11(1002).

Richart, F.E., Hall, J.R., and Woods, R.D. 1970. Vibrations of soils and foundations.

Robertson, P.K., Campanella, R.G., Gillespie, D., and Rice, A. 1986. Seismic Cpt to Measure in Situ Shear Wave Velocity. Journal of Geotechnical Engineering, **112**(8): 791–803. doi:10.1061/(ASCE)0733-9410(1986)112:8(791).

Saride, S., Puppala, A.J. and Williammee, R., 2010. Assessing recycled/secondary materials as pavement bases. Proceedings of the ICE-Ground Improvement, 163(1): 3-12.

Seed, H. B., Wong, R. T., Idriss, I. M., and Tokimatsu, K. 1986. Moduli and Damping Factors for Dynamic Analyses of Cohesionless Soils. Journal of Geotechnical Engineering,.

Seed, H.B. 1979a. Considerations in the earthquake-resistant design of earth and rockfill dams. Géotechnique,.

Seed, H.B. 1979b. Considerations in the earthquake-resistant design of earth and rockfill dams. Géotechnique, **29**(3): 215–263. doi:10.1680/geot.1979.29.3.215.

Seed, H.B. 1981. Earthquake-Resistant Design of Earth Dams. Proceedings: First International Conference on Recent Advances in Geotechnical Earthquake Engineering and Soil Dynamics, April 26 - May 3, 1981, St. Louis, Missouri,: 1157–1173.

Seed, H.B., De Alba, P.A., and Makdisi, F.I. 1978. Performance of Earth Dams during Earthquakes. Journal of the Geotechnical Engineering Division, **104**(7): 967–994.

Seed, H.B., and Idriss, I.M. 1970. Soil moduli and damping factors for dynamic response analyses. *In* Report No. EERC 70-10, Earthquake Engineering Resource Center, University of California, Berkley, California.

Seed, H.B., Idriss, I.M., Lee, K.L., and Makdisi, F.I. 1975a. Dynamic analysis of the slide in the Lower San Fernando Dam during the earthquake of February 9, 1971. Journal of Geotechnical and Geoenvironmental Engineering, **101**(ASCE# 11541 Proceeding): 889–911.

Seed, H.B., Lee, K.L., Idriss, I.M., and Makdisi, F.I. 1975b. The slides in the San Fernando Dams during the earthquake of February 9, 1971. Journal of Geotechnical and Geoenvironmental Engineering, **101**(ASCE# 11449 Proceeding).

Seed, H.B., and Martin, G.R. 1966. The seismic coefficient in earth dam design. Journal of Soil

Mechanics & Foundations Div, **92**(Proc. Paper 4824).

Shukha, R., and Baker, R. 2008. Design implications of the vertical pseudo-static coefficient in slope analysis. Computers and Geotechnics,.

Song, Z., and Su, C. 2017. Computation of Rayleigh Damping Coefficients for the Seismic Analysis of a Hydro-Powerhouse. Shock and Vibration, **2017**: 1–11. doi:10.1155/2017/2046345.

Stokoe, K.H., Rix, G.J., and Nazarian, S. 1991. In situ seismic testing with surface waves. International Journal of Rock Mechanics and Mining Sciences & Geomechanics Abstracts, **28**(2–3): A91. doi:10.1016/0148-9062(91)92397-H.

Tahar Berrabah, A., Belharizi, M., Laulusa, A., and Bekkouche, A. 2012. Three-Dimensional Modal Analysis of Brezina Concrete Arch Dam, Algeria. Earth Science Research, **1**(2). doi:10.5539/esr.v1n2p55.

Teachavorasinskun, S., Kato, H., Shibuya, S., Horii, N., and Tatsuoka, F. 1991. Stiffness and damping of sands in torsion shear. University of Missouri--Rolla.

Vick, S.G. 1996. Hydraulic tailings. Landslides: investigation and mitigation. Edited by AK Turner, RL Schuster, and LR Schuster. Transportation Research Board, Special Report, **247**: 577–584.

Vucetic, M., and Dobry, R. 1991. Effect of Soil Plasticity on Cyclic Response. Journal of Geotechnical Engineering, **117**(1): 89–107. doi:10.1061/(ASCE)0733-9410(1991)117:1(89).

W. H. Gu, N. R. Morgenstern, and P.K.R. 1993. Progressive failure of lower San Fernando Dam. **119**(2): 333–349.

Wiltshire, R.L. 2002. 100 Years of embankment dam design and construction in the US Bureau of Reclamation. Just Add Water: Reclamation Projects and Development Fantasies in the Upper Basin of the Colorado River,: 67.

Woodward, P.K., and Griffiths, D. V. 1993. Three-dimensional finite element analyses of the natural frequencies of non-homogeneous earth dams. International Journal of Rock Mechanics and Mining Sciences & Geomechanics Abstracts, **30**(3): A199. doi:10.1016/j.nic.2013.03.032.

Woodward, P.K., and Griffiths, D.V. 1996. Influence of viscous damping in the dynamic analysis of an earth dam using simple constitutive models. Computers and Geotechnics, **19**(3): 245–263. doi:10.1016/0266-352X(96)00002-X.

Wu, B. 2015. A correction of the half-power bandwidth method for estimating damping. Archive of Applied Mechanics, **85**(2): 315–320. doi:10.1007/s00419-014-0908-0.

Youd, T., Hansen, C., and Bartlett, S. 2002. Revised multilinear regression equations for prediction of lateral spread displacement. J Geotech Geoenviron Eng,.

Youd, T., and Perkins, D. 1987. Mapping of liquefaction severity index. J Geotech Eng, **113(11)**.

Zhang, G., Robertson, P.K., Asce, M., and Brachman, R.W.I. 2004. Estimating Liquefaction-

Induced Lateral Displacements Using the Standard Penetration Test or Cone Penetration Test. **130**(August): 861–871.

# Chapter 2:

# 2D and 3D Seismic Response Analyses of an Earthen Dam: A Comparative Study

## Abstract

The seismic response of a 1463m long, highly heterogeneous, hydraulic fill earthen dam, was evaluated by performing two-dimensional (2D) plane strain and three-dimensional (3D) analyses. Twenty-eight cone penetration test (CPTu) soundings were available along the crest of the dam to characterize the geomaterials. Two different scenarios were considered for the comparative study based on the extent of information used to characterize the dam: (i) Case 1 – using 6 CPTu data, with one CPTu available every 244m of the dam, and (ii) Case 2 – using all the 28 CPTu data. These two scenarios indicate the extent of information available for a particular project to characterize the material properties of the dam are: limited data and extensive information, respectively. Both 2D and 3D finite element models of the dam were developed for these two scenarios, and the seismic response analyses were then performed using two different earthquake excitations. The differences in natural frequencies, crest accelerations, and shear stresses were calculated and used to study the seismic response of the dam.

The analyses results suggest that the natural frequencies estimated from both 2D and 3D analyses are significantly different for Case 2. A drastic change in material properties along the longitudinal axis of the dam has a prominent effect on the differences in the 2D and 3D natural frequencies. Furthermore, a 2D analysis was observed to underestimate the peak crest accelerations and shear stresses as compared to a 3D analysis for both the scenarios. The findings

of this study emphasize the vital role of material variability on seismic response analyses, and enable engineers and researchers to assess the conditions that warranted a 3D analysis.

## 2.1 Introduction and Background

Stability and serviceability of earthen embankment structures such as dams and levees are of paramount importance to geotechnical engineers. The instability and excessive deformation of these structures can have catastrophic consequences on the wellbeing of the society (Seed et al. 1978, Resendiz et al. 1982, Ambraseys 1988, Harder 1991, Chakraborty et al. 2018a, 2018b). Hence, seismic response analyses are usually performed to have a better understanding of the structural behavior during potential earthquake events that may transpire in the future. One of the primary steps in seismic response analyses is the determination of natural frequency and the mode shapes of vibration. Every dynamic system has natural frequencies for different modes of vibration. If the predominant frequency of any natural or artificial source of vibration is close to the natural frequency of the structure, amplification of the vibration can result in resonance. This necessitates the determination of the natural frequency of water-retaining structures such as earthen dams and levees (Dakoulas and Gazetas 1985, Gazetas 1987, Jibson 2007, Parish et al. 2009, Zhu and Zhou 2010a, Chakraborty et al. 2018b, 2018a). Several methods are available for determining the natural frequency of structures. These methods include, analytical methods (shear beam), numerical methods (finite element or finite difference), ambient and forced vibration tests (Mononobe et al. 1936, Ishizaki and Hatakeyama 1962, Clough and Chopra 1966, Chopra 1967, Okamoto et al. 1969, Okamoto 1984, Gazetas 1987, Cetin et al. 2005).

The shear beam method considers the dam to be composed of variable wedge-shaped cross-sections and closed-form analytical solutions are used for determining the natural frequencies and mode shapes of vibration. This method was initially used to analyze one-dimensional models, and

was later improved to solve 2D analysis problems (Mononobe et al. 1936, Hatanaka 1955, Ambraseys 1960, Okamoto 1984). The assumptions made to derive the analytical solutions are not valid for analyzing the response of heterogeneous zoned earthen dams, exposed to seismic excitations with both horizontal and vertical components of disturbances. Moreover, the assumptions are valid only for the first mode when the dam experiences low intensities of seismic excitation. Numerical methods using finite element or finite difference analyses overcome the shortcomings of the shear beam method and provide a viable technique for analyzing real-field problems accurately (Ishizaki and Hatakeyama 1962, Clough and Chopra 1966, Chopra 1967, Parish et al. 2009). Seismic response analyses of earthen dams can also be studied using data recorded by seismographs placed at different locations of the dam during an earthquake event (Okamoto et al. 1969, Abdel-Ghaffar and Scott 1979a, 1979b, Cetin et al. 2005, Pelecanos et al. 2015, Yang et al. 2017). In the absence of field data recorded during earthquakes, ambient and forced vibration tests are also performed to study the response of a dam (Abdel-Ghaffar and Koh 1981, Castro et al. 1998, Jafari and Davoodi 2006, Sevim and Altunişik 2018). Natural frequency and mode shapes of the dam are then determined by analyzing the recorded induced accelerations and displacements (Petrovski et al. 1974, Abdel-Ghaffar and Scott 1981). However, the forced vibration test requires sophisticated instrumentations that are typically not available in every project (Jafari and Davoodi 2006).

Among the different analyses methods mentioned above, numerical analyses such as finite element /finite difference method (FEM/FDM) are capable of incorporating effects of variation in material properties, geometric configurations and arbitrary seismic loading conditions (Chopra 1967, Gazetas 1987, Yiagos and Prevost 1991). Hence, FEM/FDM are most frequently used to study the response and stability of earthen embankments during seismic loadings. These analyses

are performed either by modeling the dam as a two-dimensional (2D) plane strain model or three-dimensional (3D) model. Makdisi (1976) investigated the stiffening effects of narrow canyons on the natural frequencies and the dynamic response of dams using 3D finite element modeling. Mejia and Seed (1983) performed a comparative seismic response study using 2D and 3D analyses. Dams with different canyon shapes and dimensions were analyzed using 2D and 3D numerical modeling and the differences in natural frequencies were analyzed. The geometric configurations, dynamic properties of the material of dam, and nature of input motions were identified as the major factors that affect the seismic response of an earthen dam (Mejia and Seed 1983).

Many researchers have studied seismic response of earthen dams using 2D and 3D modeling. Majority of the studies emphasized the pronounced effects of 3D modeling on the results when the length to height (L/H) ratio of the dam is less than six (Mejia and Seed 1983, Woodward and Griffiths 1993, Boulanger, R.W. et al. 1995, Mejia and Dawson 2010). Hence, 2D plane strain analysis is typically considered to be valid and sufficient for analyzing long earthen dams (L/H > 6) with the same distribution of material properties (Makdisi 1976, Mejia and Seed 1983, Griffiths and Prevost 1988, Dakoulas 1993, Boulanger, R.W. et al. 1995, Parish et al. 2009, Mejia and Dawson 2010, Ozel and Arici 2012, Bybordiani and Arici 2017). However, long earthen dams with homogenous material properties are rarely found in reality. Especially, the effect of material variability is pronounced in earthen dams built with the hydraulic fill method of construction (Caballero et al. 2017a, Puppala et al. 2018a, 2018b).

In hydraulic fill method of construction, the excavated soil is mixed with water, transported through pipes and discharged along outer edges of the embankment (Heinz 1976, Küpper 1991, Vick 1996, Chatterjee and Choudhury 2014). The coarse-grained particles settle first to form the shells. The finer particles remain in suspension and eventually settle to form the core of the dam

(Vick 1996). This gradual deposition of particles under gravity result in high variability in the material properties present in the body of the dam (Morgenstern and Küpper 1988, Küpper 1991, Vick 1996). Several hydraulic-fill dams around the world have experienced stability issues during earthquake events in the past (Seed et al. 1975a, 1975b, Tezcan et al. 2001).

In this research study, seismic response analyses were performed for the Eagle Mountain (EM) dam, a hydraulic fill earthen dam located in north Texas. The effects of variations in material properties were incorporated in the analyses using extensive cone penetration tests (CPTu) conducted along the crest of the dam. Commercially available 2D and 3D FEM software packages were used to model the dam. This research study attempts to verify the applicability and limitations of the current practice that suggests 2D analysis to be sufficient for analyzing long earthen dams. The first natural frequency, earthquake-induced crest accelerations, and shear stresses estimated using 2D and 3D seismic response analyses were used to evaluate the sufficiency of 2D plane strain analysis for a long, highly heterogeneous earthen dam. The following section presents the methodology adopted and salient findings of this research study.

## 2.2 Methodology

### 2.2.1 Site details and material characterization

The seismic response analyses were performed for Eagle Mountain (EM) dam, a 1463 m long hydraulic fill earthen dam located on the West Fork Trinity River in Fort Worth, Texas, USA. The construction of this dam started in the early 1930 and was completed in 1932. It currently serves as a water supply resource and caters to industrial, municipal, and irrigation needs for the city of Fort Worth, Texas. Figure 2.1 presents the different zones of the EM dam based on the construction method adopted to build the dam. A 175 m stretch of the dam was constructed by wetting and rolling the soil, 225 m of it has a hydraulic fill core, with wetted and rolled shells, and the remaining

1063 m was entirely built by hydraulic fill method (Figure 2.1). Due to the lack of sophisticated construction machinery and equipment in the late 18$^{th}$ and early 19$^{th}$ centuries, the hydraulic fill method was frequently used to construct earthen dams.

Twenty-eight cone penetration tests with pore water pressure measurements (CPTu) were performed along the crest of the dam. Additional undisturbed samples were obtained from different sections of the dam from five exploratory boreholes. The unit weight ($\gamma$) of different soil types were obtained from the undisturbed samples (Table 2.1). Average unit weight of 20.3 kN/m$^3$ was used to model the soil layers present throughout the dam.

Table 2.1. Unit weight of different soil types present in the dam

| Soil type | Sandy lean clay | Lean clay with sand | Fat clay | Silty clay with sand | Lean clay | Sandy silt | Fat clay with sand | Clayey sand |
|---|---|---|---|---|---|---|---|---|
| Number of samples | 27 | 5 | 3 | 6 | 2 | 3 | 3 | 3 |
| Mean (kN/m$^3$) | 20.6 | 20.2 | 18.9 | 20.7 | 19.0 | 20.0 | 19.2 | 21.2 |

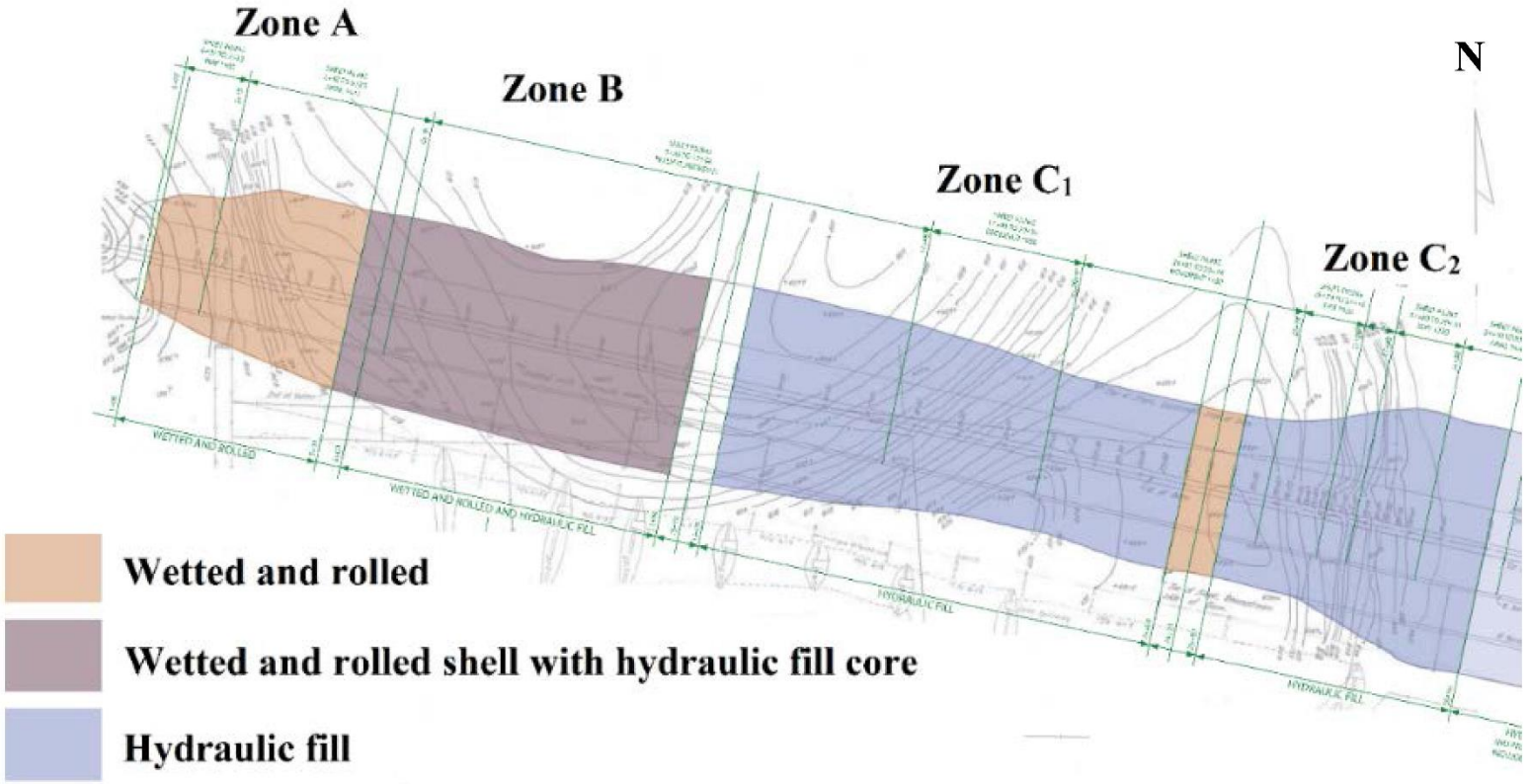


Figure 2.1: Plan view of different zones of EM dam based on the method of construction

In addition to the unit weight of the soil layers, two additional important input parameters are required for any seismic response analyses. The first parameter is the small strain shear modulus ($G_{max}$) ($G_{max} = \rho V_s^2$ where $\rho$ is the mass density of the soil and $V_s$ is shear wave velocity) which governs the propagation of seismic waves through the dam (Mayne and Rix 1995, Chaney et al. 1996, Kayen et al. 2013). $V_s$ in this study was estimated using the correlation equations developed by Hegazy and Mayne (1995) (equation 2.1). This correlation equation was categorically used because of its applicability in determining the shear wave velocity profiles for both sandy and clayey materials.

$$V_s\,(\text{m/s}) = [10.1 * (\log q_t) - 11.4]^{1.67} [(\frac{f_s}{q_t}) * 100]^{0.3} \quad (2.1)$$

The 2D and 3D models were divided into 12 layers (each with a thickness of 1.5 m), and average $V_s$ values for each layer were used to estimate the corresponding $G_{max}$ values. Since this study was performed considering the application of low-intensity ground accelerations (peak ground acceleration (PGA) = 0.01g), the soil layers were modeled as a linear elastic material. The Young's modulus ($E$) for different layers of the dam was obtained using equation 2.2.

$$E\,(\text{kPa}) = 2 \text{ x } (G_{max}) \text{ x } (1+\mu) \quad \text{where Poisson's ratio } (\mu) \text{ is } 0.33 \quad (2.2)$$

The second important input parameter for seismic response analyses is the damping ratio. The damping ratio of natural soils typically ranges between 0.5-5% (Vucetic and Dobry 1991, Kallioglou et al. 2008). A damping ratio ($D$) of 5% was used for all the soil layers that constitute the dam body.

### 2.2.2 Construction of numerical models of the EM dam

The availability of data from 28 CPTus provided a rich source of information about the different properties of the geomaterials present in the body of the dam. However, such extensive information is seldom available for all projects. Hence the usual practice is to assign material properties available from the nearest CPTu for linear interpolation to estimate the material properties at a section where CPTu data is unavailable. An attempt was made in this research study to evaluate the suitability of a 2D analysis in studying the seismic response of a long heterogeneous earthen dam (L/H=80) when (a) limited information is available and (b) when extensive information is available about the material variability existing in the dam. The 2D and 3D numerical models of the dam were developed for two different scenarios:

1) Case 1: A total of 6 CPTu data are available with one CPTu available for every 244 m segment of the dam (Figure 2.2a). This represents a scenario where limited information is available about the dam material properties.

2) Case 2: 28 CPTu data are available along the length of the dam (Figure 2.2b). This represents a scenario where extensive information is available about the dam material properties.

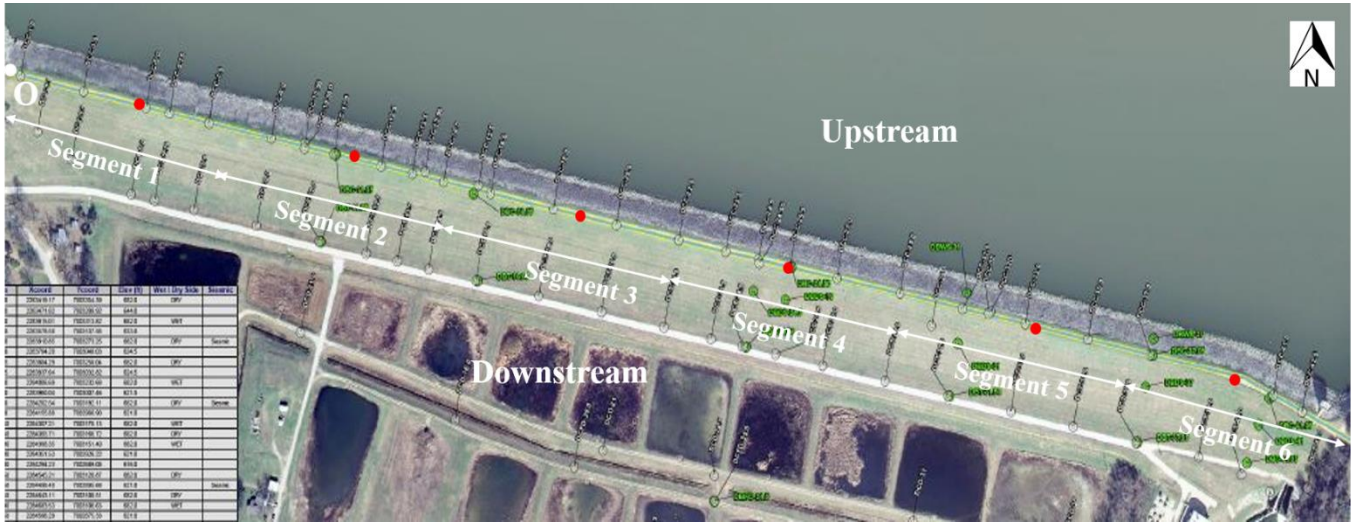


(a)

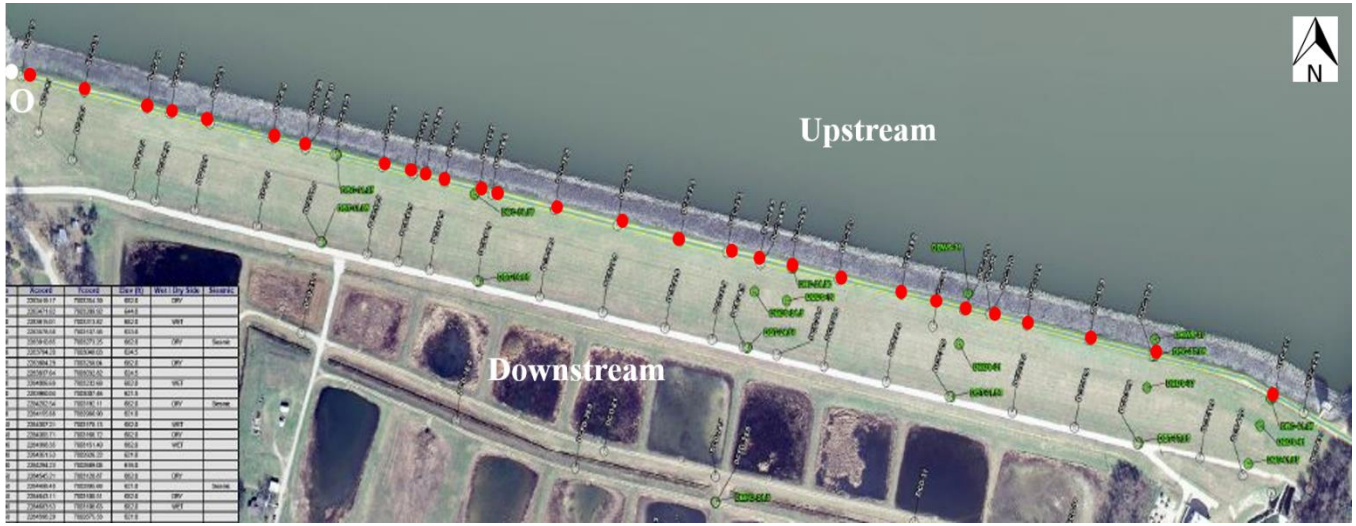


(b)

Figure 2.2: Locations of CPTu conducted along the crest of EM dam (red circles) for (a) Case 1 and (b) Case 2

*2.2.2.1 Development of 2D models*

Available as-built drawing of the dam was used to determine its geometric configuration and was used to develop the finite element model of each section. The models were divided into 12 layers of 1.5 m thickness, and soil properties such as γ, E and D were assigned to different layers basing on the tests on the undisturbed samples. Rigid base boundary condition was used assuming the earthquake time-history data represent "within motion" and was obtained by the superimposition of both upward and downward propagating components of the seismic wave (Mejia and Dawson 2006). The mesh size selected for the analyses was smaller than one-tenth of the wavelength of the highest frequency component of the input wave, in accordance with the recommendations made by Kuhlemeyer and Lysmer (1973). A mesh convergence study indicated an element size of 1 m to be sufficient for performing the 2D analysis (Figure 2.3).

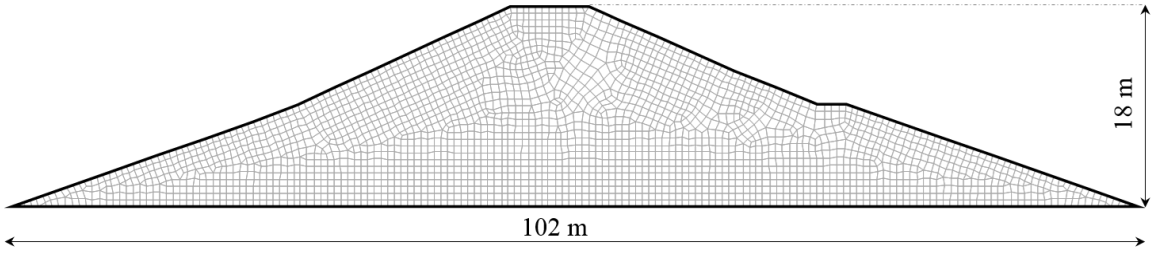


Figure 2.3: 2D finite element mesh of a typical section of the EM dam

*2.2.2.2 Development of 3D models*

The transverse cross-section of the dam was drawn using the as-built drawing, and it was expanded along the longitudinal axis of the dam to make the three-dimensional model. The model was divided into horizontal layers of 1.5 m thickness and was further divided into vertical segments to model the dam for the two analyses scenarios - Case 1 (6 segments) and Case 2 (28 segments).

The properties were assigned to each layer based on the material properties interpreted from the CPTu available for the respective segments.

*Case 1*

To make the 3D model of the dam with limited information available (Case 1), six CPTus at distances of 152.4, 381, 609.6, 883.9, 1066.8, 1249.7 m, were selected (Figure 2.2a). Subsequently, the length of the dam was divided into six segments; one CPTu data was assumed to be available for each 244 m long segments. Shear wave velocity profile obtained for Case 1 is presented in Figure 2.4.

Each of these six segments was horizontally divided every 1.5 m, and $\rho$, $\mu$, and $E$ were assigned to the layers in each segment. Figure 2.5 presents the 3D model of the dam with the effect of material variability captured using a limited number of in-situ tests (i.e., 6 CPTus).

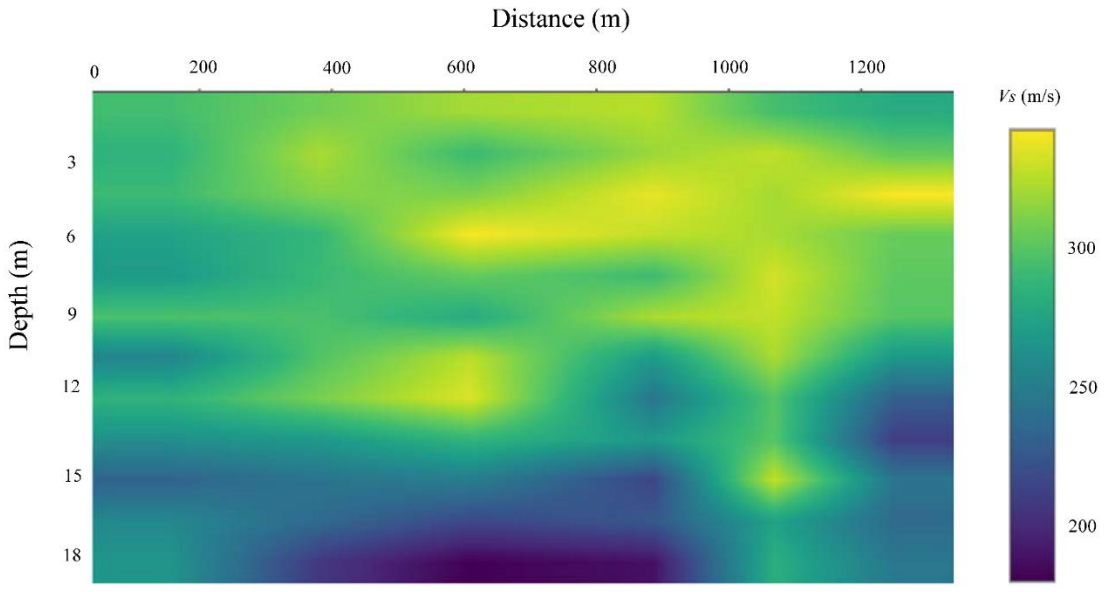


Figure 2.4: Shear wave velocity profile of the EM dam for Case 1

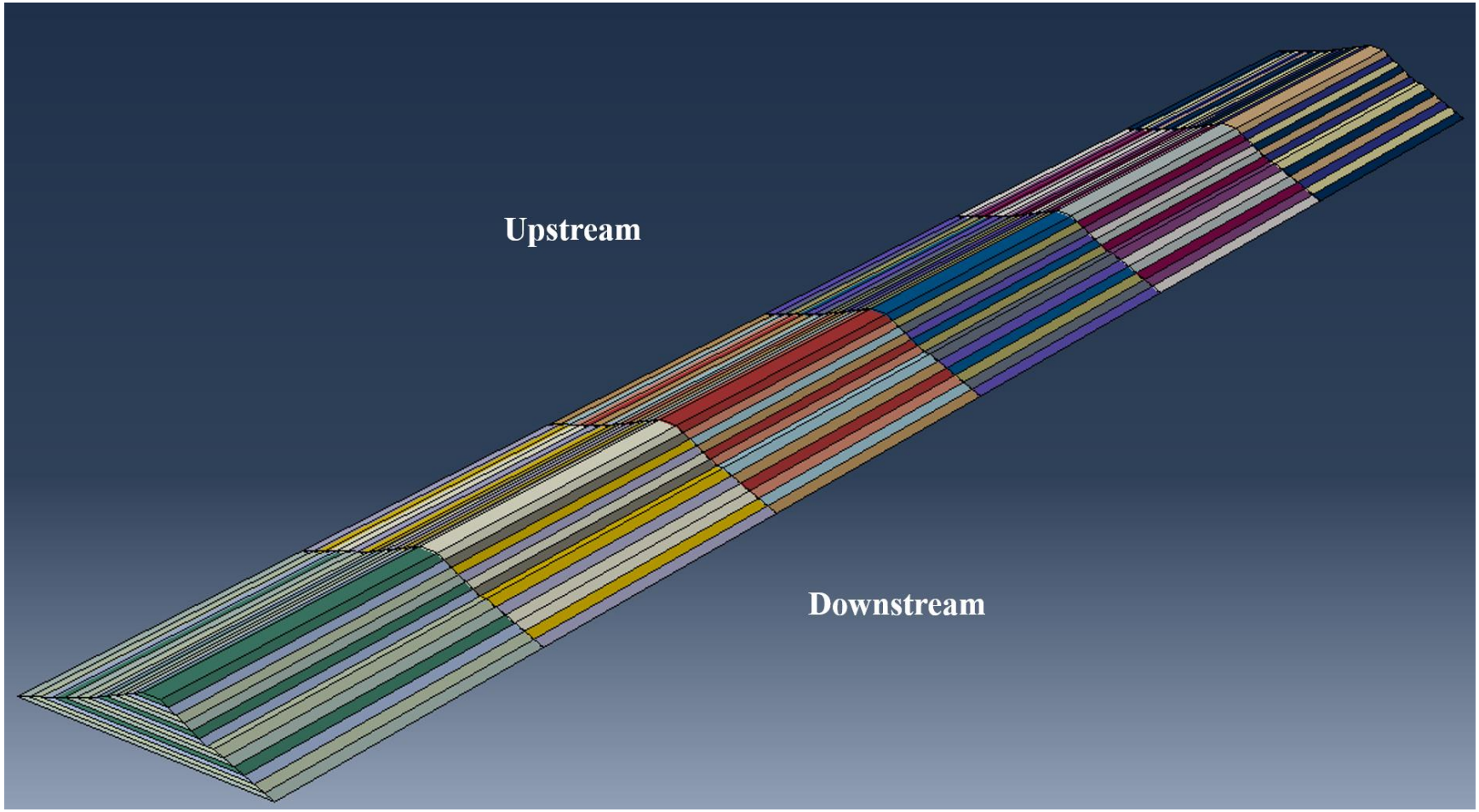


Figure 2.5: 3D model of the EM dam for Case 1

*Case 2*

A total of 28 segments with unequal lengths were considered, with one CPTu data available in the middle of each segment. Similar to Case 1, each section was horizontally divided every 1.5 m, and the corresponding material properties (ρ, μ, and E) were assigned to the layers in each segment. The shear wave velocity profile obtained for Case 2 is presented in Figure 2.6. A stark difference in the shear wave velocity profile of the same dam can be observed from Figures 2.4 and 2.6, for Case 1 and Case 2 analyses. Figure 2.7 shows the heterogeneous model of the dam with material variability portrayed using data interpreted from 28 CPTus.

The extreme ends along the longitudinal axis of the dam were fixed in the z-direction, and the base was fixed in all directions. Similar to 2D model, a mesh convergence study was performed to determine the appropriate mesh size and 3 m element size was suitable for the 3D analysis (Figure 2.8).

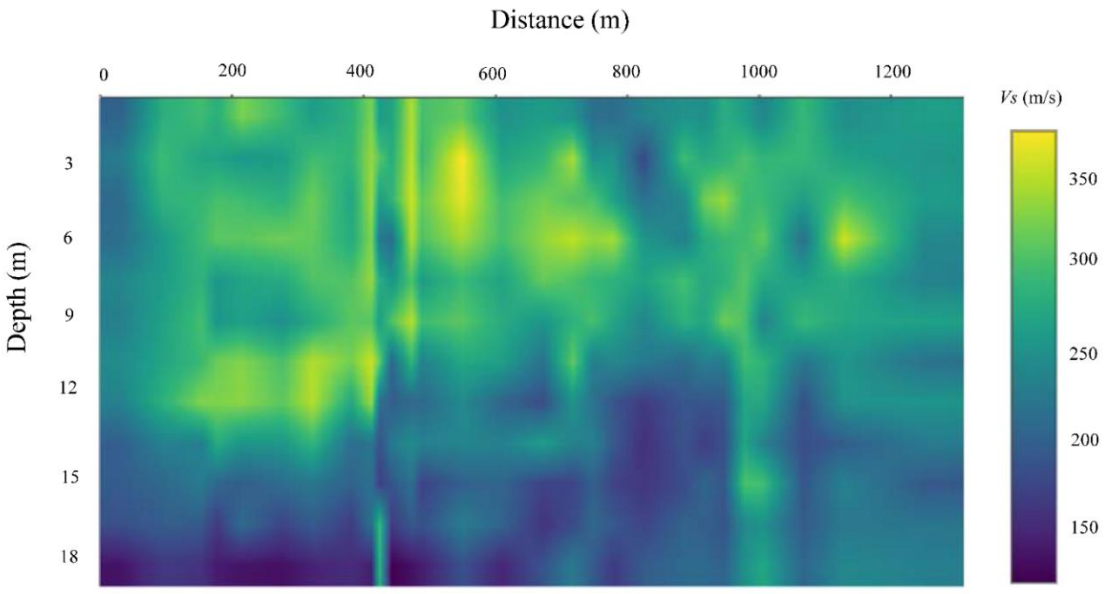


Figure 2.6: Shear wave velocity profile of the EM dam for Case 2

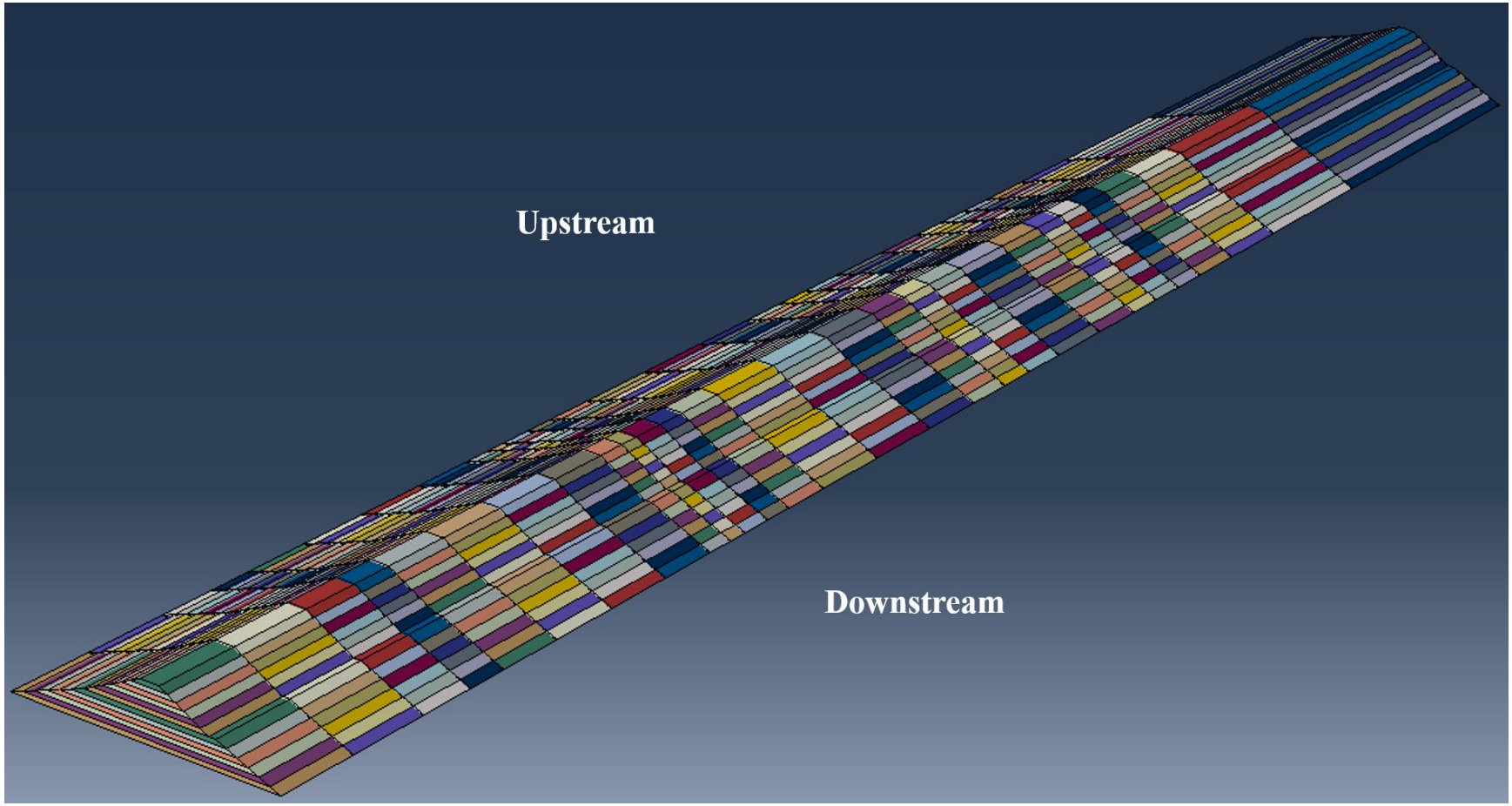


Figure 2.7: 3D model of the EM dam for Case 2

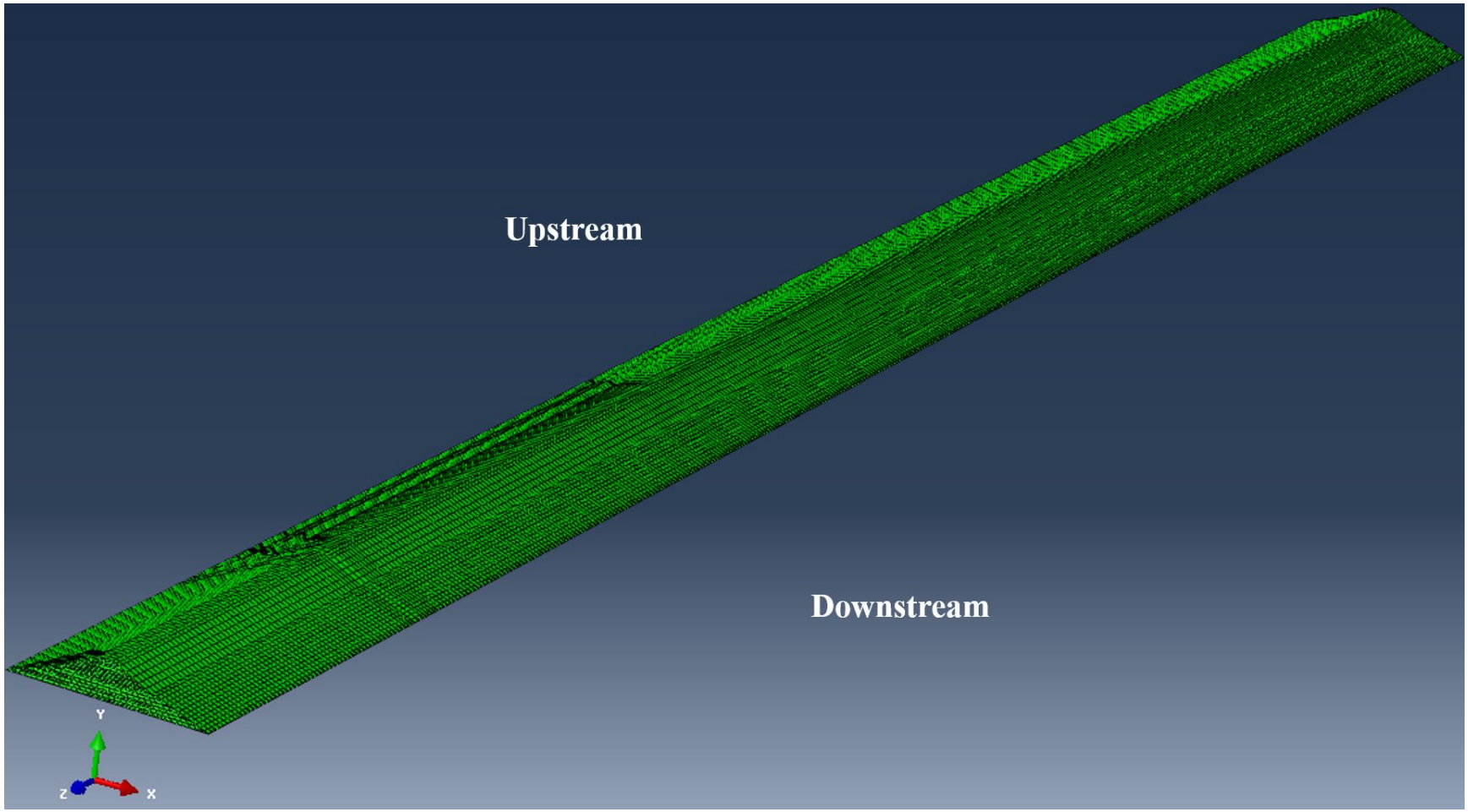


Figure 2.8: 3D finite element mesh of the EM dam

### 2.2.3 Estimation of natural frequency

The natural frequency determination is one of the essential steps in any seismic response analyses. This study was performed considering scenarios where low-intensity earthquakes occur (PGA = 0.01g). The contribution of the second and higher modes of vibration of a dam is usually not significant under such low-PGA earthquake events (Chopra and Chakrabarti 1972, 1973, Prevost et al. 1985, Charatpangoon et al. 2014). Therefore, the scope of this research study was limited to estimating the first natural frequency of the EM dam. The natural frequency of 2D and 3D models of the dam were compared to identify the scenarios where the natural frequency values are widely different. It was hypothesized that a significant difference in natural frequency values would also be associated with a widely different response when subjected to earthquake excitations. A synthesized multi-sine base excitation (sum of sines), obtained by superposition of sinusoidal waves of frequencies from 0.01Hz to 25 Hz, was applied at the base of the 2D model to determine the natural frequency of the 2D dam model sections. The sum of sines method relies on the premise that earthen dams act as filters to seismic waves, and only those waves having frequency close to the natural frequency of the structure are amplified at the crest (Zhu and Zhou 2010b, Chakraborty et al. 2018b). Since Eigenvalue analysis and the sum of sines method provide similar results, Eigenvalue analysis was not performed for the 2D analysis (Chakraborty et al. 2018b).

Previous research studies have not demonstrated the applicability of the sum of sines method to estimate the natural frequency of 3D models of earthen dams. Therefore, the natural frequencies of the 3D models were determined using both Eigenvalue analysis and the sum of sines method. Figure 2.9 depicts the schematic of the process involved in estimating the natural frequency by applying the sum of sines excitation at the base of the 2D and 3D models.

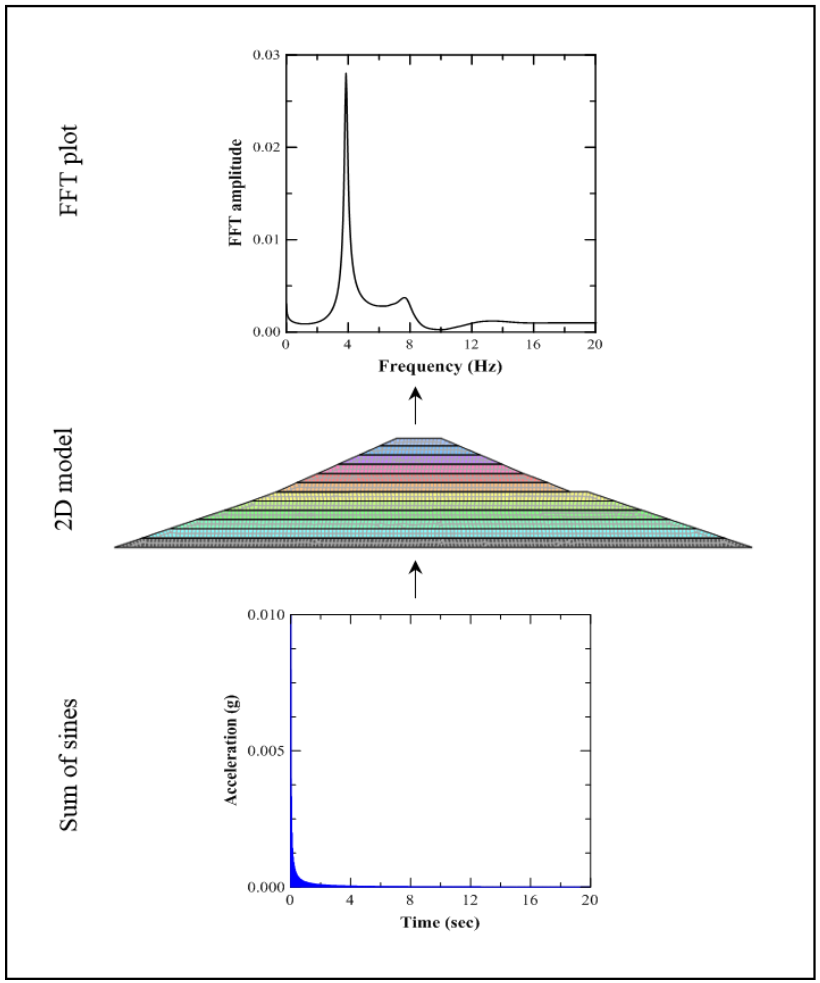


(a)

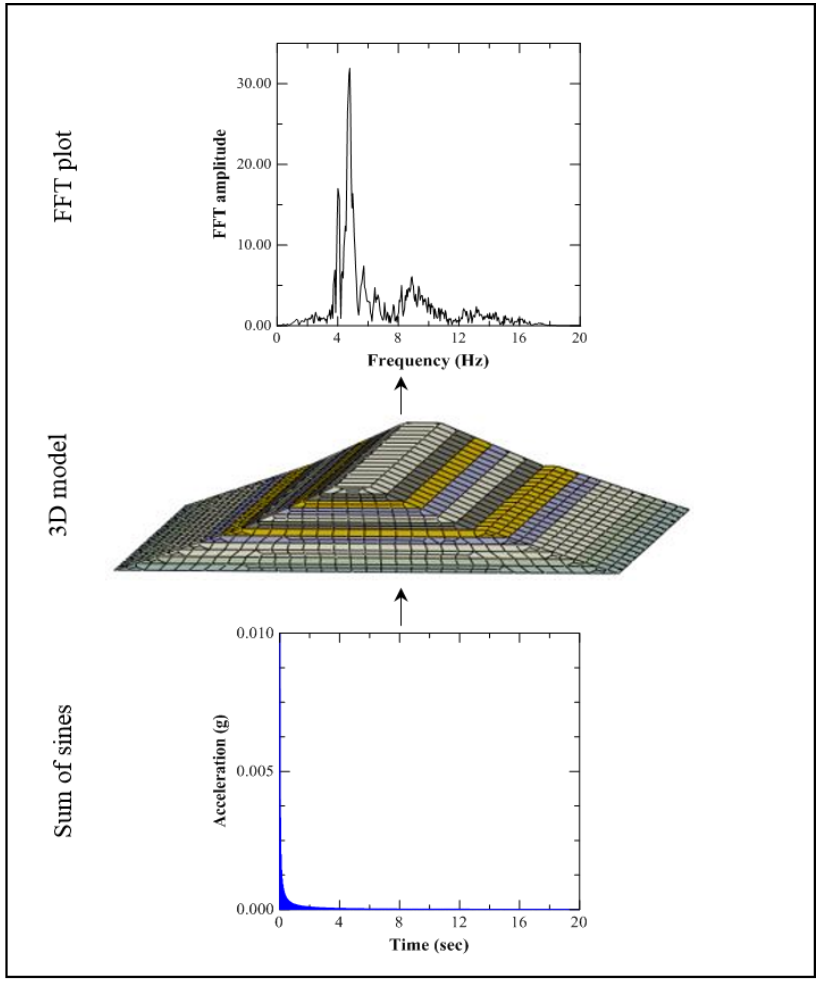


(b)

Figure 2.9: Natural frequency estimation using ‘sum of sines’ method for a typical (a) 2D section and (b) 3D segment

The first natural frequency was obtained by identifying the location of the first strong peak in the Fast Fourier Transform (FFT) plot of the acceleration history recorded at the crest of the dam.

### 2.2.4 Seismic response when subjected to earthquakes

The first natural frequency of the dam models was estimated by applying the sum of sines excitation - a synthesized wave with a wide range of frequency components having an equal contribution from each of the constituent frequencies. However, real earthquake data are typically random in nature and consist of waves of different frequencies with unequal contributions. Hence, responses of the dam were also analyzed considering two real earthquake events. Figure 2.10 presents the time history data and FFT plots of two induced seismic events in Oklahoma (OK), USA, recorded at stations Pawnee, OK (M4.5, USGS Station OK044, Nov 1, 2016) and Norfolk, OK (M5.0, USGS Station OK034, Nov 6, 2016), respectively. The earthquake data recorded at Pawnee and Norfolk had predominant frequencies of 4.74 Hz and 11.87 Hz, respectively. These earthquake data were scaled to PGA of 0.01g and were applied at the base of the models.

Peak accelerations on the crest of each section were determined for both 2D and 3D models. This will provide a better understanding of the impact of earthquake excitation on the structural response while considering the material variability along the dam. Also, average crest accelerations were determined to comprehend the overall response of the dam during the entire time duration of the earthquake. Besides estimating the natural frequency and crest accelerations, the shear stresses at select sections were analyzed at the time-step corresponding to the peak crest acceleration (which was similar for 2D and 3D). The earthquake-induced shear stress dictates the chances of failure of a dam section, and hence was computed and compared for the 2D and 3D analyses. Two segments located at distances of 175 m and 1250 m from the origin were selected

to study the differences in the earthquake-induced shear stress along the vertical centerline. These segments were selected to study the impact of segment widths; the segments at 175 m and 1250 m had widths of 38 m and 244 m, respectively. The following section presents the analyses and discussion of the results and highlights the salient findings of this research study.

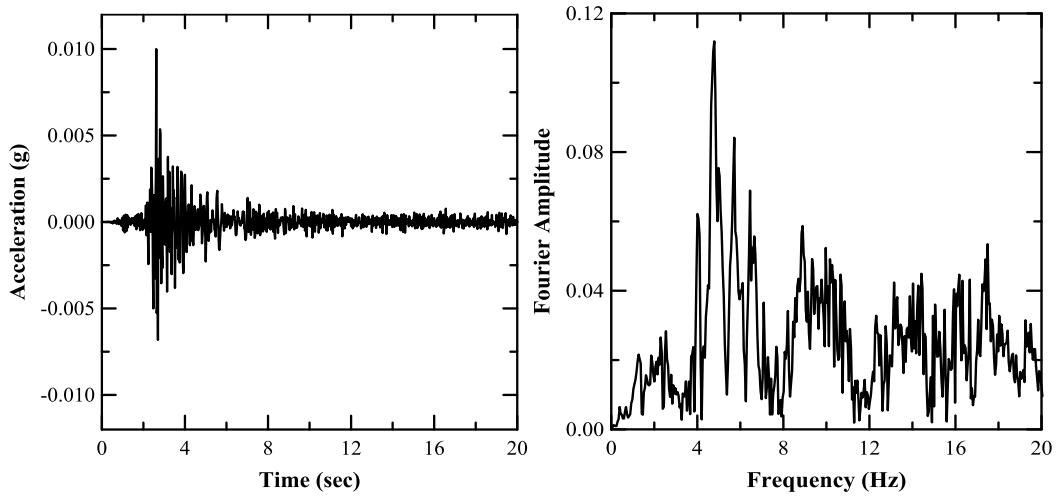


(a)

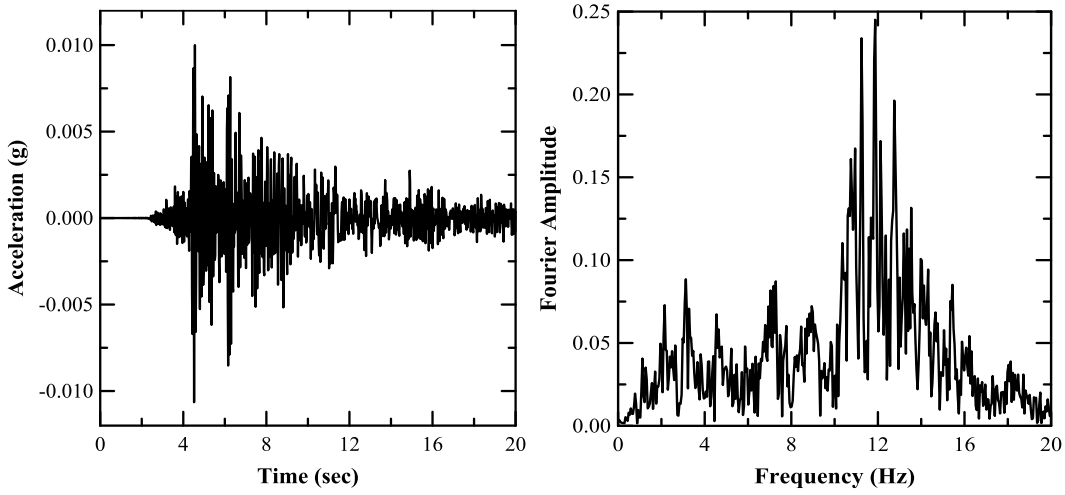


(b)

Figure 2.10: Acceleration-time data and FFT plot for Oklahoma earthquake, November 2016 recorded at stations (a) Pawnee, OK and (b) Norfolk, OK

## 2.3 Results and Discussion

This section presents the results of the 2D and 3D seismic response analyses of the Eagle Mountain dam. These analyses were performed under two different scenarios; Case 1 – with limited information available to portray the variation in material properties existing at the dam site and Case 2 – extensive information available to comprehensively incorporate the effect of material variability into the FEM models of the dam. The different parameters considered to study the behavior of the dam during seismic events include (i) the first natural frequency, (ii) peak and average crest acceleration values, and (iii) shear stress at the time of peak crest acceleration. The differences in the results obtained from the 2D and 3D analyses and the scenarios which warrant a 3D analysis instead of a simplistic 2D analysis are elucidated in the following sections.

### 2.3.1 Estimation of first natural frequency

The first mode of transverse vibration of a dam is typically characterized by a unidirectional lateral movement of the entire structure. However, for the EM dam model, no such deformed mode shape was observed from Eigenvalue analysis results shown in Figure 2.11. Rather, the deformed mode shapes for Case 1 analyses were localized at the individual six segments, for different frequencies ranging between 3.7 Hz and 5.6 Hz (Figure 2.12). This localized deformation suggests that the notion of a single first natural frequency is solely applicable for earthen dam models with the same material properties along the length of the dam. However, for a heterogeneous earthen dam model, the first natural frequency depends on the shear moduli of the different segments and varies along the length of the dam.

In addition to performing Eigenvalue analysis, the first natural frequency of the 3D model of EM dam was estimated using the sum of sines method. The results indicate that the first natural

frequency values obtained from the two methods are nearly similar (Figure 2.12). This suggests that the sum of sines method is capable of providing an accurate estimate of variation in the first natural frequency of a 3D heterogeneous earthen dam model.

Unlike the Case 1 analyses, the deformed mode shapes and corresponding frequencies were difficult to be detected from Case 2 Eigenvalue analysis. The presence of thin segments and drastic changes in material properties resulted in an overlap of the deformed mode shapes (Figures 2.2b, 2.6 and 2.13). Therefore, it was not possible to visually distinguish the deformed mode shapes and detect the corresponding first natural frequencies of the 28 segments. Instead, the first natural frequency was identified using the sum of sines method. The sum of sines method does not rely on visual identification of the mode shape of vibration and provides an easy approach for identifying the first natural frequency of any earthen dam. The first natural frequency of the different segments of the dam were estimated for the 2D and 3D models of the dam using the sum of sines method. The variation in natural frequency obtained for Case 1 and Case 2 analyses are presented in Figure 2.14.

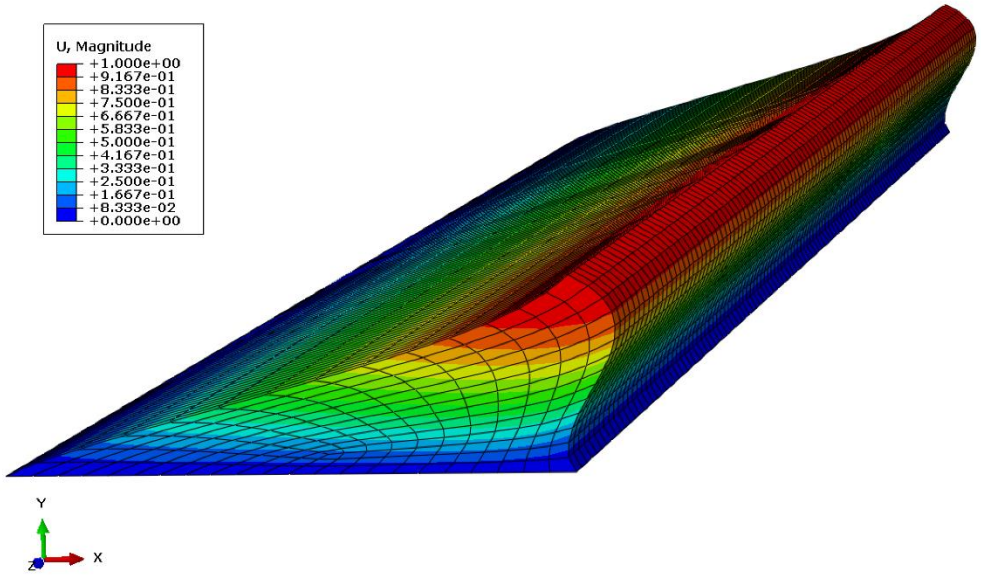


Figure 2.11: First mode of vibration obtained from Eigenvalue analysis for a homogeneous dam adopted from Clough and Chopra (1966)

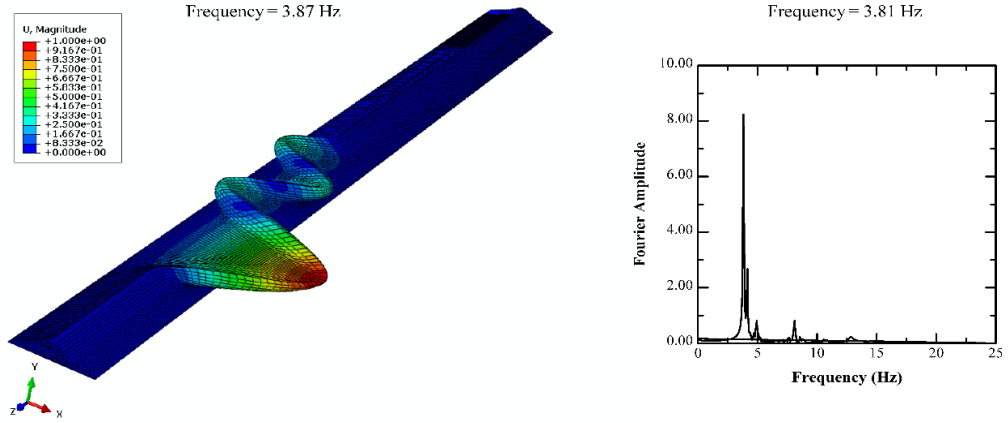


(a)

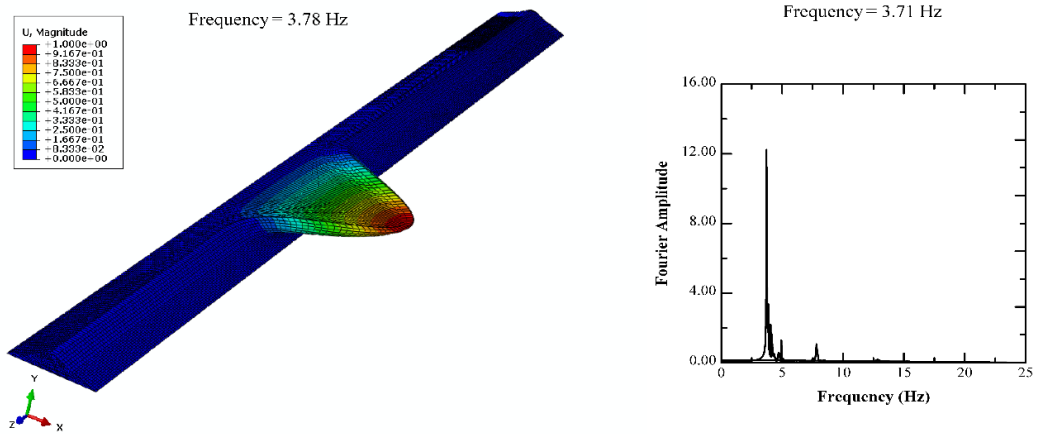


(b)

Figure 2.12: First natural frequency obtained from Eigenvalue analysis and the sum of sines method for two typical segments of Case 1 model at distances of (a) 380 m and (b) 610 m

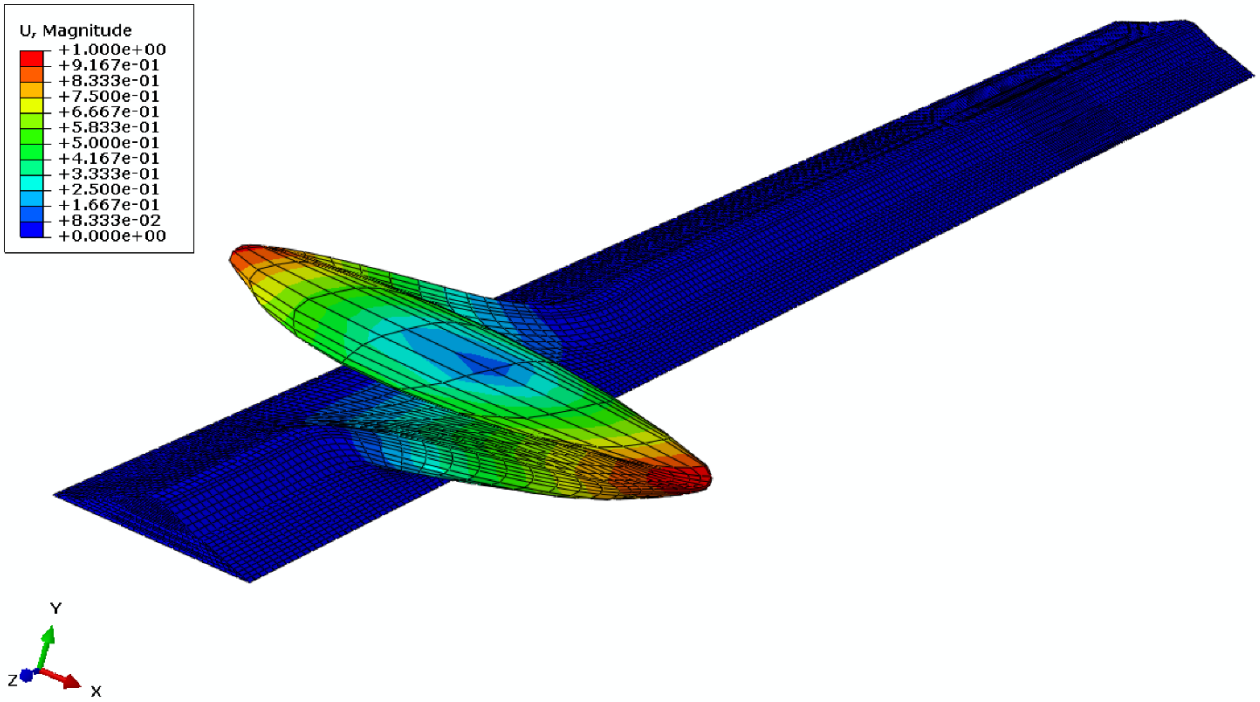


Figure 2.13: Overlapping mode shapes for 3 segments between 175 m to 250 m for Case 2 model

Figure 2.14 also highlights the similarity in the natural frequencies obtained from 2D and 3D analyses for Case 1 and the differences observed for Case 2. Previous researchers observed that the effect of adjacent boundaries had a prominent influence on the natural frequencies in a 3D analysis for a dam segments with L/H value less than 6. Past studies have shown that the natural frequency obtained from 2D and 3D analyses are practically the same for the L/H ratio greater than 6. The L/H ratio of the individual segment for Case 1 analyses is close to 13, which is higher than the threshold value suggested by previous researchers (Mejia and Seed 1983, Woodward and Griffiths 1993, Boulanger, R.W. et al. 1995, Mejia and Dawson 2010). Therefore the differences in 2D and 3D natural frequencies are negligible for Case 1 analyses. This indicates that each of the segments tends to behave independently with negligible influence of the adjacent sections. Contrarily, similar natural frequencies were not obtained for 2D and 3D analyses for Case 2 (Figure 2.14).

In Case 2, the same dam was modeled using extensive in-situ test data available. The availability of such extensive information from 28 CPTu tests facilitated in defining the variation in material properties over shorter spans of the dam. Hence several thin segments were defined with L/H less than 6. The presence of narrow sections coupled with drastic changes in stiffness had an appreciable impact on the 3D natural frequency as compared to that obtained from a 2D analysis (Figures 2.2b, 2.6, and 2.14). In case of a 2D analysis, the sections are assumed to respond independently without any influence of the adjacent sections. However, in a 3D analysis, the behavior of any segment depends on the stiffening or weakening effect of the adjacent segments. For instance, the natural frequencies of segments located at a distance of 380 m to 490 m have less fluctuation in the 3D analysis as compared to 2D analysis results (Figure 2.14b). The five narrow segments present in this 110 m stretch of the dam interact with each other and tend to vibrate as a

single unit in a 3D analysis. Such a synergistic response cannot be captured using a 2D plane strain analysis, resulting in the observed fluctuations and differences from the 3D analyses results. Contrarily, natural frequencies obtained from 2D and 3D analyses are similar at a distance of 1250 m due to the higher length of the segment with L/H = 12.8 (> 6).

The extent of difference in the 2D and 3D natural frequencies is not the same along the length of the dam (Figure 2.14b). The width of the segment and the differences in stiffness properties with respect to the adjacent sections were hypothesized to be the two primary factors influencing the differences in the 2D and 3D natural frequency values. Since the shear wave velocities of twelve (12) horizontal layers were used to model the individual segments of the dam, it was necessary to identify a measure of the average stiffness of a segment of the dam that predominantly dictates the natural frequency.

Regression analyses was performed to find the relationship between the natural frequency and the average shear modulus of the top, middle, and bottom one-third of a segment. The p-values of the regression analyses were used as a measure of identifying the layer, which predominantly influences the natural frequencies. A high p-value for a particular dependent parameter indicates the corresponding coefficient of zero, implying an insignificant contribution. The p-values provided in Table 2.2 clearly indicate that the average shear modulus of the bottom one-third of the dam has predominant influence on the natural frequency values. This finding is similar to the observations made by Chakraborty et al. (2017, 2018).

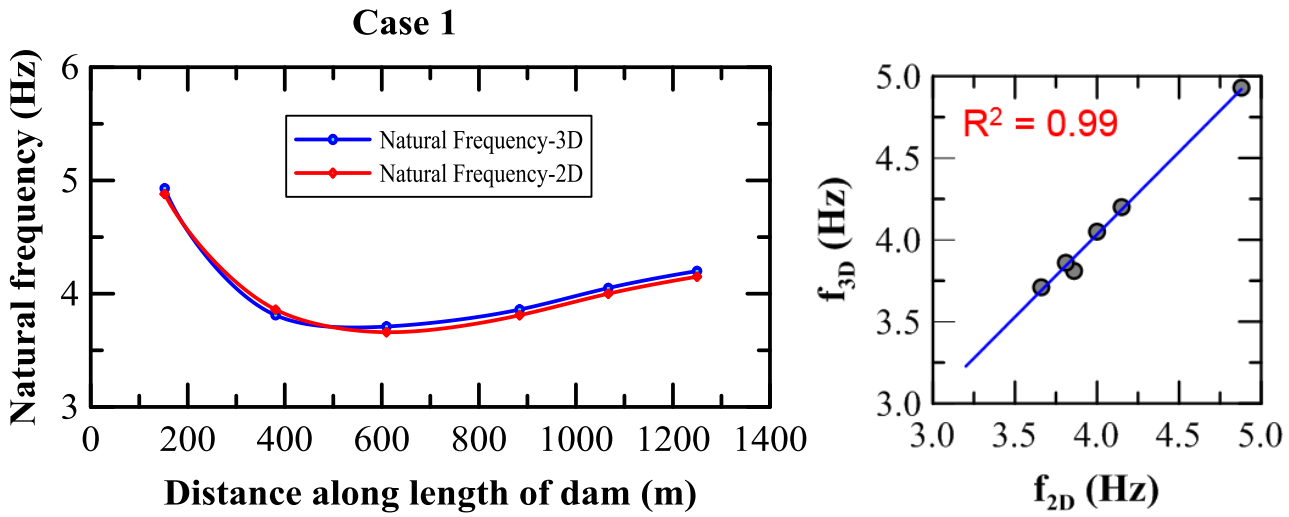


(a)

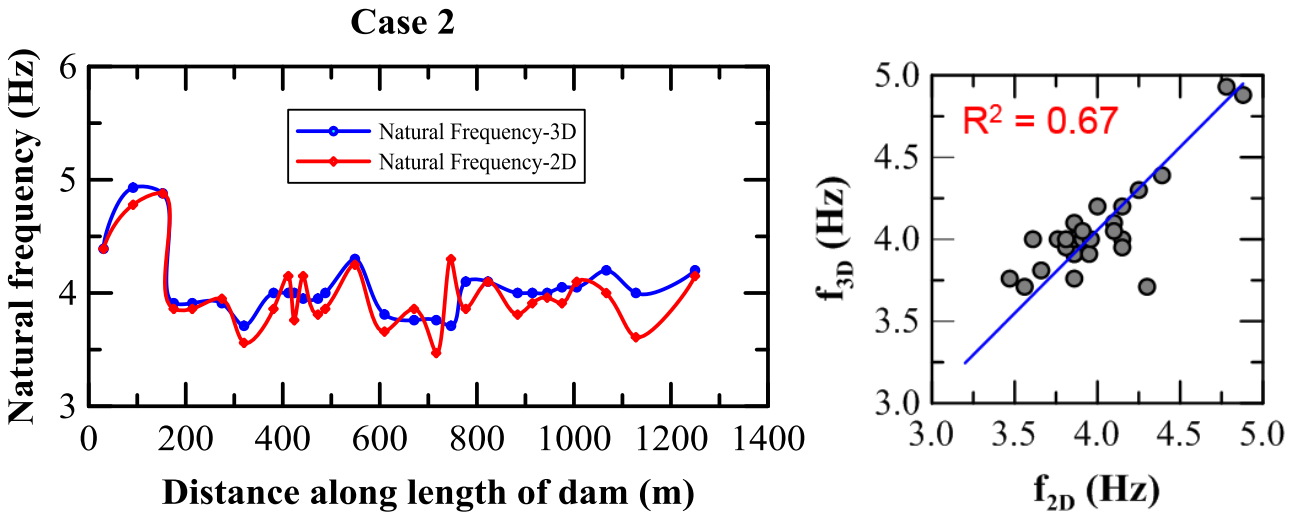


(b)

Figure 2.14: Comparison of natural frequencies obtained from 2D and 3D models for (a) Case 1 and (b) Case 2

Table 2.2. p-values from the regression analyses

| *Average* $G_{max}$ | p-value |
|---|---|
| Top one-third | $8.890 \times 10^{-1}$ |
| Middle one-third | $9.370 \times 10^{-1}$ |
| Bottom one-third | $9.516 \times 10^{-6}$ |

The width and the differences in stiffness properties of a segment are the two common factors affecting natural frequency values. They were incorporated in the analyses in terms of the shear modulus gradient (SMG) (equation 2.3). Figure 2.15a presents the variation of SMG along the length of the dam, and Figure 2.15b depicts the absolute differences in 3D and 2D natural frequencies, expressed as a percentage with respect to 2D natural frequencies. Figure 2.15 shows a good similarity in the pattern of the variation in SMG and differences in natural frequencies, along the length of the dam. This implies that a change in shear modulus over a short span is expected to result in a higher difference in 3D and 2D natural frequencies. Therefore, it may be inferred that 3D analysis of a heterogeneous earthen dam will yield additional information compared to a 2D analysis, if and only if, extensive information about material properties are available to capture the material variability existing along the length of the dam.

$$SMG = \frac{|G_i - G_{i+1}|}{\frac{L_i + L_{i+1}}{2}} - \frac{|G_{i-1} - G_i|}{\frac{L_{i-1} + L_i}{2}} \quad (2.3)$$

where $G_i$ is the average shear modulus of bottom one-third of the dam and $L_i$ is thickness of the $i^{th}$ segment, respectively.

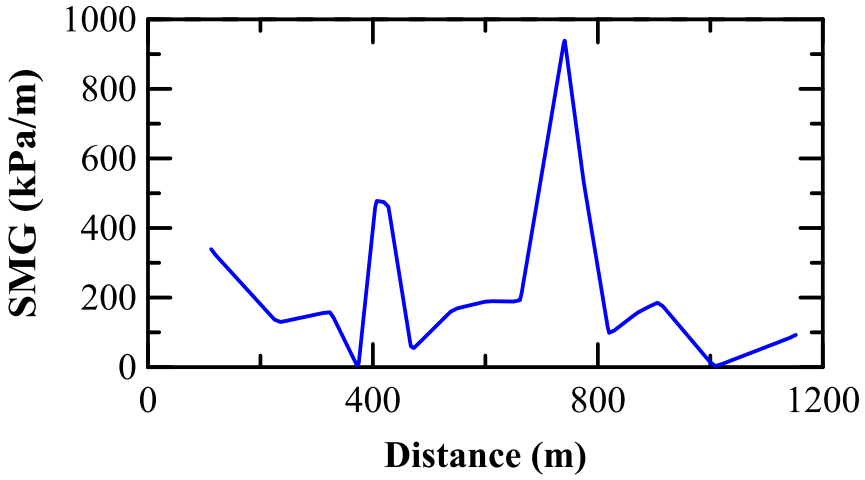


(a)

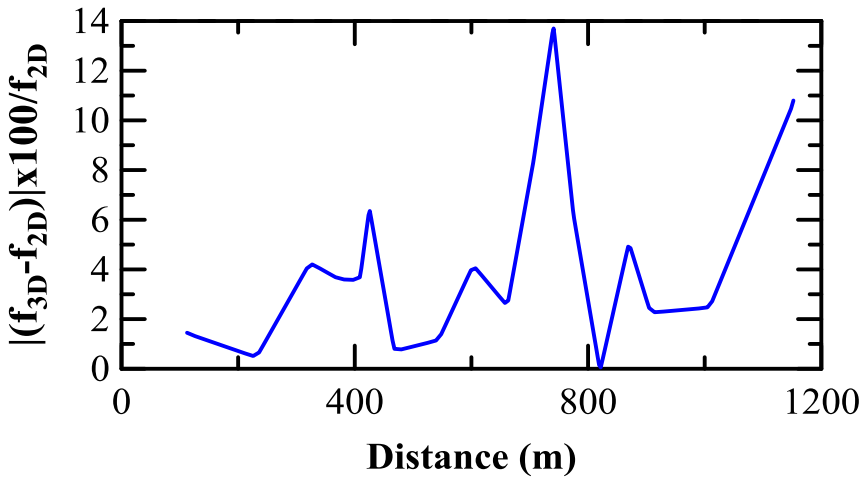


(b)

Figure 2.15: Variation of (a) shear modulus gradient and (b) percentage difference (absolute) in 2D and 3D natural frequencies

The comparison between 2D and 3D natural frequencies presented so far was based on the first natural frequencies estimated using the sum of sines method. The frequency of the first strong peak was considered as the first natural frequency for both 2D and 3D analyses. Unlike the sharp, strong peak obtained in the FFT plot for 2D analysis, a broad, blunt peak was observed for the 3D analyses of Case 2 (Figure 2.16). This can be attributed to the influence of the different material

properties of the adjacent segments. Therefore, the notion of a single-valued first natural frequency is not applicable in the case of 3D analysis. Instead, the first natural frequency needs to be represented as a band of frequencies over which a particular segment of the dam tends to vibrate in the first mode. This hypothesis was validated by applying single-frequency sinusoidal base excitations with frequencies ranging between the lower limit to the upper limit of the frequency bandwidth observed for a typical segment located at a distance of 175m.

The first natural frequency band was observed to exist between 3.9 Hz to 4.9 Hz. Hence, three single-frequency sinusoidal waves with frequencies of 3.9 Hz, 4.4 Hz, and 4.9 Hz were individually applied at the base of the 3D dam model. The absolute value of the relative X-displacements along the centerline of the dam, at different time steps of the excitation, were used to identify the mode shape of vibration. Figure 2.17 suggests that the segment experienced first mode of vibration for all three frequencies. The observations confirm that a band of first natural frequencies exists for heterogeneous earthen dams, primarily due to the influence of material variability of adjacent segments. Figure 2.18 presents the frequency bandwidth obtained from 3D analyses of Case 2. Besides estimating the natural frequency of the EM dam, the seismic response was further studied based on the earthquake-induced accelerations and shear stresses, details of which are provided in the next section.

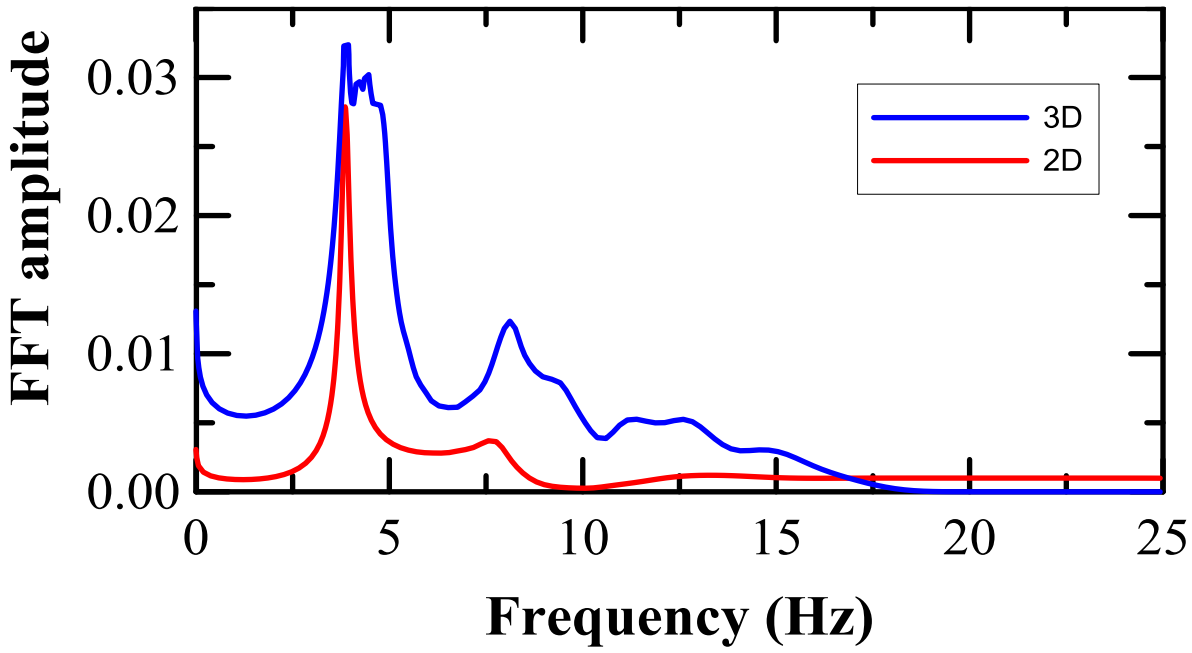


Figure 2.16: Comparison of single-valued natural frequency for 2D analysis and band of natural frequency for 3D analysis

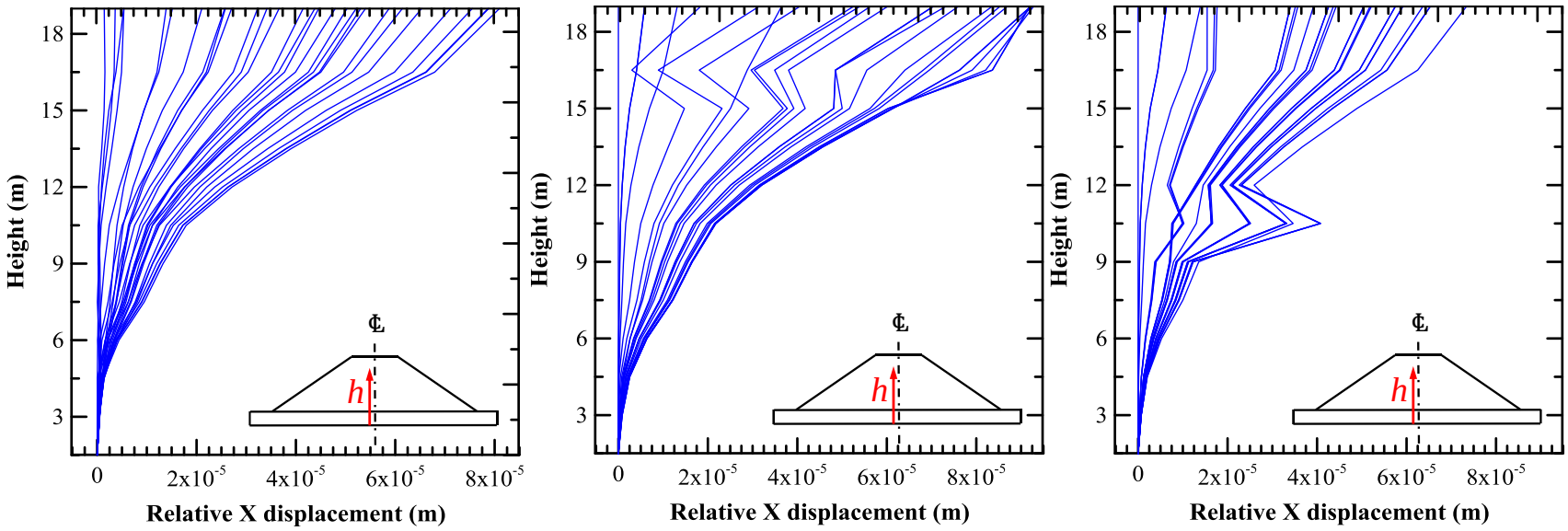


Figure 2.17: First mode of vibration after applying sinusoidal waves of frequency (a) f1= 3.9 Hz, (b) f2= 4.4 Hz and (c) f3= 4.9 Hz

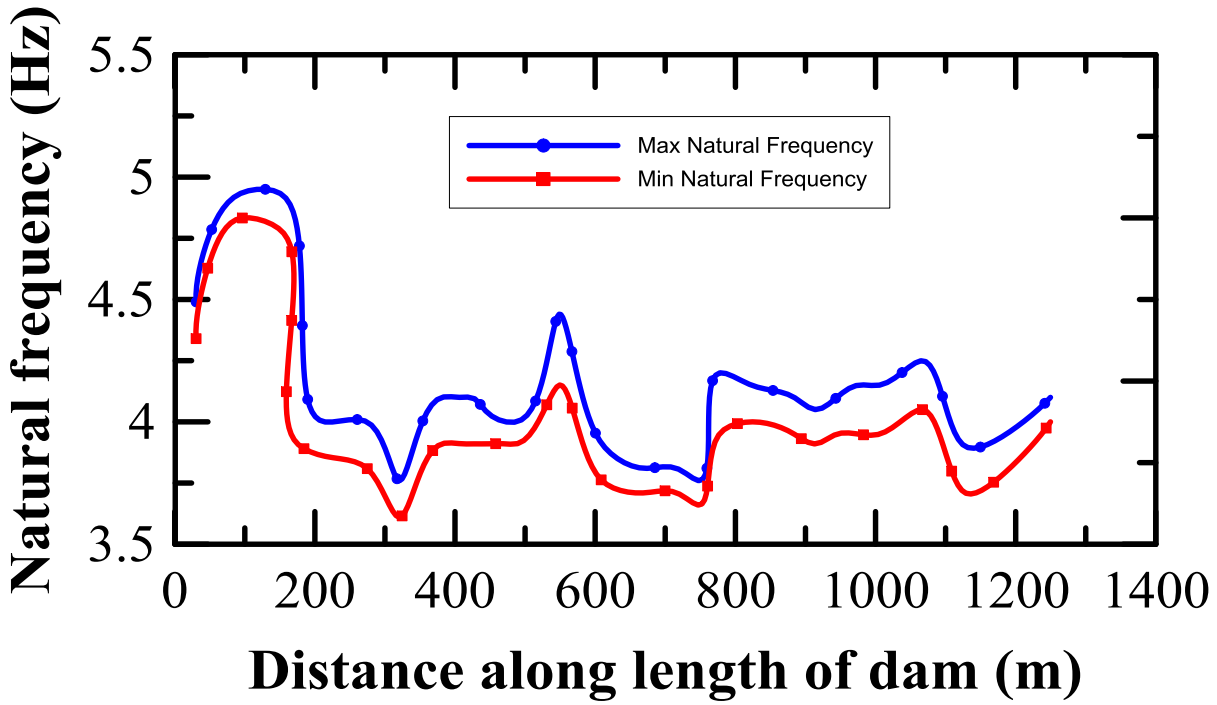


Figure 2.18: Variation of natural frequency band for Case 2 3D analyses

### 2.3.2 Earthquake-induced acceleration and shear stresses

The peak crest acceleration values of Case 1 and Case 2 were obtained for two different earthquake excitations (Figures 2.19a and b). The peak crest acceleration values obtained from the 3D analyses is higher than the 2D analyses results, for both case scenarios and earthquake excitations considered in this study. The average crest acceleration, which provides a measure of the average earthquake-induced force acting on the dam, also exhibited a similar trend as the peak acceleration, irrespective of the frequency content of the earthquakes. A higher peak and/or average acceleration values indicate that the earthquake-induced forces computed from a 3D analyses are higher than that obtained from the 2D analyses. This implies that the earthquake-induced forces are underestimated in a 2D analyses, and hence a slope will be declared safe from a 2D analyses. In reality, the slope might experience stability issues. This is in agreement with the observations made by Mejia and Seed (1983).

The failure of a dam occurs when the shear stresses exceed the shear strength of the materials. Therefore, the earthquake-induced shear stresses computed from 2D and 3D analyses were compared, besides analyzing the peak and average crest acceleration values. The shear stresses along the centerline of the dam were compared at sections located at distances of 175 m and 1250 m at the time corresponding to peak crest acceleration values at the respective segments. The segments located at 175 m and 1250 m were purposefully selected for the comparative study due to their widely different thicknesses of 38 m and 244 m, respectively. The shear stresses induced during Pawnee and Norfolk earthquakes, and the deformations along the centerline of the dam are presented in Figures 2.20 and 2.21, respectively.

The shear stresses computed from the 3D analyses were higher than that computed from 2D analyses for the Pawnee earthquake (Figure 2.20). The higher peak crest acceleration and

lateral movement of the dam induced higher shear stress in the 3D analyses (Figures 2.19a and 2.20). The extent of difference in computed shear stresses (2D versus 3D) is greater for the 38 m thick section as compared to the 244 m thick section. The adjacent segments have a stronger influence on the response of a thin segment, as compared to a thick segment. Therefore, the difference in shear stresses is expected to be prominent for a thin segment (similar to Case 2), as compared to a thick segment (similar to Case 1).

In the case of Norfolk earthquake, the shear stresses computed from the 3D analyses were higher than the 2D analyses for major portions of the dam (Figure 2.21). A greater 2D shear stress was observed for the layers located between 4m and 8m from the base of the dam. This apparent anomaly can be attributed to the lower relative displacement of the centerline of the dam for the 3D analyses, as compared to the 2D analyses (Figure 2.21). This peculiar behavior was not observed for Pawnee earthquake as the deformation of the centerline of the dam was consistently higher for the 3D analyses (Figure 2.20). Nevertheless, higher shear stress close to the upper half of the dam indicates chances of slope stability issues, which may be overlooked from a 2D analyses (Figure 2.21).

The magnitude of the earthquake-induced shear stresses are not appreciable for either of the earthquake scenarios considered in this study (Figures 2.20 and 2.21). This is attributed to the use of low-intensity earthquake excitation with PGA of 0.01g. Nevertheless, the findings of this study highlight the chances of underestimation of earthquake-induced forces and shear stresses by performing a 2D analysis. In the case of heterogeneous earthen dams with scarce in-situ test data, performing a 3D analysis may not yield appreciable additional information over that obtained from a 2D analysis. However, it is preferable to perform a 3D analysis for a project where extensive information is available to capture the material variability existing at site. The findings of this

study can facilitate future researchers to develop guidelines that can be used by practicing engineers to select between 2D or 3D analyses based on the extent of in-situ test data available for a given project. Further studies are needed to develop such guidelines and validate their applicability. This research study was limited to studying the behavior of the dam at small strain levels, and the effect of water present on the upstream side of the dam was not considered. Future studies will be required to study the effect of reservoir water, non-linear behavior of soil, and development of excess pore water pressure, on the 2D and 3D seismic response analyses results.

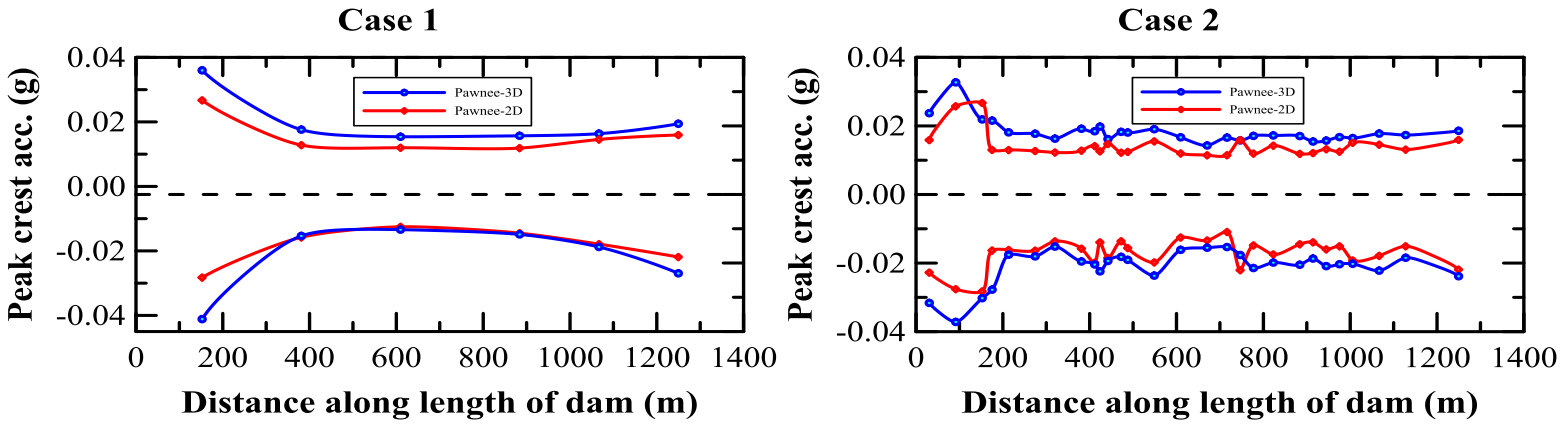


(a)

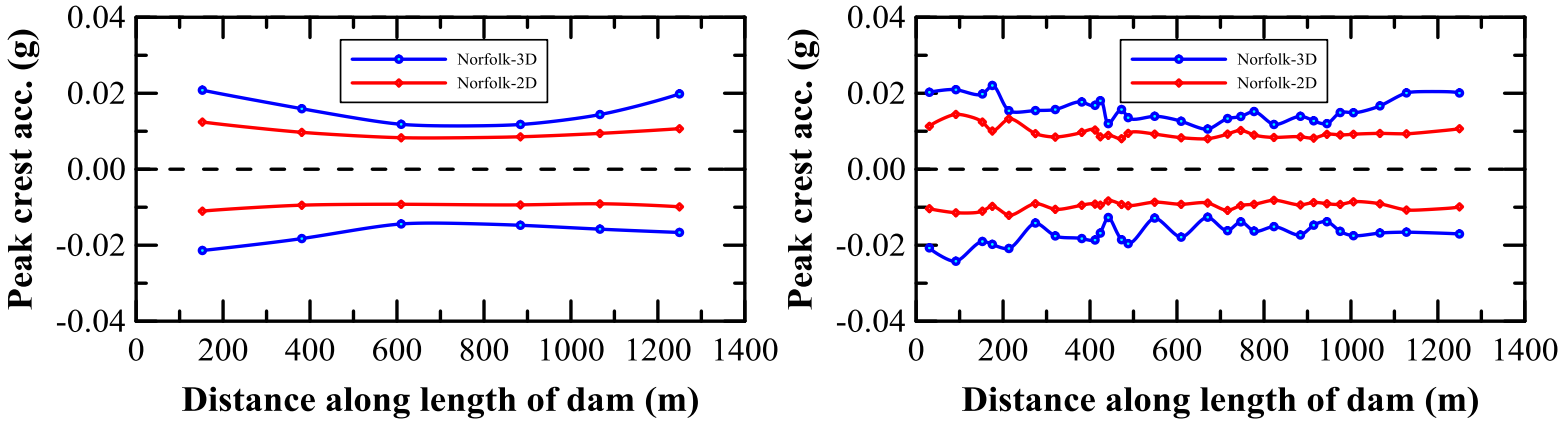


(b)

Figure 2.19: Case 1 and Case 2 peak crest accelerations from 2D and 3D analyses for earthquakes recorded at stations (a) Pawnee, OK and (b) Norfolk, OK

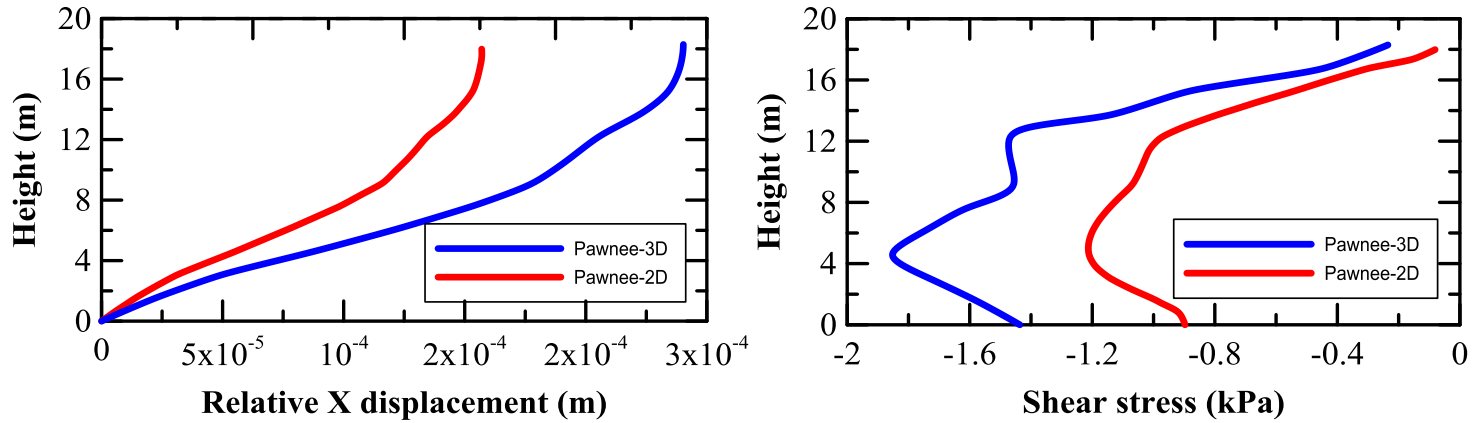


(a)

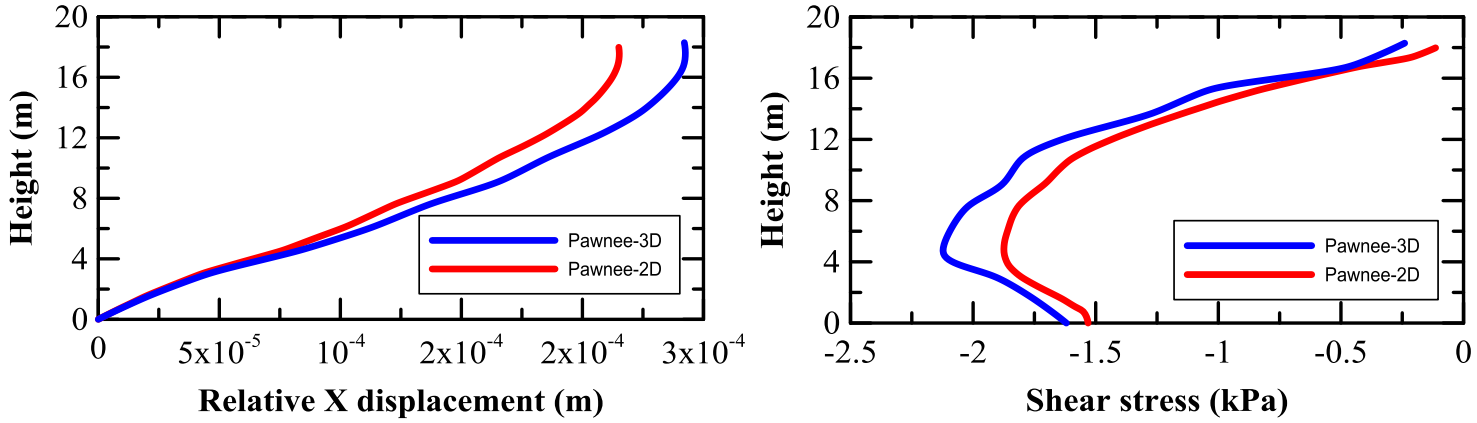


(b)

Figure 2.20: Relative x-displacement and shear stress data for Pawnee earthquake (a) segment at 175 m and (b) segment at 1250 m

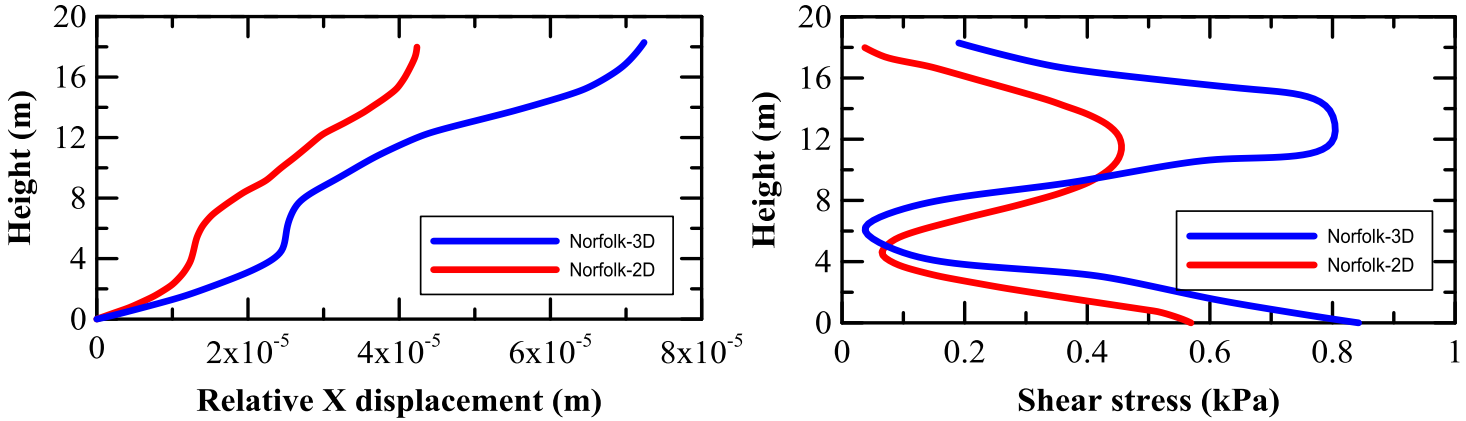


(a)

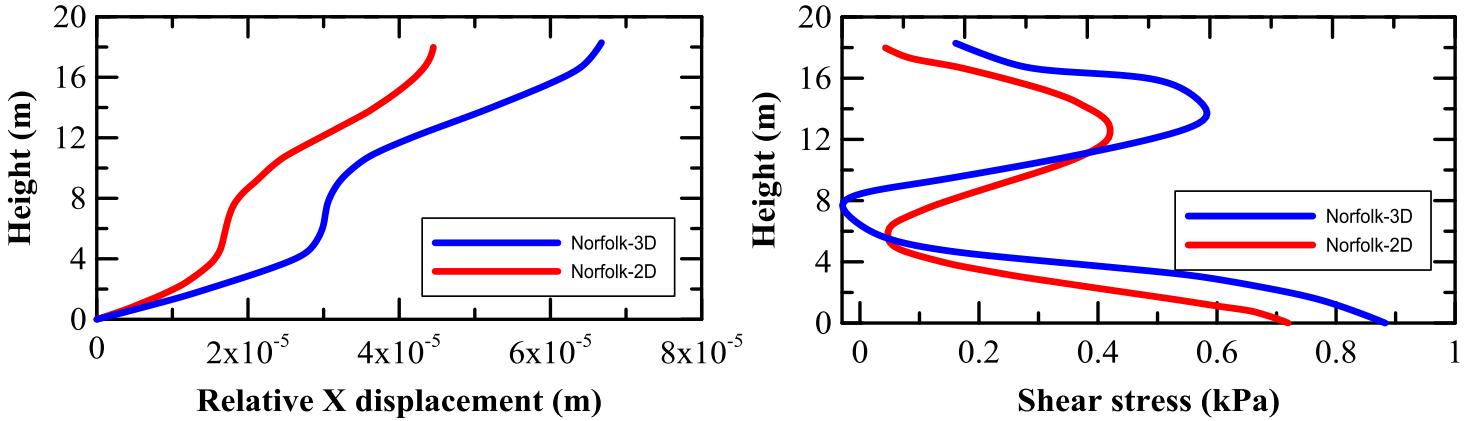


(b)

Figure 2.21: Relative x-displacement and shear stress data for Norfolk earthquake (a) segment at 175 m and (b) segment at 1250 m

## 2.4 Summary and Conclusions

The objective of this study was to evaluate the applicability and limitations of the conventional 2D seismic response analyses for studying the behavior of a long, heterogeneous, hydraulic fill earthen dam. The hydraulic fill dam was modeled using commercially available 2D and 3D FEM-based software packages for two different scenarios: Case 1 – material characterization based on the limited information available from 6 CPTus and Case 2 – extensive information available about the material variability from 28 CPTus. A comparative study was performed using different parameters, including the first natural frequency, earthquake-induced peak crest acceleration values and shear stresses, computed from 2D and 3D analyses. The following major conclusions can be drawn from the findings of this study:

- The 2D analyses results, for Case 1 and Case 2, indicate a significant variation in the first natural frequency due to the material variability existing along the length of the hydraulic fill dam. Therefore, a single-valued, first natural frequency of the entire dam, is not applicable for a heterogeneous earthen dam.
- The mode shapes obtained from the 3D Eigenvalue analysis showed localized first mode of deformation corresponding to first natural frequencies of the six different segments considered for Case 1. Hence, a uniform, laterally deformed mode shape, typically observed for long homogeneous dams, is not applicable for heterogeneous earthen dams.
- The estimation of first natural frequency from 3D Eigenvalue analyses was difficult for Case 2 analyses due to the influence of overlapping first modes of vibration of adjacent segments. The utilization of the sum of sines method was found to be an easier approach for estimating the variation of natural frequency along the length of the dam, for both Case

1 and Case 2 analyses. Thus, the sum of sines method is applicable for estimating the natural frequencies for any 2D or 3D models of earthen dams.

- The 2D and 3D natural frequencies were similar for Case 1 analyses. However, the 3D natural frequencies observed for Case 2 analyses were significantly different from the 2D analyses results. The extent of difference is expected to be pronounced for the segments where the available in-situ test results can be used to capture drastic changes in material properties along the dam. In such situations, a 2D plane strain analysis cannot portray the actual response of the dam, and performing a 3D analysis is desirable.
- The seismic response of a particular segment of the dam was influenced by the material properties of the adjacent segments in 3D analyses of Case 2. Consequently, the segment exhibited first mode of vibration over a band of natural frequencies in a 3D analysis. This effect is ignored in a 2D analysis but can be captured by a 3D analysis when extensive information about the properties of the influencing neighboring segments is available.
- For both Case 1 and Case 2 analyses, the earthquake-induced acceleration values, forces, and shear stresses computed from a 2D analysis were found to be lower than those computed from a 3D analysis, irrespective of the frequency contents of the earthquake excitations. This indicates that the 2D analysis underestimates the earthquake-induced forces and shear stresses, and may overlook potential stability issues of an earthen dam.

# References


Abdel-Ghaffar, A.M., and Koh, A.-S. 1981. Longitudinal vibration of non-homogeneous earth dams. Earthquake Engineering & Structural Dynamics, **9**(3): 279–305. doi:10.1002/eqe.4290090308.

Abdel-Ghaffar, A.M., and Scott, R.F. 1979a. Analysis of earth dam response to earthquakes. Available from http://resolver.caltech.edu/CaltechAUTHORS:20151104-154157041.

Abdel-Ghaffar, A.M., and Scott, R.F. 1979b. Shear Moduli and Damping Factors of Earth Dam. Journal of the Geotechnical Engineering Division, **105**(12): 1405–1426.

Abdel-Ghaffar, A.M., and Scott, R.F. 1981. Vibration tests of full-scale earth dam. doi:10.1016/0148-9062(81)91322-X.

Ambraseys, N. 1960. On the shear response of a two-dimensional truncated wedge subjected to an arbitrary disturbance. Bulletin of the Seismological Society of America, **50**(1): 45–56.

Ambraseys, N.N. 1988. Engineering Seismology. International Journal of Earthquake Engineering and Structural Dynamics,.

Boulanger, R.W., Bray, J.D., Merry, S.M., and Mejia, L.H. 1995. Three-dimensional dynamic response analyses of Cogswell dam. Canadian Geotechnical Journal,.

Bybordiani, M., and Arici, Y. 2017. The use of 3D modeling for the prediction of the seismic demands on the gravity dams. Earthquake Engng Struct. Dyn.,.

Castro, R.R., Mucciarelli, M., Pacor, F., Federici, P., and Zaninetti, A. 1998. Determination of the characteristic frequency of two dams located in the region of Calabria, Italy. Bulletin of the Seismological Society of America, **88**(2): 503–511.

Cetin, K., Isik, N.S., Batmaz, S., and Karabiber, S. 2005. A comparative study on the actual and estimated seismic response of kiralkizi dam in turkey. Journal of Earthquake Engineering, **9**(4): 445–460. doi:10.1080/13632460509350550.

Chakraborty, S., Banerjee, A., Das, J.T., Mosadegh, L., and Puppala, A.J. 2018a. Impact of Variation of Small Strain Shear Modulus on Seismic Slope Stability Analysis of a Levee: A Sensitivity Analysis. Ifcee 2018,: 302–313. doi:10.1061/9780784481608.029.

Chakraborty, S., Das, J.T., Puppala, A.J., and Banerjee, A. 2018b. Natural frequency of earthen dams at different induced strain levels. Engineering Geology, **248**(August 2018): 330–345. Elsevier. doi:10.1016/j.enggeo.2018.12.008.

Chakraborty, S., Das, J.T., Banerjee, A., and Puppala, A.J. 2017. Effect of Erroneous Estimation of Small Strain Shear Moduli on Seismic Response of an Earth Dam. *In* Indian Geotechnical Conference. Guwahati. pp. 1–5.

Chaney, R., Demars, K., Brignoli, E., Gotti, M., and Stokoe, K. 1996. Measurement of Shear Waves in Laboratory Specimens by Means of Piezoelectric Transducers. Geotechnical Testing Journal, **19**(4): 384–397. doi:10.1520/GTJ10716J.

Charatpangoon, B., Kiyono, J., Furukawa, A., and Hansapinyo, C. 2014. Dynamic analysis of earth dam damaged by the 2011 Off the Pacific Coast of Tohoku Earthquake. Soil Dyn Earthq Eng,.

Chatterjee, K., and Choudhury, D. 2014. Seismic Analysis of Soil Slopes Using FLAC2D and Modified Newmark Approach. *In* Geo-Congress 2014 Technical Papers. American Society of Civil Engineers, Reston, VA. pp. 1196–1205. doi:10.1061/9780784413272.116.

Chopra, A., and Chakrabarti, P. 1972. The earthquake experience at Koyna dam and stresses in concrete gravity dams. Earthq Eng Struct Dyn,.

Chopra, A., and Chakrabarti, P. 1973. The Koyna earthquake and the damage to Koyna dam. Bull Seismol Soc Am,.

Chopra, A.K. 1967. Earthquake Response of Earth Dams.

Clough, R.W., and Chopra, A.K. 1966. Earthquake Stress Analysis in Earth Dams. Journal of the Engineering Mechanics Division, **92**(2): 197–212. Available from http://cedb.asce.org/cgi/WWWdisplay.cgi?14349%5Cnfiles/160/WWWdisplay.html.

Dakoulas, P. 1993. Earth dam-canyon interaction effects for obliquity incident SH waves. Journal of Geotechnical and Geoenvironmental Engineering,.

Dakoulas, P., and Gazetas, G. 1985. A class of inhomogeneous shear models for seismic response of dams and embankments. International Journal of Soil Dynamics and Earthquake Engineering, **4**(4): 166–182. doi:10.1016/0261-7277(85)90037-3.

Gazetas, G. 1987. Seismic response of earth dams : some recent developments. **6**(1).

Griffiths, D. V., and Prevost, J.H. 1988. Two and three-dimensional dynamic finite element analyses of Long Valley dam.pdf.

Harder, L.F. 1991. Performance of Earth Dams During the Loma Prieta Earthquake. *In* Proceedings: Second International Conference on Recent Advances in Geotechnical Earthquake Engineering and Soil Dynamics.

Hatanaka, M. 1955. Fundamental Considerations on the Earthquake Resistant Properties of the Earth Dam. Part I On the Vibration of Earth Dam. Bulletins - Disaster Prevention Research Institute, Kyoto University, **11**: 1–36.

Hegazy, Y., and Mayne, P. 1995. Statistical correlations between VS and cone penetration data for different soil types. *In* Proc., International Symposium on Cone Penetration Testing, CPT '95, Linkoping.

Heinz, R.A. 1976. Hydraulic Fill Dams/Earthquake Stability. Civil Engineering—ASCE, **46**(5): 55–60. ASCE.

Ishizaki, H., and Hatakeyama, N. 1962. Considerations on the Vibrational Behaviors of Earth Dams. Bulletins - Disaster Prevention Research Institute, Kyoto University, **52**: 1–23.

Jafari, M.K., and Davoodi, M. 2006. Dynamic characteristics evaluation of Masjed Soleiman Dam using in situ dynamic tests. Canadian Geotechnical Journal, **43**(10): 997–1014. doi:10.1139/t06-059.

Jibson, R.W. 2007. Regression models for estimating coseismic landslide displacement.

Kallioglou, P., Tika, T., and Pitilakis, K. 2008. Shear Modulus and Damping Ratio of Cohesive Soils. Journal of Earthquake Engineering,.

Kayen, R., Moss, R.E.S., Thompson, E.M., Seed, R.B., Cetin, K.O., Kiureghian, A. Der, Tanaka, Y., and Tokimatsu, K. 2013. Shear-Wave Velocity–Based Probabilistic and Deterministic Assessment of Seismic Soil Liquefaction Potential. Journal of Geotechnical and Geoenvironmental Engineering, **139**(3): 407–419. doi:10.1061/(ASCE)GT.1943-5606.0000743.

Kuhlemeyer, R.L., and Lysmer, J. 1973. Finite Element Method Accuracy for Wave Propagation Problems. Journal of the Soil Mechanics and Foundations Division, **99**(5): 421–427. ASCE.

Küpper, A.M.A.G. 1991. Design of hydraulic fill. University of Alerta.

Makdisi, F.L. 1976. Performance and Analysis of Earth Dams During Strong Earthquakes.

Mayne, P.W., and Rix, G.J. 1995. Correlations between Shear Wave Velocity and Cone Tip Resistance in Natural Clays. Soils and Foundations, **35**(2): 107–110. doi:10.3208/sandf1972.35.2_107.

Mejia, L., and Dawson, E. 2010. 3D Analysis of the Seismic Response of Seven Oaks Dam. In 3D analysis of the seismic response of Seven Oaks Dam. pp. 1–13.

Mejia, L.H., and Dawson, E.M. 2006. Earthquake deconvolution for FLAC. *In* 4th International FLAC Symposium on Numerical Modeling in Geomechanics. pp. 4–10.

Mejia, L.H., and Seed, H.B. 1983. Comparison of 2D and 3D Dynamic Analyses of Earth Dams. Journal of Geotechnical Engineering, **109**(11): 1383–1398. doi:10.1061/(ASCE)0733-9410(1983)109:11(1383).

Mononobe, N., Takata, A., and Matumura, M. 1936. Seismic stability of the earth dam. *In* Proceeding of the 2nd Congress on Large Dams. Washington , DC. pp. 435–442.

Morgenstern, N.R., and Küpper, A.A.G. 1988. Hydraulic fill structures-a perspective. *In* Hydraulic Fill Structures. pp. 1–31.

Okamoto, S. 1984. Introduction to Earthquake Engineering. *In* Second Edi. University of Tokyo Press. pp. 474–477.

Okamoto, S., Hakuno, M., Kato, K., and Kawakami, F. 1969. On the dynamical behavior of an earth dam during earthquakes. Available from http://www.iitk.ac.in/nicee/wcee/article/vol2_II-443.pdf.

Ozel, H.F., and Arici, Y. 2012. Comparison of 2D vs. 3D Modeling Approaches for the Analyses of Concrete Faced Rockfill Dams. 15th World Conference on Earthquake Engineering (15WCEE),.

Parish, Y., Sadek, M., and Shahrour, I. 2009. Review article: Numerical analysis of the seismic behaviour of earth dam. Natural Hazards and Earth System Science, **9**(2): 451–458. doi:10.5194/nhess-9-451-2009.

Pelecanos, L., Kontoe, S., and Zdravković, L. 2015. A case study on the seismic performance of earth dams. Géotechnique, **65**(11): 923–935. doi:10.1680/jgeot.SIP.15.P.009.

Petrovski, J., Paskalov, T., and Jurukovski, D. 1974. Dynamic full-scale test of an earthfill dam. Géotechnique, **24**(2): 193–206. doi:10.1680/geot.1974.24.2.193.

Prevost, J., Abdel-ghaffar, A., and Lacy, S. 1985. Nonlinear Dynamic Analyses of an Earth Dam. Journal of Geotechnical Engineering, **111**(7): 882–897. doi:10.1061/(ASCE)0733-9410(1985)111:7(882).

Resendiz, D., M. Romo, and E.M. 1982. El Infiernillo and La Villita Dams: Seismic Behavior. ASCE Journal of the Geotechnical Division,.

Seed, H.B., De Alba, P.A., and Makdisi, F.I. 1978. Performance of Earth Dams during Earthquakes. Journal of the Geotechnical Engineering Division, **104**(7): 967–994.

Seed, H.B., Idriss, I.M., Lee, K.L., and Makdisi, F.I. 1975a. Dynamic analysis of the slide in the Lower San Fernando Dam during the earthquake of February 9, 1971. Journal of Geotechnical and Geoenvironmental Engineering, **101**(ASCE# 11541 Proceeding): 889–911.

Seed, H.B., Lee, K.L., Idriss, I.M., and Makdisi, F.I. 1975b. The slides in the San Fernando Dams during the earthquake of February 9, 1971. Journal of Geotechnical and Geoenvironmental Engineering, **101**(ASCE# 11449 Proceeding).

Sevim, B., and Altunişik, A.C. 2018. Determination of Natural Frequencies of Arch Dams Based on Reservoir Levels Using Ambient and Forced Vibration Tests. Civil Engineering Research Journal, **3**(5). doi:10.19080/CERJ.2018.03.555623.

Tezcan, S.O., Bhatia, S.K., and Fiegle, S. 2001. Seismic Stability and Rehabilitation Analysis of a Hydraulic Fill Dam. (Seed 1981): 1–16.

Vick, S.G. 1996. Hydraulic tailings. Landslides: investigation and mitigation. Edited by AK Turner, RL Schuster, and LR Schuster. Transportation Research Board, Special Report, **247**: 577–584.

Vucetic, M., and Dobry, R. 1991. Effect of Soil Plasticity on Cyclic Response. Journal of Geotechnical Engineering, **117**(1): 89–107. doi:10.1061/(ASCE)0733-9410(1991)117:1(89).

Woodward, P.K., and Griffiths, D. V. 1993. Three-dimensional finite element analyses of the natural frequencies of non-homogeneous earth dams. International Journal of Rock Mechanics and Mining Sciences & Geomechanics Abstracts, **30**(3): A199. doi:10.1016/j.nic.2013.03.032.

Yang, J., Jin, F., Wang, J.-T., and Kou, L.-H. 2017. System identification and modal analysis of an arch dam based on earthquake response records. Soil Dynamics and Earthquake Engineering, **92**: 109–121. doi:10.1016/j.soildyn.2016.09.039.

Yiagos, A.N., and Prevost, J.H. 1991. Two-phase elasto-plastic seismic response of earth dams: theory. Soil Dynamics and Earthquake Engineering, **10**(7): 357–370. doi:10.1016/0267-7261(91)90025-U.

Zhu, S., and Zhou, J. 2010a. Study on Seismic-spectrum Characteristics for 300m-grade Earth-Rockfill Dam. *In* 2010 Asia-Pacific Power and Energy Engineering Conference. IEEE. pp. 1–4. doi:10.1109/APPEEC.2010.5449316.

Zhu, S., and Zhou, J. 2010b. Study on seismic-spectrum characteristics for 300 m-grade earth-Rockfill dam. *In* Asia-Pacific Power and Energy Engineering Conference. pp. 1–4. doi:10.1109/APPEEC.2010.5449316.

# Chapter 3:

# Comparison of Earthquake-Induced Pore Water Pressure and Deformations in Earthen Dams Using Non-Linear and Equivalent Linear Analyses

## Abstract

Earthquake excitations often cause an increase in pore water pressure in contractive sands resulting in liquefaction, which can lead to catastrophic consequences. Therefore, it is imperative to assess the earthquake-induced excess pore water pressure and deformations to evaluate the post-earthquake serviceability of the important structures such as earthen dams. The analyses are usually performed using the equivalent linear method or the non-linear method. The purpose of this research is to evaluate and compare the excess pore water pressure and associated deformations predicted using these two methods of analyses. Two numerical models of a typical zoned earthen dam were subjected to two earthquake time-history data with significantly different frequency contents to comprehend the differences in the outcome. The analyses results are similar for dams with dense sand shells when subjected to low-intensity earthquake excitations with the predominant frequency significantly different from the first natural frequency of the structure.

## 3.1 Introduction and Background

Natural hazards such as earthquake excitations often have a detrimental effect on the stability of water retaining structures (Chakraborty et al. 2018a, 2018b). Hence seismic response and stability analysis of earthen dams have been an important topic to geotechnical engineers for decades. Such analyses facilitate understanding the performance of the structure and are necessary for asset management and safety assessment (Puppala et al. 2019a, 2019b). The state of practice for

dynamic analysis of earthen dams is to compute earthquake-induced shear stresses, assess the liquefaction potential and then estimate permanent displacement as an indicator of post-earthquake serviceability of the structure (Rathje and Bray 2000a, Wang et al. 2006).

The simplest method to perform dynamic analysis of earthen dams is based on linear elastic behavior consideration of the soil (Idriss and Sun 1992, Wang et al. 2006). In this method, shear modulus of the soil is assumed to remain constant during seismic shaking. However, in reality, the shear modulus decreases with an increase in the earthquake-induced strains (Rathje and Bray 2000b, Krahn 2004). The equivalent linear or non-linear methods of analysis are used in practice to incorporate the non-linear behavior of the soil (Prevost et al. 1985, Gazetas 1987, Wang et al. 2006, Elia et al. 2011). The equivalent linear analysis involves performing an iterative analysis (Gazetas 1987, Zhai et al. 2004, Jibson 2011). The analysis starts with the small strain shear modulus ($G_{max}$) values assigned to the different soil layers. The shear modulus is recalculated using the respective modulus degradation curves at the end of each iteration. Many studies have found that the equivalent linear method predictions to be satisfactory (Abdel-Ghaffar and Scott 1979, Mejia and Seed 1983, Prevost et al. 1985, Rathje and Bray 2000a). Despite its popularity, some shortcomings are observed in this method; the equivalent linear analysis is typically valid when the stiffness reduction is less than 40% during shaking (Shiomi et al. 2000, Kaklamanos et al. 2013). Moreover, the dynamic response analysis results indicate that the geomaterials exhibit extra softness at the start of excitation and higher stiffness towards the end (Zhai et al. 2004, Wang et al. 2006).

In the non-linear analysis, the changes in pore water pressure, strain and the subsequent changes in shear modulus are computed at every time-step of the earthquake loading, using sophisticated constitutive models (Prevost et al. 1985, Abouseeda and Dakoulas 1998, Krahn 2004,

Boulanger and Ziotopoulou 2015). These models need to be calibrated based on extensive laboratory tests on undisturbed samples (Boulanger and Montgomery 2016). In many projects, extensive advanced laboratory test results and input parameters needed for the non-linear analysis may not be available. Hence it is necessary to identify the scenarios in which both the methods of analyses can provide similar results, thereby avoiding the need for performing the comparatively complex non-linear analysis in such scenarios. In this research study, a hypothetical zoned earthen dam with two different sets of material properties for the shells was exposed to two different earthquake excitations with widely different frequency contents, and the behavior of the structures was studied using the aforementioned analysis methods. Parameters such as shear stresses, pore water pressure ratio ($r_u$), and post-earthquake deformations were used to identify the scenarios in which the non-linear and equivalent linear analyses provide similar results.

## 3.2 Methodology

This section presents the procedure for numerical modeling of the earthen dam, and details of the material properties and boundary conditions assigned to the model. Two dimensional (2D), plane strain, time-history analyses were performed using two commercially available software packages capable of performing non-linear and equivalent linear analyses. The geometric configuration of the dam model has been adopted from Parish et al. (2009), which represents a typical zoned earthen dam with distinct core, shells, and foundation (Figure 3.1). The same material properties of different parts of the model have been assigned consistently for both analyses. Figure 3.2 presents the scaled acceleration-time data and spectral acceleration (SA) plots (5% damping) of two induced seismic events in Oklahoma (OK), USA, recorded at stations Pawnee, OK (M4.5, USGS Station OK044, Nov 1 2016) and Norfolk, OK (M5.0, USGS Station OK034, Nov 6 2016). These earthquake data were scaled to peak ground acceleration (PGA) of 0.1g and 0.6g, and were applied

at the base of the dam models. The predominant frequency of Pawnee EQ is closer to the first natural frequency of the structure (2.1 Hz), as compared to Norfolk EQ (Figure 3.2). At the end of the seismic excitations, vertical deformations of node A and pore water pressure ratios at node B were determined and used for the comparative study. The location of A and B is presented in Figure 3.1.

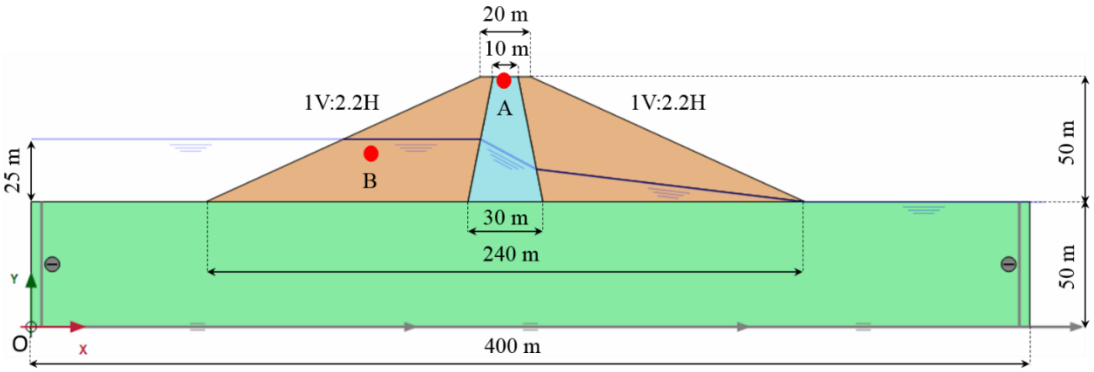


Figure 3.1: Cross-section of the typical zoned earthen embankment dam and location of predefined nodes at the crest (A) and at coordinates (130 m, 64 m) (B)

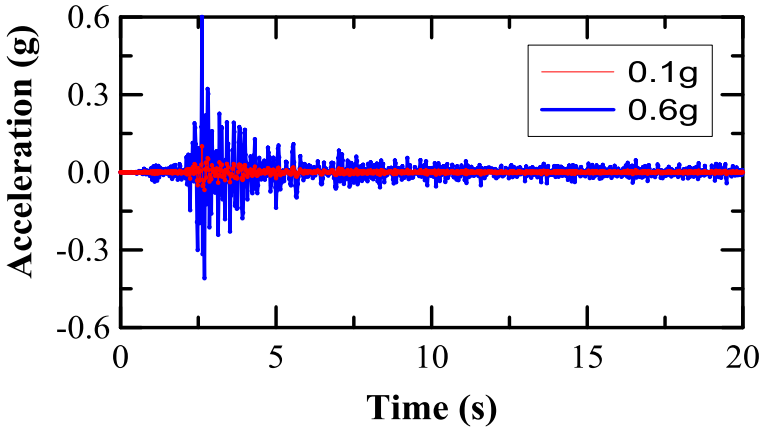


(a)

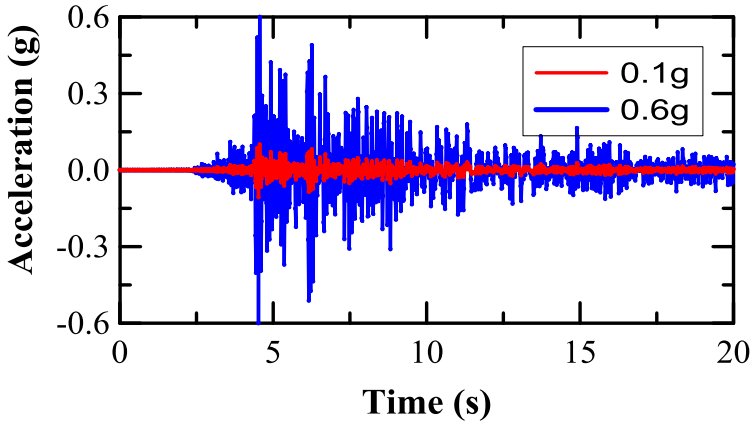


(b)

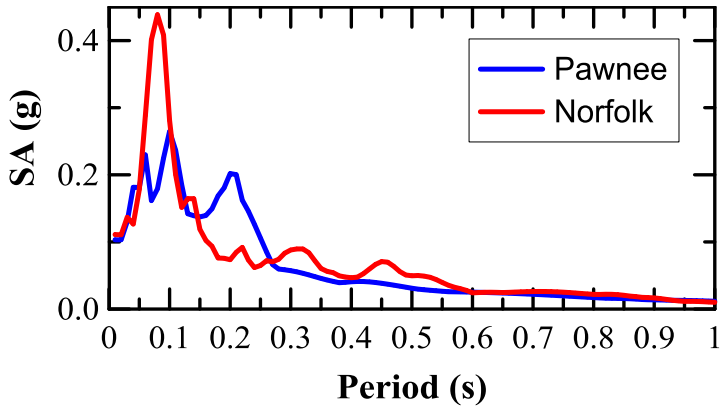


(c)

Figure 3.2: Scaled acceleration-time data for Oklahoma earthquakes (Nov 2016) recorded at stations (a) Pawnee (b) Norfolk and (c) Acceleration response spectra of both earthquakes

### 3.2.1 Fully coupled non-linear analysis modeling

Non-linear behavior of the soil is usually captured using different fully coupled non-linear models. In this research, shells, and core of the dam, were modeled using PM4Sand and HS small strain models, respectively. The foundation was modeled as a linear-elastic model owing to the extremely high $G_{max}$ values as compared to the shell or core of the dam (Table 3.1). The procedure adopted to estimate different input parameters needed for these material models have been presented in detail in the next section. Table 3.1 shows some of the basic soil properties assigned to the numerical models.

Table 3.1. Material properties assigned to the numerical model

| Material properties | Unit weight (kN/m$^3$) | Poisson's ratio | Small strain shear modulus (kPa) | Effective elastic modulus (kPa) | Permeability (m/s) |
|---|---|---|---|---|---|
| Core | 17.66 | 0.20 | 46,000 | [$E^{ref}$ =7,886] Stress dependent | $5 \times 10^{-7}$ |
| Shells $(N_1)_{60}$ =9 | 19.62 | 0.35 | [$G^{ref}$ =45,130] Stress dependent | [$E^{ref}$ =15,230] Stress dependent | $1 \times 10^{-5}$ |
| Shells $(N_1)_{60}$ =20 | 19.62 | 0.30 | [$G^{ref}$ =67,060] Stress dependent | [$E^{ref}$ =21,790] Stress dependent | $1 \times 10^{-5}$ |
| Foundation | 21.58 | 0.25 | 400,000 | 1,000,000 | $1 \times 10^{-7}$ |

#### *3.2.1.1 Core – Hardening Soil with Small Strain*

The clay core of the dam was modeled using the Hardening soil model with small-strain stiffness (HS small). The HS small model can capture the response of soil better than the more commonly used Mohr-Coulomb model by computing a stress-dependent stiffness value. Table 3.2 presents

the stiffness moduli used in the model which were selected to satisfy the Alpan criteria chart (Alpan 1970).

Table 3.2. Stiffness values used for the HS Small model (core)

| | | |
|---|---|---|
| Secant stiffness in standard drained triaxial test (kPa) | $E_{50}^{ref}$ | 7,886 |
| Tangent stiffness for primary oedometer loading (kPa) | $E_{oed}^{ref}$ | 7,886 |
| Unloading/reloading stiffness (kPa) | $E_{ur}^{ref}$ | 20,000 |

The variation of shear modulus and damping ratio for clay core was calculated using the respective equations from Brinkgreve et al. (2007). Since the HS Small model uses a damping ratio close to 0 at very small strain levels, Rayleigh damping coefficients (α and β) have been suitably selected to provide 5% damping at 0.75 and 3 Hz.

*3.2.1.2 Shells – PM4Sand*

The sand shells were modeled using the PM4Sand model to estimate the excess pore water pressure generated during dynamic loading conditions. The PM4Sand model requires three important input parameters, namely (i) shear modulus coefficient ($G_0$), (ii) relative density ($D_{R0}$) and (iii) contraction rate parameter ($h_{p0}$) (Boulanger and Ziotopoulou 2015).

$$G_0 = 167 * \sqrt{(N_1)_{60} + 2.5} \tag{3.1}$$

$$D_{R0} = \sqrt{\frac{(N1)_{60}}{46}} \tag{3.2}$$

Where, $(N_1)_{60}$ is the SPT blow counts corrected for overburden pressure and a hammer energy efficiency of 60%. For this research, $(N_1)_{60}$ values of 9 and 20 have been used for the analysis to study the differences in the pore water pressure ratio and associated deformations,

estimated from the non-linear and equivalent linear methods, for sands with two different relative densities. $(N_1)_{60}$ values of 9 and 20 correspond to sands having relative densities of 0.442 (loose sand) and 0.660 (dense sands), respectively. Lastly, the contraction rate parameter $h_{p0}$ was calibrated using single-element undrained cyclic direct simple shear simulations to estimate the proper resistance to liquefaction based on the $(N_1)_{60}$ and an earthquake magnitude of 7.5. Table 3.3 presents parameters used in PM4Sand model.

Table 3.3. Parameters used for PM4Sand model (shells)

| | $D_{R0}$ | $G_0$ | $h_{p0}$ |
|---|---|---|---|
| $(N_1)_{60}$ =20 | 0.660 | 792.0 | 0.34 |
| $(N_1)_{60}$ =9 | 0.442 | 566.3 | 0.90 |

The applied earthquake excitations (Figures 3.2a and 3.2b) were considered to represent "within motion," obtained by the superimposition of both upward and downward propagating components of the wave. Hence, a rigid base boundary condition was used (Mejia and Dawson 2006), and free-field boundary condition was provided at the vertical sides. The selected mesh size was smaller than one-tenth the wavelength corresponding to the highest frequency component of the input wave (Kuhlemeyer and Lysmer 1973). The pore water pressure ratio at node B and the vertical deformations at node A were estimated by the software package based on the induced dynamic stresses and constitutive models used to model the dam. A similar analysis was performed using the equivalent linear method, and the results were compared with the non-linear method. Details of the equivalent linear method of analysis are provided in the next section.

### 3.2.2 Decoupled equivalent linear analysis modeling

Parameters provided in Table 3.1 were also used in the equivalent linear model. Equations provided by Brinkgreve et al. (2007) were used to calculate parameters for the clay core. The modulus reduction curve, variation of $G_{max}$ value versus effective vertical stress and cyclic number

function (cyclic stress ratio versus the number of cycles required to cause liquefaction ($N_L$)) were estimated for the sand shells using the single-element undrained cyclic direct simple shear test simulations in the non-linear software package. This numerical simulations mimicked laboratory test conditions and ensured the use of similar input parameters as those used for the non-linear analysis. For the shells, the variation of damping ratio with strain was estimated based on plasticity index and average effective confining stress estimated from the initial static analysis using the method outlined in Ishibashi and Zhang (1993). The excess pore water pressure during earthquake shaking was calculated for the saturated shell area below water table using the procedure outlined by Lee and Albaisa (1974) and De Alba et al. (1976).

After the estimation of excess pore water pressure, the permanent deformation of the dam was computed by estimating incremental loads based on the stress difference between two time steps. The vertical displacement was computed by the software package using the hyperbolic constitutive models used to model the dam. The comparison of the results obtained using equivalent and non-linear methods of analyses is presented in the next section.

## 3.3 Results and Discussion

The dynamic response analysis of an earthen dam was carried out using both equivalent linear and non-linear analyses to recognize the range of differences between the excess pore water pressure and deformation results obtained from the two methods. Three parameters were considered in this research study to identify the scenarios where both the analysis methods yield similar results. These parameters are: (i) intensity of earthquake shaking (PGA) (ii) frequency content of the applied earthquake and (iii) relative density of the material located on the shells and slopes of the dam.

The effect of the first parameter was studied by selecting two levels of ground motion; one with PGA of 0.1g which can be considered for operating basis earthquake (OBE) and the other one with PGA of 0.6g which can be considered as the maximum credible earthquake (MCE) (FEMA 2005). The second parameter incorporates the effect of probable near-resonance conditions and its impact on the two analyses results. It is important to realize that every system has a definite natural frequency for a given mode of vibration and if the frequency of any natural or artificial source of vibration is close to the natural frequency the system, resonance will happen. Such resonance is associated with amplified vibrations, which may cause severe damages to structures and have a detrimental effect on society. In this study, the predominant frequency of the selected earthquakes did not exactly match with the natural frequency of the structure (Figure 3.2). Nonetheless, one of the earthquakes (Pawnee) was selected to represent an earthquake excitation with the predominant frequency closer to the natural frequency as compared to another one to gain insight into the effect of near-resonance condition on the analyses results. The last parameter includes the effect of different types of sand present in the shells where the development of excess pore water pressure can lead to occurrence of liquefaction and exacerbate the post-earthquake deformations. The vertical deformations at the crest were estimated using non-linear and equivalent linear analyses after applying (i) two levels of earthquake excitations, (ii) two earthquakes with different frequency contents, and (iii) considering the presence of loose and dense sand in the shell. The observed vertical displacements at the crest of the dam were compiled and are presented in Table 3.4.

From the results, it can be observed that the equivalent linear analysis tends to compute larger vertical deformation values compared to the non-linear analysis. This can be attributed to the type of material model used in the analysis. In spite of the ability of hyperbolic stress-strain

relationships (which was used in equivalent linear analysis) in incorporating non-linear behavior of the soil in the estimation, it is important to notice that hyperbolic modeling is inherently elastic. Hence, the modeling of plastic deformations might not be fully considered in the computations.

The peak acceleration on the crest of the dam was higher for the equivalent linear model, thereby resulting in accumulation of larger deformation. Especially for PGA=0.6g, where the non-linear behavior of geomaterials was more pronounced, the plastic deformation considerations in non-linear material models were significant, and differences between the results are more prominent (Table 3.4). The vertical deformations at the crest were nearly similar for both the methods of analysis when (i) the shell of the dam was composed of dense sand, (ii) the dam was subjected to a low PGA earthquake excitation (0.1g), and (iii) the predominant frequency of the earthquake was significantly different from the first natural frequency of the structure (2.1 Hz).

Figure 3.3 presents the vertical deformation and pore water pressure ratio corresponding to this scenario. It can be observed that the estimated vertical deformation and the cumulative excess pore water pressure at the end of the shaking were nearly similar. On the other hand, the differences between the results at the end of shaking were appreciable for a dam with loose sand shell, subjected to strong seismic shaking (PGA=0.6g), and the frequency content of the earthquake was close to the natural frequency of the structure (Figure 3.4).

Table 3.4. Vertical deformation obtained on the crest of the dam from non-linear and equivalent linear analysis

| EQ | Soil type | PGA | Deformation (m) | | |
|---|---|---|---|---|---|
| | | | Non-linear | Equivalent-linear | Difference |
| Pawnee | $(N_1)_{60}$ =9 | 0.1g | 0.008 | 0.070 | 0.060 |
| | | 0.6g | 0.110 | 0.370 | 0.260 |
| | $(N_1)_{60}$ =20 | 0.1g | 0.007 | 0.030 | 0.020 |
| | | 0.6g | 0.100 | 0.300 | 0.200 |
| Norfolk | $(N_1)_{60}$ =9 | 0.1g | 0.020 | 0.080 | 0.060 |
| | | 0.6g | 0.300 | 0.540 | 0.240 |
| | $(N_1)_{60}$ =20 | 0.1g | 0.020 | 0.024 | 0.004 |
| | | 0.6g | 0.270 | 0.470 | 0.200 |

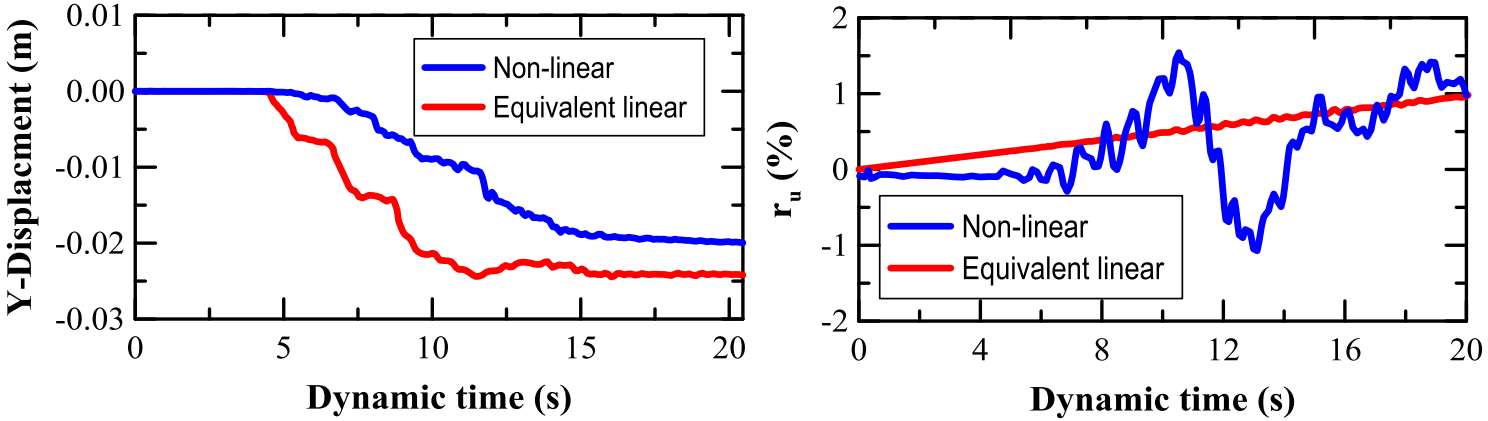


(a) (b)

Figure 3.3: Norfolk earthquake with PGA=0.1g and $(N_1)_{60}$ =20 (a) Vertical deformation at the crest and (b) $r_u$ (%) at x=130 and y=64 m

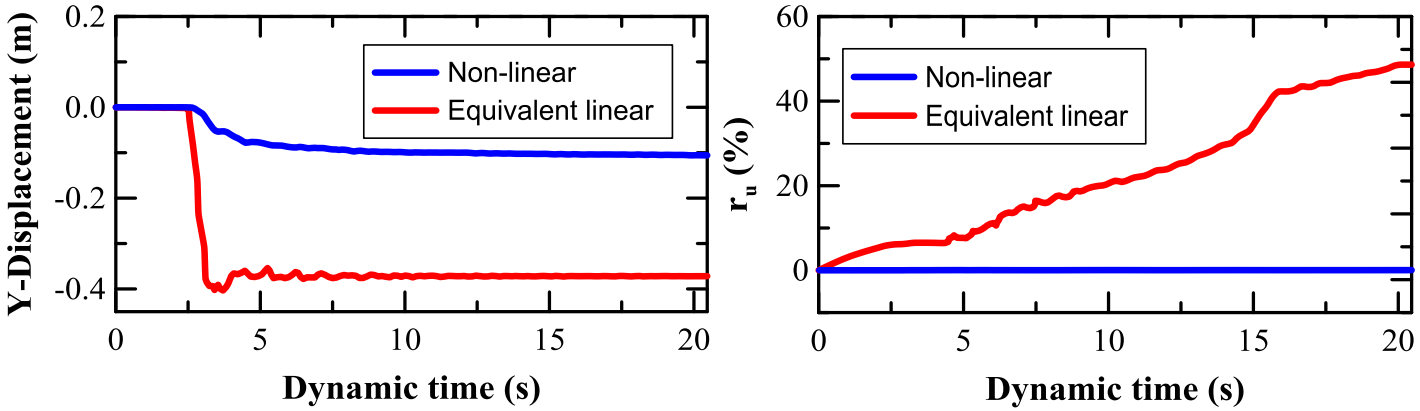


(a) (b)

Figure 3.4: Pawnee earthquake with PGA=0.6g and $(N_1)_{60}$ =9 (a) Vertical deformation at the crest and (b) $r_u$ (%) at x=130 m and y=64 m

In case of equivalent linear analysis, the earthquake-induced shear stresses were observed to be larger in the shell, near the face of the slope, as compared to non-linear analysis. As can be observed in Figure 3.5, the value of shear stress near the upstream slopes in the non-linear method is in the range of 0-20 kPa while this value in the equivalent linear analysis is 20-60 kPa and this value increases to 80 kPa on the downstream slope. Subsequently, an increase in excess pore water pressure was more pronounced near the surface of the slope for the equivalent linear analysis as compared to non-linear analysis (Figure 3.4b). This resulted in liquefaction-induced instability of the shell of the dam and induced higher vertical deformation at node A in case of the equivalent linear analysis (Figure 3.4a).

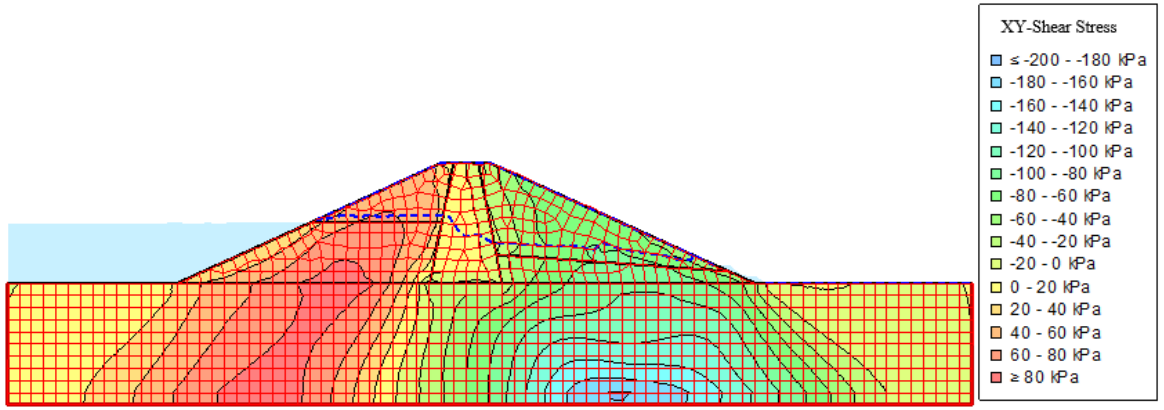


(a)

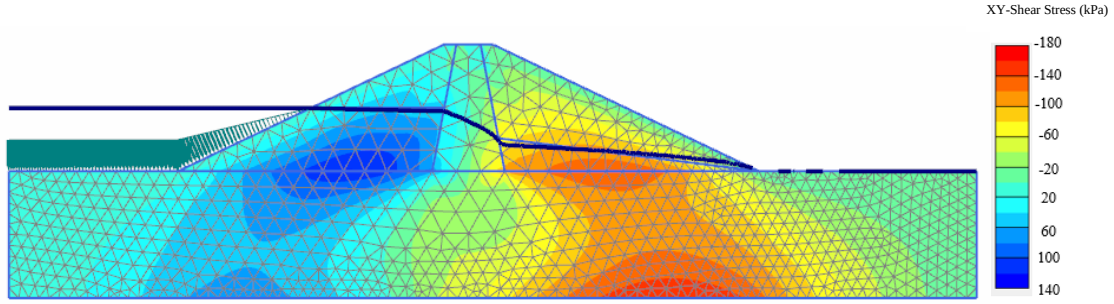


(b)

Figure 3.5: XY-Shear stress contours for Pawnee earthquake with PGA=0.6g and $(N_1)_{60}$ =9 (a) equivalent linear model and (b) non-linear model

## 3.4 Conclusion

This research study focused on recognizing the differences in the pore water pressure ratio and associated deformations of a zoned earthen dam, analyzed using the equivalent linear analysis and fully-coupled non-linear analysis. The analyses were performed encompassing three criteria related to the properties of the dam and earthquake excitations: (i) level of earthquake shaking (PGA) (ii) frequency content of the applied earthquake, and (iii) relative density of the sand shells of the dam. The results suggest that it is more convenient to use the relatively simple equivalent linear analysis method when dams with dense sand shells experience earthquakes with low intensity of excitation, without chances of near-resonance condition. Under such scenarios, the results obtained from these two methods are similar. Scenarios in which strong excitations with chances of liquefaction are expected to occur, the equivalent linear analysis tend to provide higher estimates of the post-earthquake deformation. To avoid estimating unrealistically high values of the earthquake-induced deformation, the non-linear analysis is the preferred analysis method, especially when the dam shells consist of loose sand, and the probability of strong vibration and liquefaction is high due to high PGA base excitation and/or resonance condition. The findings of this research study provide an approach of selecting suitable analysis methods based on numerical modeling of a hypothetical dam subjected to a limited number of earthquake excitations. Further studies are required where actual post-earthquake deformation and pore water pressure data of real earthen dams are available for comparative studies with the numerical analyses results.

# References


Abdel-Ghaffar, A.M., and Scott, R.F. 1979. Shear Moduli and Damping Factors of Earth Dam. Journal of the Geotechnical Engineering Division, **105**(12): 1405–1426.

Abouseeda, H., and Dakoulas, P. 1998. Non-linear dynamic earth dam-foundation interaction using a BE-FE method. Earthquake Engineering & Structural Dynamics, **27**(9): 917–936. doi:10.1002/(SICI)1096-9845(199809)27:9<917::AID-EQE763>3.0.CO;2-A.

De Alba, P., Chan, C.K., and Seed, H.B. 1976. Determination of soil liquefaction characteristics by large-scale laboratory tests. Shannon & Wilson.

Alpan, I. 1970. The geotechnical properties of soils. Earth-Science Reviews,.

Boulanger, R.W., and Montgomery, J. 2016. Nonlinear deformation analyses of an embankment dam on a spatially variable liquefiable deposit. Soil Dynamics and Earthquake Engineering, **91**: 222–233. doi:10.1016/j.soildyn.2016.07.027.

Boulanger, R.W., and Ziotopoulou, K. 2015. Pm4Sand (Version 3): a Sand Plasticity Model for Earthquake Engineering.

Brinkgreve, R., Bonnier, P., and Kappert, M. 2007. Hysteretic damping in a small-strain stiffness model. Numerical Models in Geomechanics,: 737–742. doi:10.1201/noe0415440271.ch106.

Chakraborty, S., Banerjee, A., Das, J.T., Mosadegh, L., and Puppala, A.J. 2018a. Impact of Variation of Small Strain Shear Modulus on Seismic Slope Stability Analysis of a Levee: A Sensitivity Analysis. Ifcee 2018,: 302–313. doi:10.1061/9780784481608.029.

Chakraborty, S., Das, J.T., Puppala, A.J., and Banerjee, A. 2018b. Natural frequency of earthen dams at different induced strain levels. Engineering Geology, **248**(August 2018): 330–345. Elsevier. doi:10.1016/j.enggeo.2018.12.008.

Elia, G., Amorosi, A., Chan, A.H.C., and Kavvadas, M.J. 2011. Fully coupled dynamic analysis of an earth dam. Geotechnique, (7): 549–563. doi:10.1680/geot.8.P.028.

FEMA. 2005. Federal Guidelines for Dam Safety - Earthquake Analyses and Design of Dams.

Gazetas, G. 1987. Seismic response of earth dams : some recent developments. **6**(1).

Idriss, I.M., and Sun, J.I. 1992. SHAKE91: A computer program for conducting equivalent linear seismic response analyses of horizontally layered soils deposits.

Ishibashi, I., and Zhang, X. 1993. Unified dynamic shear moduli and damping ratios of sand and clay. Soils and Foundations, **33**(1): 182–191. doi:10.3208/sandf1972.33.182.

Jibson, R.W. 2011. Methods for assessing the stability of slopes during earthquakes—A retrospective. Engineering Geology,.

Kaklamanos, J., Bradley, B.A., Thompson, E.M., and Baise, L.G. 2013. Critical parameters affecting bias and variability in site-response analyses using KiK-net downhole array data. Bulletin of the Seismological Society of America, **103**(3): 1733–1749. doi:10.1785/0120120166.

Krahn, J. 2004. Dynamic modeling with QUAKE/W: an engineering methodology. GEO-SLOPE.

Kuhlemeyer, R.L., and Lysmer, J. 1973. Finite Element Method Accuracy for Wave Propagation Problems. Journal of the Soil Mechanics and Foundations Division, **99**(5): 421–427. ASCE.

Lee, K.L., and Albaisa, A. 1974. Earthquake Induced Settlements in Saturated Sands. Journal of the Geotechnical Engineering Division, **100**(4): 387–406. ASCE.

Mejia, L.H., and Dawson, E.M. 2006. Earthquake deconvolution for FLAC. *In* 4th International FLAC Symposium on Numerical Modeling in Geomechanics. pp. 4–10.

Mejia, L.H., and Seed, H.B. 1983. Comparison of 2D and 3D Dynamic Analyses of Earth Dams. Journal of Geotechnical Engineering, **109**(11): 1383–1398. doi:10.1061/(ASCE)0733-9410(1983)109:11(1383).

Parish, Y., Sadek, M., and Shahrour, I. 2009. Review article: Numerical analysis of the seismic behaviour of earth dam. Natural Hazards and Earth System Science, **9**(2): 451–458. doi:10.5194/nhess-9-451-2009.

Prevost, J., Abdel-ghaffar, A., and Lacy, S. 1985. Nonlinear Dynamic Analyses of an Earth Dam. Journal of Geotechnical Engineering, **111**(7): 882–897. doi:10.1061/(ASCE)0733-9410(1985)111:7(882).

Puppala, A. J., Congress, S. S., & Banerjee, A. 2019a. Research advancements in expansive soil characterization, stabilization and geoinfrastructure monitoring. In Frontiers in geotechnical engineering (pp. 15-29). Springer, Singapore.

Puppala, A. J., & Congress, S. S. C. 2019b. A Holistic Approach for Visualization of Transportation Infrastructure Assets Using UAV-CRP Technology. In International Conference on Inforatmion technology in Geo-Engineering (pp. 3-17). Springer, Cham.

Rathje, E.M., and Bray, J.D. 2000a. An examination of simplified earthquake-induced displacement procedures for earth structures: Reply. Canadian Geotechnical Journal, **37**(3): 731–732. doi:10.1139/cgj-37-3-731.

Rathje, E.M., and Bray, J.D. 2000b. Nonlinear Coupled Seismic Sliding Analysis of Earth Structures. Journal of Geotechnical and Geoenvironmental Engineering, **126**(11): 1002–1014. doi:10.1061/(ASCE)1090-0241(2000)126:11(1002).

Shiomi, T., Chan, A., Nukui, Y., Hijikata, K., and Koyama, K. 2000. Comparison of Equivalent Linear Analysis and Nonlinear Analysis for A Liquefaction Problem. *In* Proc. 12th World Conference on Earthquake Engineering, Auckland, New Zealand. pp. 1–8.

Wang, Z.L., Makdisi, F.I., and Egan, J. 2006. Practical applications of a nonlinear approach to analysis of earthquake-induced liquefaction and deformation of earth structures. Soil Dynamics and Earthquake Engineering, **26**(2-4 SPEC. ISS.): 231–252. doi:10.1016/j.soildyn.2004.11.032.

Zhai, E., Roth, W., Dawson, E., and Davis, C. 2004. Seismic deformation analysis of an earth dam-A comparison study between equivalent linear and non-linear effective-stress approaches. *In* 13th World Conference on Earthquake Engineering.

# Chapter 4:

# Estimation of Liquefaction-Induced Lateral Displacement of Eagle Mountain Dam using Numerical and Semi-empirical Approaches

## Abstract

Liquefaction-induced lateral displacements have caused extensive damages to infrastructures such as bridge piers, water retaining structures, and pipelines in the past. Several methods, including analytical solutions, physical and numerical modeling, and empirical/semi-empirical equations, have been used to estimate liquefaction-induced lateral displacements. In this research study, an attempt was made to predict the liquefaction-induced lateral displacement of the foundation of the Eagle Mountain dam (EM), located in Fort Worth, Texas, using numerical and semi-empirical methods. The soil behavior type (SBT) interpreted from available cone penetration test (CPTu) soundings were used to identify the potential liquefiable layers present in the downstream foundation of the dam. A commercially available finite element method (FEM) based software package was used to create numerical models of the sections that are susceptible to liquefaction. Two different earthquake time-history data with widely different predominant frequencies were obtained from the United States Geological Survey (USGS), scaled to peak ground acceleration (PGA) of 0.3g and 0.6g, and applied at the base of the models. Pore water pressure ratio ($r_u$) profiles and lateral displacements were estimated to assess the chances of liquefaction-induced damage to the dam. Semi-empirical equations developed by Zhang et al. (2004) were also used to estimate the lateral displacements using the CPTu results. The estimated displacements indicate

that the EM dam is expected to be safe and have no issues associated with liquefaction-induced lateral displacement.

## 4.1 Introduction and Background

The development of excess pore water pressure during seismic excitations can reduce the shear strength of loose sand layers and cause severe damages to the overlying structures due to liquefaction of the soil (Marcuson 1978, Liu 2008). Liquefaction-induced ground failures can be categorized into sand boils, ground oscillations, flow failures, and deformation failures (Youd 1993, 1995, Bardet 1999, Zhang et al. 2004). A rapid upward flow of pore water caused by liquefaction can carry sand particles up to the surface, resulting in sand boils.

Sand boils are explicit signs that support the occurrence of high excess pore water pressure. The ground oscillation occurs when liquefied subsurface soils at greater depths separate from the surficial soils. The surficial soils usually break apart into blocks and are separated by fissures. Unlike sand boils, ground oscillation is hard to identify and predict. Among the different facets of liquefaction-induced ground failures, flow failures are the most dangerous ones (Youd 1993, 1995). These failures usually happen on slopes with a gradient greater than 6% and are accompanied by the rapid movement of flows with deformations as high as tens of feet (Youd 1993, 1995, Zhang et al. 2004). Deformation failure, which occurs in forms of lateral displacements, is one of the most common consequences of liquefaction (Bardet 1999).

Lateral displacement occurs on gently sloping grounds when the combination of earthquake-induced dynamic forces and the gravitational force on soil layers on top of liquefied layers lead to lateral movement of the soil mass (Rauch 1997). Open fissures and scarps on the ground surface are considered as signs of occurrence of lateral displacement (Youd 1995). Liquefaction-induced lateral displacement has caused extensive damages to civil infrastructures in

the past (Bardet 1999, Franke and Kramer 2014). Hence, it is imperative to evaluate the chances of such deformations under probable earthquake events that may occur in the future and assess the consequence of such events.

Several methods, including analytical solutions, physical and numerical modeling, and empirical/semi-empirical equations, have been used to estimate liquefaction-induced lateral displacements (Youd 1995, Bardet 2003). In analytical solutions, elastic beam and sliding-block methods are used for lateral displacement predictions (Newmark 1965, Hamada et al. 1987, Towhata et al. 1991). However, the assumed elastic or perfectly plastic behavior of soil results in erroneous displacements estimated by the analytical solutions (Youd 1995, Bardet 1999). In physical modeling, centrifuges and shake tables are used to simulate desired dynamic loading conditions to measure the possible lateral displacements (Bardet 2003, Javadi et al. 2006, Liu 2008). Physical models are rarely used in practice due to the difficulty in precisely simulating the field conditions (Arulanandan and Scott 1993, Youd 1995, Kagawa et al. 1997, Towhata 2005).

The lateral displacement can also be computed by numerical analysis using the finite element or finite difference method that uses suitable constitutive stress-strain relationships to predict the lateral displacements experienced by a liquefied soil stratum during an earthquake (Yasuda et al. 1992; Gu et al. 1993, 1994). The efficacy of the analysis and accuracy of the results depend on the choice of the constitutive model used (Javadi et al. 2006, Chakraborty et al. 2018a, 2018b). In the absence of extensive laboratory tests typically required for calibrating the constitutive models, empirical/semi-empirical equations, developed based on data available from case histories, are extensively used for estimating lateral displacement (Bardet 1999).

Youd and Perkins (1987) developed an empirical equation considering parameters such as earthquake magnitude and distance of event to the site to calculate liquefaction-induced lateral

displacement. Bartlett and Youd (1992) developed two separate models for ground slope of infinite extent, and for free face. This equation was later updated by Youd et al. (2002) by adding more data and is most frequently used by engineers when Standard Penetration Test (SPT) results are available for the site (Khoshnevisan et al. 2015). Zhang et al. (2004) developed a semi-empirical approach for lateral displacement estimation that can be used when either SPT or CPTu data are available. A suitable equation is selected for estimating the liquefaction-induced lateral displacement based on the condition of the site, availability of in-situ test results, and the scope and limitations of the equations.

In this research study, an attempt was made to predict the liquefaction-induced lateral displacement for Eagle Mountain dam, an earthen dam located in Fort Worth, Texas, using numerical and semi-empirical methods. Based on CPTu data available, two locations where the extensive sand layers are present were selected for liquefaction analysis and estimation of possible lateral displacements (Puppala et al. 2018a, 2018b). A commercially available FEM-based software was used to model the selected areas. Two different earthquake time-history data recorded in Oklahoma (OK) and Missouri (MO) were obtained from USGS (United States Geological Survey) and were scaled to different PGA values to simulate earthquake events with different intensities.

The scaled earthquake data were applied at the base of the models, and the pore water pressure ratio ($r_u$) profiles were used to identify the liquefiable areas, and lateral displacements were estimated after shaking. Since CPTu data were available for this specific site, semi-empirical equations developed by Zhang et al. (2004) were also used for estimating the lateral displacements. The estimated lateral displacements were compared and used to assess the chances of liquefaction-induced damages to the earthen dam.

## 4.2 Methodology

The EM dam is an 87-years-old earthen dam located on the West Fork Trinity River in Tarrant County, Fort Worth, Texas, USA. The dam is currently maintained and operated by Tarrant Regional Water District (TRWD) and is a major water resource for the city of Fort Worth, Texas. A series of CPTu were conducted along the downstream toe of the EM dam. The soil behaviour type (SBT) of the downstream foundation layers was determined using the charts developed by Robertson (1990). The soil layers with SBT of 5 to 7 (on a scale of 1 to 9) indicated the presence of silty sand to sand layers. Two locations, namely DCD 11 and DCT 18 (Figure 4.1), had extensive sand layer deposits that might be susceptible to liquefaction. The lateral displacements at these locations were estimated using numerical and semi-empirical approaches, which are explained in detail in the next sections.

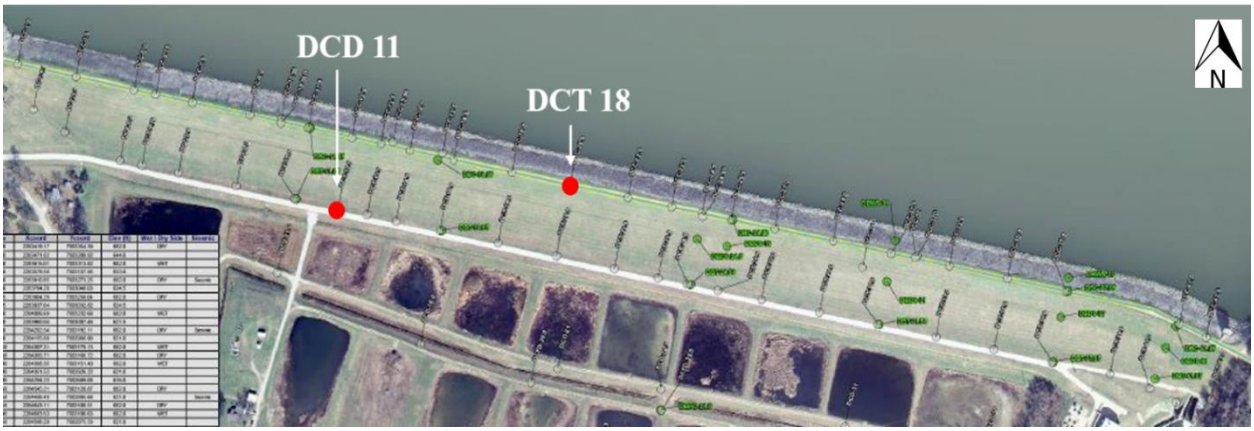


Figure 4.6: Plan view of EM dam showing the locations of DCD 11 and DCT 18

### 4.2.1 Numerical approach

Based on available SBT data, soil layers at the two locations shown in Figure 4.1 were delineated and modeled in a commercially available 2D FEM based software package. The subsurface profile of the numerical model consists of four soil layers for DCD 11 and three soil layers for DCT 18.

Table 4.1 presents the layer name ($L_i$), depth of the base of each layer from the ground surface ($z$), average tip resistance ($q_t$), and average skin friction ($f_s$).

Table 4.1. CPTu data

| DCD 11 | | | | DCT 18 | | | |
|---|---|---|---|---|---|---|---|
| $L_i$ | $z$ (m) | $q_t$ (kPa) | $f_s$ (kPa) | $L$ | $z$ (m) | $q_t$ (kPa) | $f_s$ (kPa) |
| $L_1$ | 1.22 | 9205 | 66 | $L_1$ | 5.18 | 5650 | 70 |
| $L_2$ | 2.74 | 3438 | 36 | $L_2$ | 6.71 | 21106 | 96 |
| $L_3$ | 3.35 | 6885 | 30 | $L_3$ | 7.32 | 4922 | 29 |
| $L_4$ | 5.18 | 3188 | 21 | - | - | - | - |

The average unit weight ($\gamma$) of each soil layer was calculated using equation 4.1 where $R_f$ is friction ratio ($\frac{f_s}{q_t}$ *100%), $\gamma_w$ is the unit weight of water, and $p_a$ is atmospheric pressure in the same units as $q_t$. The coefficient of permeability ($k$) was estimated using equations 4.2, 4.3, and 4.4 where $Q_t$ is normalized cone penetration resistance ($\frac{q_t - \sigma_{v0}}{\sigma'_{v0}}$) ($\sigma_{v0}$ is overburden pressure and $\sigma'_{v0}$ is effective overburden pressure), and $F_r$ is normalized friction ratio ($\frac{f_s}{q_t - \sigma_{v0}} * 100\%$) (Robertson and Cabal 2015). The shear wave velocity ($V_s$) was determined using equations 4.5 and 4.6 due to their applicability for all soil types (Hegazy and Mayne 1995, Mayne 2006). The average of the $V_s$ values obtained from equations 4.5 and 4.6 was then used in equation 4.7 to estimate the small strain shear modulus ($G_{max}$).

$$\frac{\gamma}{\gamma w} = 0.27 * \left[\log R_f\right] + 0.36 * \left[\log \frac{q_t}{p_a}\right] + 1.236 \quad (4.1)$$

$$k(\mathrm{m/s}) = 10^{(0.952 - 3.04 I_c)} \qquad 1.0 < I_c \leq 3.27 \quad (4.2)$$

$$k(\mathrm{m/s}) = 10^{(-4.52 - 1.37 I_c)} \qquad 3.27 < I_c < 4.0 \quad (4.3)$$

$$I_c = ((3.47 - logQ_t)^2 + (logF_r + 1.22)^2)^{0.5} \quad (4.4)$$

$$V_s(\text{m/s}) = [10.1 * (\log\ q_t) - 11.4]^{1.67}[(\frac{f_s}{q_t}) * 100]^{0.3} \quad (4.5)$$

$$V_s(\text{m/s}) = 118.8 * \log(f_s) + 18.5 \quad (4.6)$$

$$G_{max}(\text{kPa}) = (\frac{\gamma}{g}) * {V_{s,avg}}^2 \quad (4.7)$$

Choosing an appropriate constitutive model for lateral displacement estimation in numerical modeling is an important step (Javadi et al. 2006). In this research study, the PM4Sand model was used to estimate the excess pore water pressure developed during dynamic loading conditions and compute the liquefaction-induced lateral displacement at the two locations. The PM4Sand model requires three important input parameters, namely (i) shear modulus coefficient ($G_0$), (ii) relative density ($D_{R0}$) and (iii) contraction rate parameter ($h_{p0}$), where $G_0$ and $D_{R0}$ were calculated from equations 4.8 and 4.9 (Kulhawy and Mayne 1990, Boulanger and Ziotopoulou 2015). Lastly, the contraction rate parameter $h_{p0}$ was calibrated using single-element undrained cyclic direct simple shear simulations to provide appropriate resistance to liquefaction during an earthquake of magnitude 7.5, corresponding to the measured CPTu resistance (Boulanger and Ziotopoulou 2015).

$$G_0 = \frac{G_{max}}{p_a} * \sqrt{\frac{p_a}{p'}} \quad (4.8)$$

$$D_{R0} = \sqrt{\frac{Q_{tn}}{350}} \quad (4.9)$$

Where, $p'$ is the overburden pressure and $Q_{tn}$ is the normalized CPTu tip resistance, which is corrected for overburden pressure (Robertson and Cabal 2015). Figure 4.2 presents the developed numerical models of sections located at DCD 11 and DCT 18, and Table 4.2 presents the parameters used in the PM4Sand models. Each section was modeled with ground surface slope of 2%.

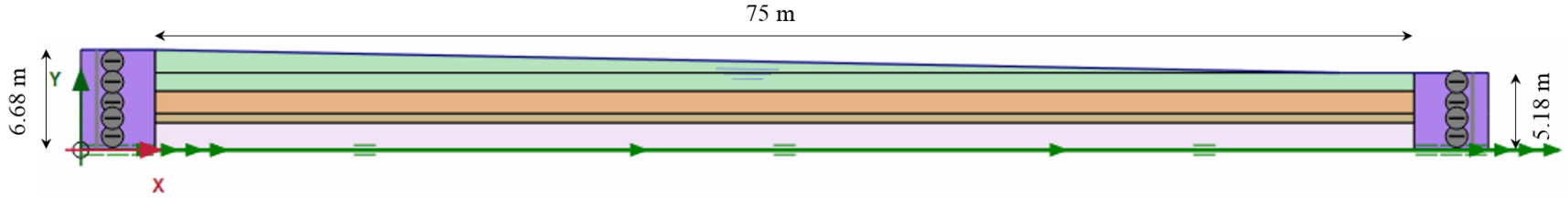


(a)

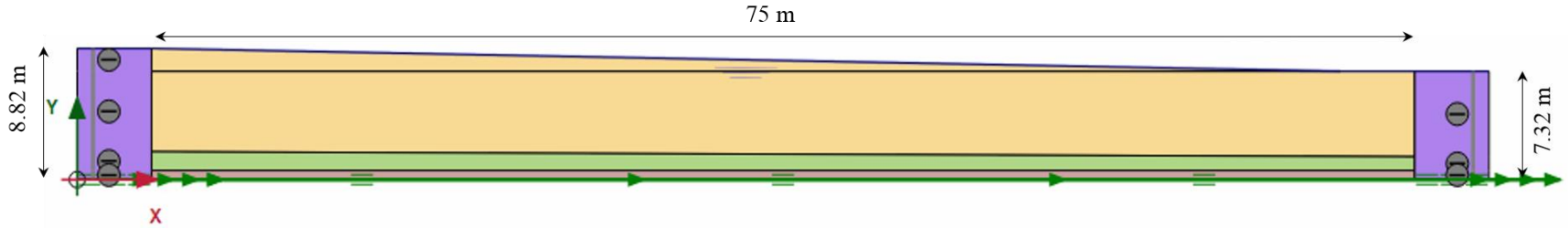


(b)

Figure 4.7: Numerical models of sections located at (a) DCD 11 and (b) DCT 18

Table 4.2. Parameters used in numerical modeling

| Location | $z$ (m) | Thickness (m) | $\Upsilon$ (kN/m$^3$) | $V_s$ (m/s) | $D_{R0}$ (%) | $G_{max}$ (kPa) | $G_0$ | $h_{p0}$ | $k$ (m/s) |
|---|---|---|---|---|---|---|---|---|---|
| DCD 11 | 1.22 | 1.22 to 2.72 (Variable) | 18.69 | 240 | 90 | 109873 | 4696 | $2 \times 10^{-3}$ | $3 \times 10^{-4}$ |
| | 2.74 | 1.52 | 17.59 | 207 | 53 | 76927 | 1869 | 2.7 | $1 \times 10^{-5}$ |
| | 3.35 | 0.61 | 17.75 | 194 | 60 | 68172 | 1353 | 4 | $1 \times 10^{-4}$ |
| | 5.18 | 1.83 | 16.97 | 177 | 41 | 54237 | 924 | 1.05 | $8 \times 10^{-6}$ |
| DCT 18 | 5.18 | 5.18 to 6.68 (Variable) | 18.61 | 246 | 60 | 114636 | 2389 | 4.65 | $2 \times 10^{-5}$ |
| | 6.71 | 1.52 | 19.48 | 258 | 90 | 131795 | 1802 | $7 \times 10^{-3}$ | $7 \times 10^{-4}$ |
| | 7.32 | 0.61 | 17.53 | 193 | 43 | 66855 | 840 | 1 | $1 \times 10^{-5}$ |

Since earthquake data recorded at the EM dam site was unavailable, earthquakes from nearby states were obtained from USGS and used for the time-history analyses. Figure 4.3 presents the acceleration-time data and Fast Fourier transform (FFT) plots of seismic events in Oklahoma (OK), USA, recorded at stations Dexter, MO (M5.6, USGS Station 2457, Nov 5, 2011) and, Salt Plains, OK (M4.7, USGS Station OK032, Nov 19, 2015). These earthquake data were scaled to PGA of 0.3g and 0.6g. The PGA of 0.3g value was considered based on the probabilistic seismic hazard analysis for the Eagle Mountain dam site (Caballero 2017b, Petersen et al. 2017). The extent of lateral displacement during a stronger hypothetical earthquake scenario was also studied with the earthquake data scaled to PGA of 0.6g. The mesh size selected for the numerical models was smaller than one-tenth of the wavelength of the highest frequency component of the input wave (Kuhlemeyer and Lysmer 1973). A rigid base boundary condition was used, assuming the earthquake excitations to represent "within motion" (Mejia and Dawson 2006). The free-field boundary condition was provided at the vertical sides to incorporate the effect of earthquake-

induced forces exerted by the adjacent soil layers that were not modeled for this study. The lateral displacements on the surface of the models were determined at the end of each shaking simulation.

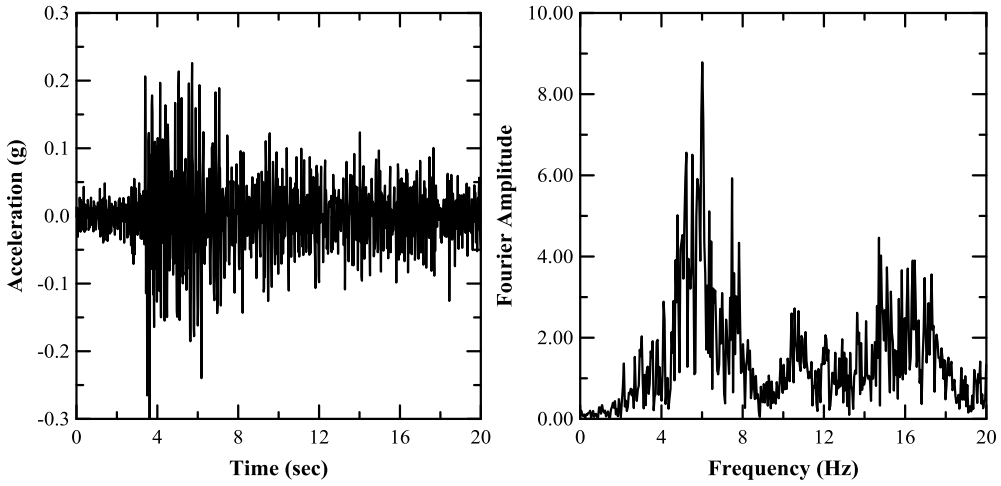


(a)

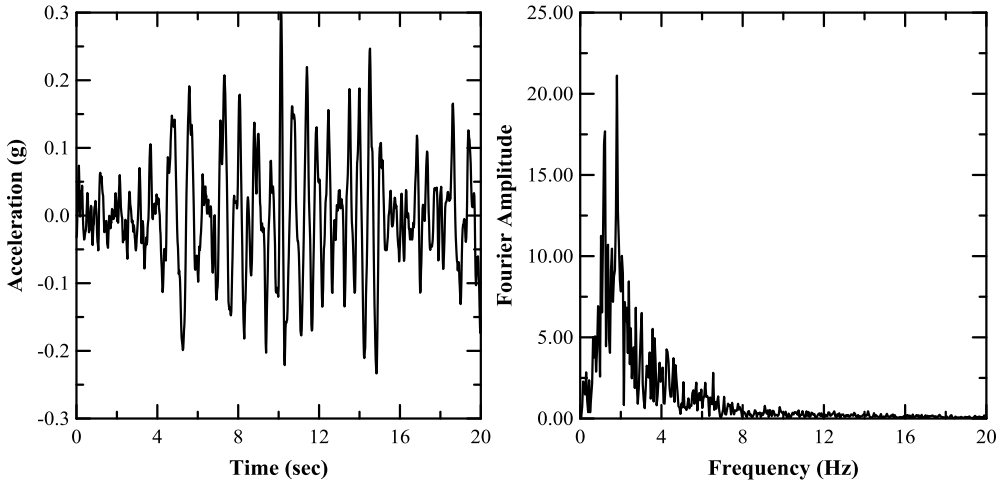


(b)

Figure 4.8: Acceleration-time data and FFT plots for earthquake recorded at stations (a) Salt Plains, and (b) Dexter (scaled to PGA = 0.3g)

4.2.2 Semi-empirical approach

A CPTu-based liquefaction analysis was performed to identify the liquefiable layers. The factor of safety (*FOS*) against liquefaction was calculated by estimating and comparing the cyclic resistance ratio (*CRR*) and cyclic stress ratio (*CSR*) corresponding to different seismic events (Robertson 1990, 2009) (equations 4.10-4.16). The maximum acceleration at the ground surface ($a_{max}$) and

earthquake magnitude (*M*) are the only seismic parameters that are used in the CPTu-based liquefaction assessment. However, these two parameters are not used directly as input parameters in the numerical analysis. Therefore, the $a_{max}$ values computed from the numerical analysis were used in calculating the *FOS* against liquefaction to ensure consistency in both the analyses and perform the comparative study for similar seismic events.

$$CSR = \frac{\tau_{av}}{\sigma'_{v0}} = 0.65 * (\frac{a_{max}}{g}) * (\frac{\sigma_{v0}}{\sigma'_{v0}}) * r_d \quad (4.10)$$

$$CRR_{7.5} = 93 * \left(\frac{Q_{tn,cs}}{1000}\right)^3 + 0.08 \qquad 50 \leq Q_{tn,cs} \leq 160 \quad (4.11)$$

$$CRR_{7.5} = 0.833 * \left(\frac{Q_{tn,cs}}{1000}\right) + 0.05 \qquad Q_{tn,cs} < 50 \quad (4.12)$$

$$Q_{tn,cs} = K_c\, Q_{tn} \quad (4.13)$$

$$K_c = 1 \qquad \text{if } I_c \leq 1.64 \quad (4.14)$$

$$K_c = 5.581\, I_c^3 - 0.403\, I_c^4 - 21.63\, I_c^2 + 33.75\, I_c - 17.88 \qquad \text{if } I_c > 1.64 \quad (4.15)$$

$$FOS = \left(\frac{CRR_{7.5}}{CSR}\right) * (MSF), \quad MSF = \frac{174}{M^{2.56}} \quad (4.16)$$

Where $r_d$ is a stress reduction factor, $Q_{tn,cs}$ is normalized clean sand equivalent cone resistance, $K_c$ is a correction factor, $I_c$ is soil behavior type index and *MSF* is magnitude scaling factor. The lateral displacement of the ground surface was then estimated using the semi-empirical equations developed by Zhang et al. (2004). Based on studies performed by Zhang et al. (2004), two types of conditions were considered for lateral displacement calculation: (a) gently sloping ground without a free-face, and (b) level ground with a free-face. Free-face ground displacements are not impeded by structural resistance, ground modification, or a natural boundary (Zhang et al. 2004). Since liquefiable layers were observed in the downstream toe area of the dam, it can be considered a case of gently sloping ground without a free-face. The maximum cyclic shear strain ($\gamma_{max}$) was calculated for each layer based on the $D_{R0}$ and *FOS* against liquefaction estimated using the procedure outlined by Zhang et al. (2004). The lateral displacement (*LD*) accumulated

at the ground surface was then calculated for the two locations (DCD 11 and DCT 18) using equations 4.17 to 4.19.

$$\gamma_{max,i} = \begin{cases} C_1 * FOS^{-C_2}, & \gamma_{max} < \text{limiting maximum shear strains} \\ C_3, & \gamma_{max} \geq \text{limiting maximum shear strains} \end{cases}, \quad (4.17)$$

Where, $C_1$, $C_2$, and $C_3$ depend on $D_{R0,}$ and these values are presented in Zhang (2004).

$$LDI_i = \left(\frac{\gamma_{max,i}}{100}\right) * H_i \quad (4.18)$$

$$LD(m) = (S + 0.2) * (\sum_{i=1}^{i=n} LDI) \quad (4.19)$$

Where $LDI_i$ is lateral displacement index and $H_i$ is the thickness of ith layer, n is the number of layers at a given section and $S$ is the slope of the ground surface.

Typically, liquefaction-induced lateral displacement value less than 0.3 m is considered as a small deformation (Holzer et al. 2005). Hence a maximum lateral displacement of 0.3 m was considered to represent the allowable deformation limit. The estimated lateral displacement values were compared with the allowable limit and used to evaluate the performance of the EM dam when exposed to earthquake events similar to those considered in this study. The following section presents the analyses results and highlights the salient findings of this study.

## 4.3 Results and Discussion

Two locations at the downstream toe of the EM dam were found to have extensive silty sand to sand deposits, based on the SBT profile. The liquefaction susceptibility and lateral displacements were estimated using the available CPTu data at stations DCD 11 and DCT 18. Two methods were selected for the analysis - numerical method using finite element based software and widely used semi-empirical equations. The analyses of the results are presented and compared in this section.

The $r_u$ profile obtained at sections DCD 11 and DCT 18, when the acceleration time-history data recorded at Dexter were scaled to PGA of 0.3g and 0.6g, are presented in Figures 4.4 and 4.5.

According to Table 4.2, loose sandy materials ($D_{R0}$<45%) are located at the bottom layer ($L_4$) for DCD 11 and at the bottom layer ($L_3$) of DCT 18. These layers experienced an increase in pore water pressure (pwp) ($r_u \approx 1$) and liquefied for both levels of shaking (Figures 4.4 and 4.5). The layers $L_2$ and $L_3$ of DCD 11 and $L_1$ of DCT 18 contain medium dense sand layers ($D_{R0}$<65%) and did not completely liquefy, as evident from maximum $r_u \approx 0.8$ (Figures 4.4 and 4.5). The remaining layers in the two sections were predominantly dense sand layers ($D_{R0}$>85%) that did not liquefy when exposed to Dexter earthquake data scaled to PGA of 0.3g and 0.6g.

The $r_u$ profiles of the sections, when exposed to the earthquake data recorded at Salt Plains (PGA scaled to 0.3g and 0.6g), are presented in Figures 4.6 and 4.7. The bottom layer ($L_4$) for DCD 11 did not fully liquefy for 0.3g (Figure 4.6a), but completely liquefied when exposed to the same earthquake excitations with the PGA scaled to 0.6g (Figure 4.7a). Figures 4.6b and 4.7b present $r_u$ profiles of DCT 18, which indicate liquefaction of the bottom layer ($L_3$) for both levels of shaking.

The $a_{max}$ values were measured at the ground surface during the shaking to study the seismic response of the foundation layers (Table 4.3). Table 4.3 shows the deamplification of acceleration at the ground surface when the sections were subjected to Salt Plains earthquake data.

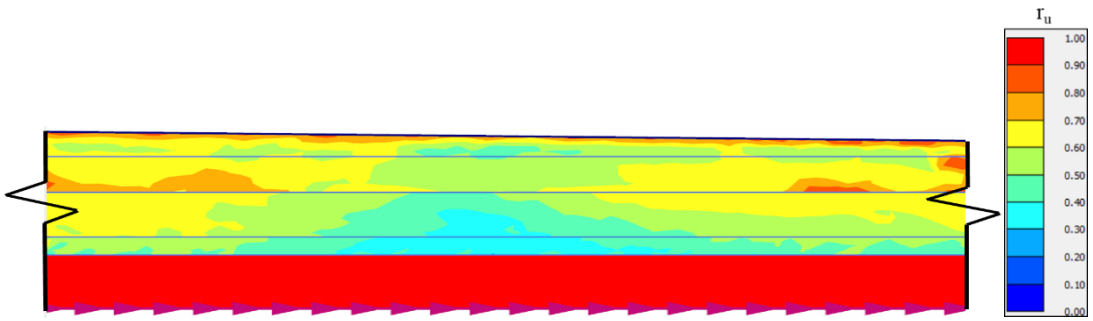


(a)

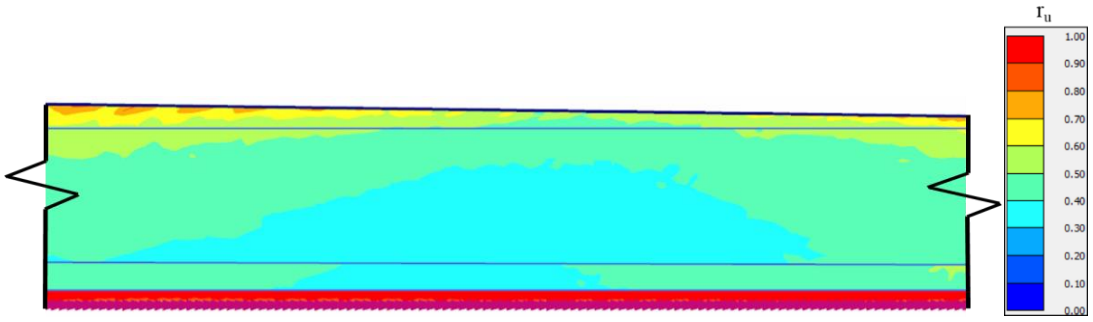


(b)

Figure 4.9: $r_u$ profiles obtained after applying Dexter acceleration-time data (scaled to 0.3g) at (a) DCD 11 and (b) DCT 18

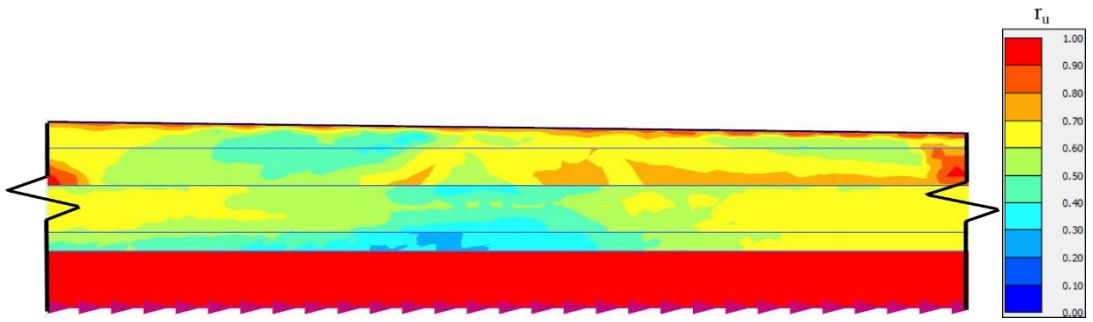


(a)

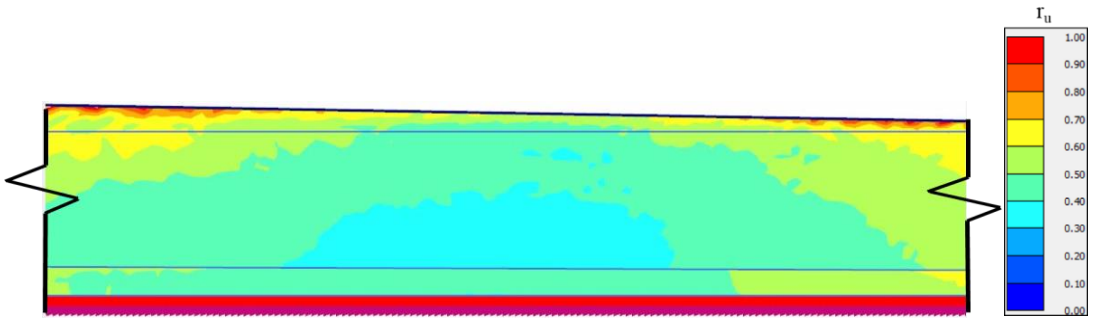


(b)

Figure 4.10: $r_u$ profiles obtained after applying Dexter acceleration-time data (scaled to 0.6g) at (a) DCD 11 and (b) DCT 18

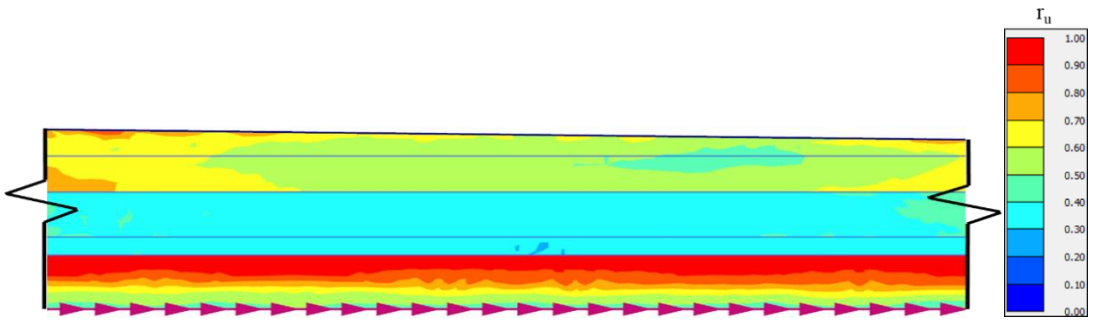


(a)

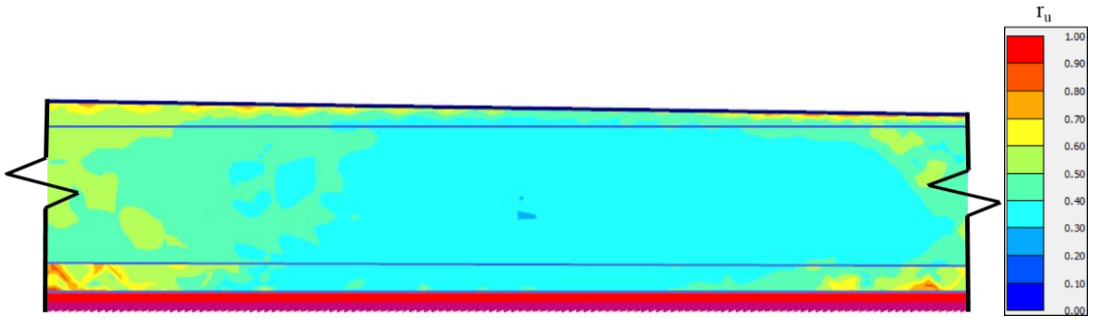


(b)

Figure 4.11: $r_u$ profiles obtained after applying Salt Plains acceleration-time data (scaled to 0.3g) at (a) DCD 11 and (b) DCT 18

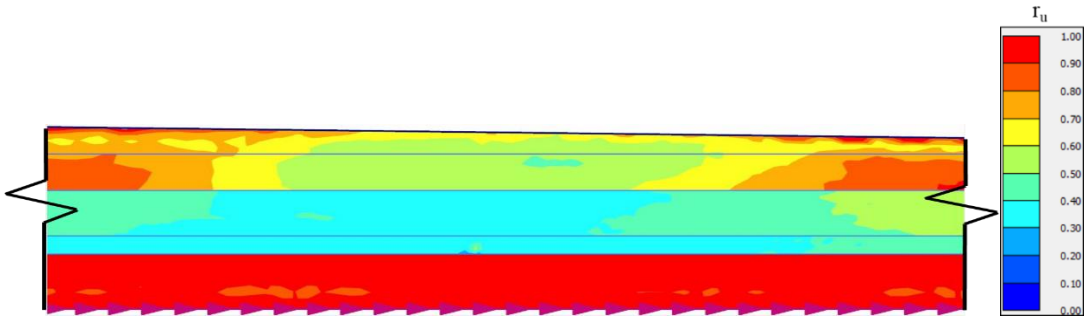


(a)

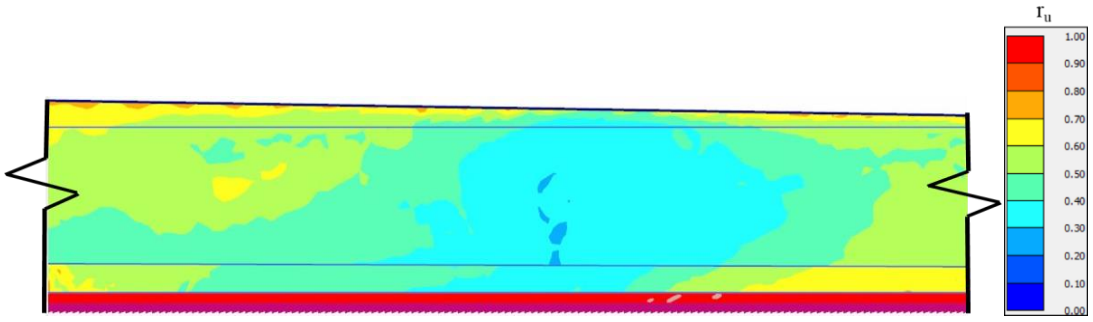


(b)

Figure 4.12: $r_u$ profiles obtained after applying Salt Plains acceleration-time data (scaled to 0.6g) at (a) DCD 11 and (b) DCT 18

This deamplification of the base excitation was attributed to the liquefaction of the soil layers, which is an agreement with the observations made by Montoya-Noguera and Lopez-Caballero (2016) (Figure 4.8b). However, the base excitation got amplified at the ground surface when the Dexter earthquake was applied. The maximum acceleration was realized at the ground surface at 5.44 s the same time instant when the excess pore water pressure was negative (Figure 4.9b).

The negative excess pore water pressure increased the mean effective stresses and the shear moduli. The increase in the material stiffness at 5.44 s resulted in a spontaneous amplification of the base acceleration at the ground surface (Figure 4.9b). The acceleration deamplified at the ground surface after 7.5 s due to an increase in excess pore water pressure and liquefaction of the soil layers, similar to those observed in the case of Salt Plains earthquake data (Figures 4.8 and 4.9).

Table 4.3. Maximum acceleration obtained on the top layer in numerical modeling

| CPTu | Acceleration at the base of the model (g) | | | |
|---|---|---|---|---|
| | Salt Plains | | Dexter | |
| | 0.30 | 0.60 | 0.30 | 0.60 |
| | $a_{max}$ at ground surface (g) | | | |
| DCD 11 | 0.15 | 0.18 | 0.41 | 0.78 |
| DCT 18 | 0.17 | 0.21 | 0.31 | 0.67 |

Since some of the layers in the numerical model analysis experienced the development of excess pore water pressure and liquefied, the changes in shear moduli and damping ratios affected the natural frequencies. Therefore, the influence of the frequency content of different earthquakes was masked by the degradation of shear moduli and subsequent reduction in the natural frequencies of the sections. The $a_{max}$ values presented in Table 4.3 were also used to estimate the factor of safety (*FOS*) and lateral displacement values using equations 4.16 to 4.19.

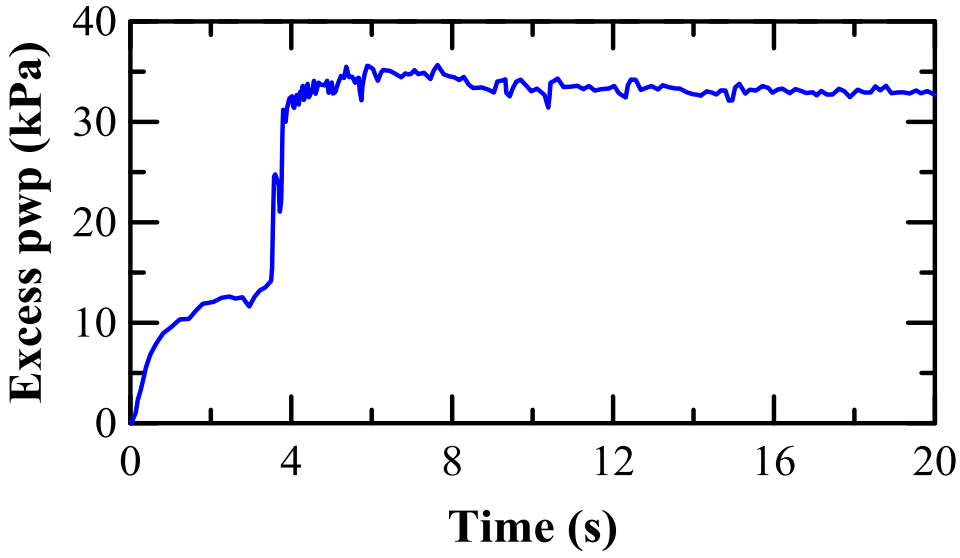


(a)

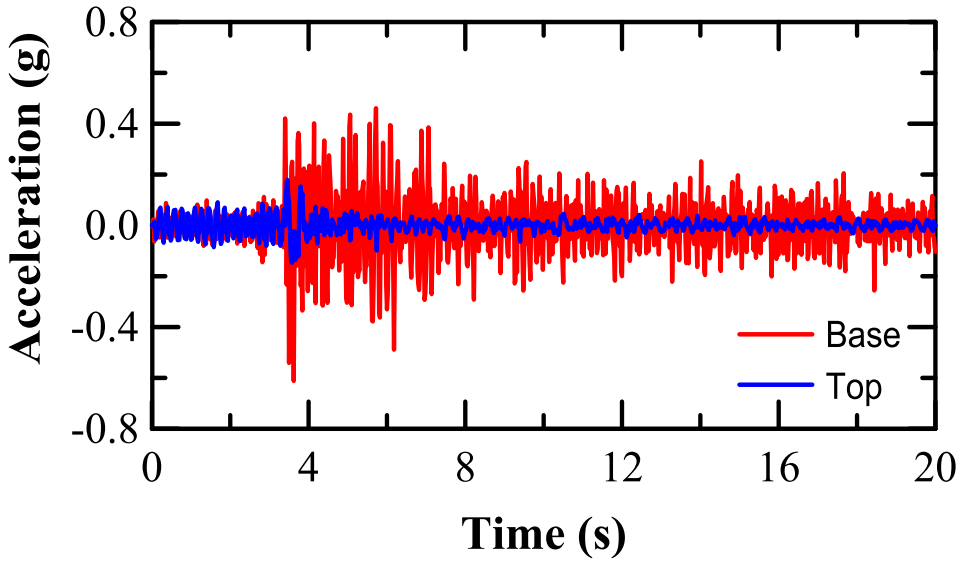


(b)

Figure 4.13: (a) Excess pore water pressure at a node (x=48 and y=2 m) located in L4, and (b) deamplification of base excitation for Salt Plains acceleration-time data (scaled to 0.6g) at DCD 11 (typical section)

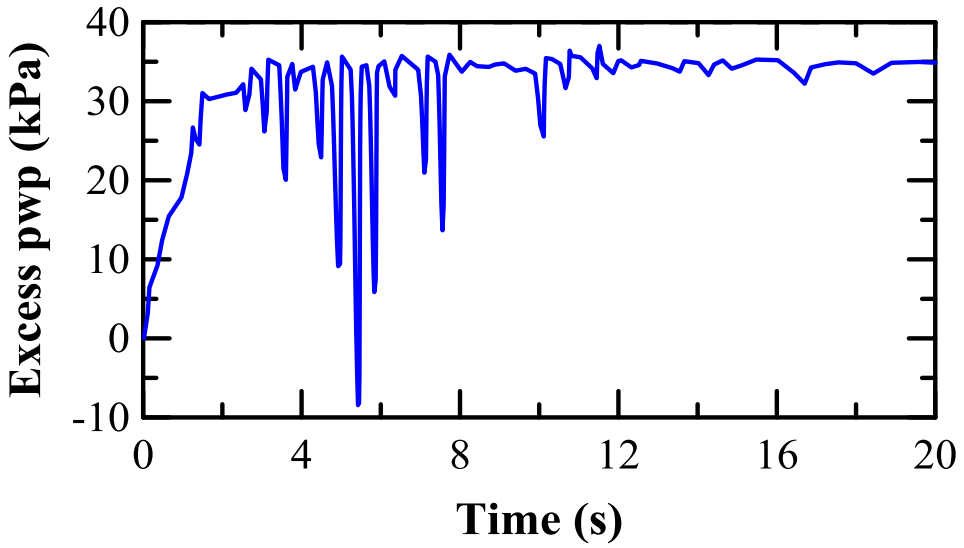


(a)

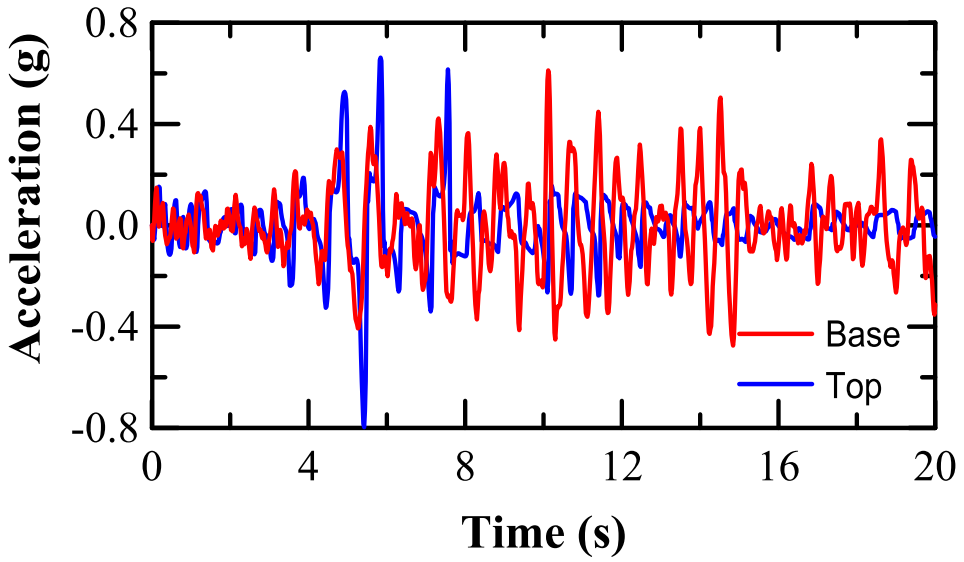


(b)

Figure 4.14: (a) Excess pore water pressure at a node (x=48 and y=2 m) located in L4, and (b) amplification of base excitation for Dexter acceleration-time data (scaled to 0.6g) at DCD 11 (typical section)

The lateral displacements estimated from the numerical analysis and semi-empirical equations for the different earthquake scenarios are presented in Figures 4.10 and 4.11 for DCD 11 and DCT 18, respectively. The lateral displacement obtained from numerical analysis solely depends on the earthquake time-history data applied at the base of the model and is independent of the earthquake magnitude. However, for each of the $a_{max}$ values computed from the numerical analysis (Table 4.3), an array of possible lateral displacement values were estimated for assumed earthquake magnitudes ranging from 3 to 7.

In general, the lateral displacements estimated using numerical analysis were smaller for the Salt Plains earthquake as compared to the Dexter earthquake (Figures 4.10 and 4.11). This can be due to the higher average acceleration values for the Dexter earthquake that induced greater accelerations and shear stresses (Figure 4.3). The higher average acceleration in the case of Dexter earthquake data resulted in $r_u \approx 1$ for $L_4$ of DCD 11 and $L_3$ of DCT 18 for PGA of 0.3g (Figures 4.4 and 4.5). The extent of liquefaction was similar for both the earthquake intensities of the Dexter earthquake (Figures 4.4 and 4.5), unlike that observed for the Salt Plains earthquake (Figures 4.6 and 4.7). Thus, the lateral displacements computed using numerical analyses were similar for the Dexter earthquake data scaled to PGA of 0.3g and 0.6g (Figures 4.10b and 4.11b).

In most of the scenarios, the lateral displacements computed using semi-empirical and numerical approaches show similar results for earthquake magnitudes greater than 6. An earthquake with low magnitude, generating a high-PGA disturbance necessary to liquefy a layer, may not feasible in reality. Hence the lateral displacements calculated using the semi-empirical equations are close of 0 for low earthquake magnitudes (< 4). The differences between the lateral displacements obtained from the semi-empirical equations for the different earthquake intensities are more prominent in the case of Dexter earthquake as compared to Salt Plains earthquake. This

can be attributed to the greater difference in $a_{max}$ values for the two different PGAs in case of Dexter earthquake, as compared to Salt Plains (Table 4.3). Based on equations 4.16 to 4.19, a higher $a_{max}$ value results in a reduction in the FOS, and subsequently increases the $Y_{max}$ and lateral displacement.

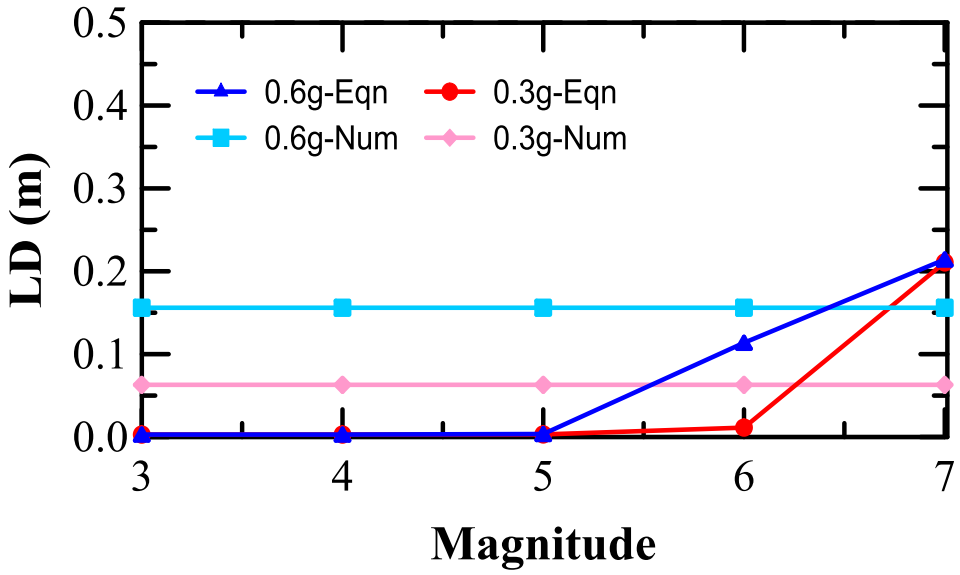


(a)

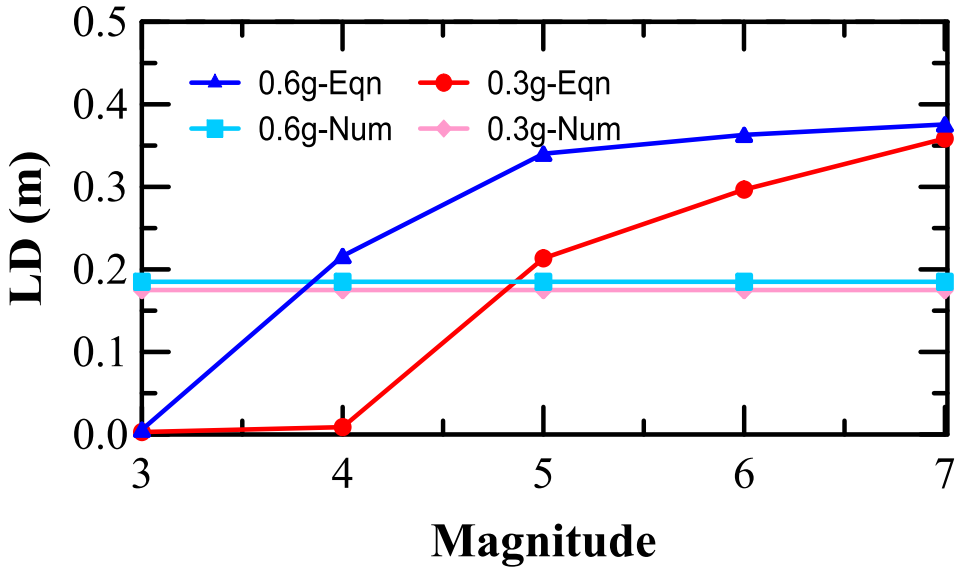


(b)

Figure 4.15: Lateral displacement (LD) estimated using numerical (Num) and semi-empirical (Eqn) methods for DCD 11 after applying (a) Salt Plains earthquake, and (b) Dexter earthquake

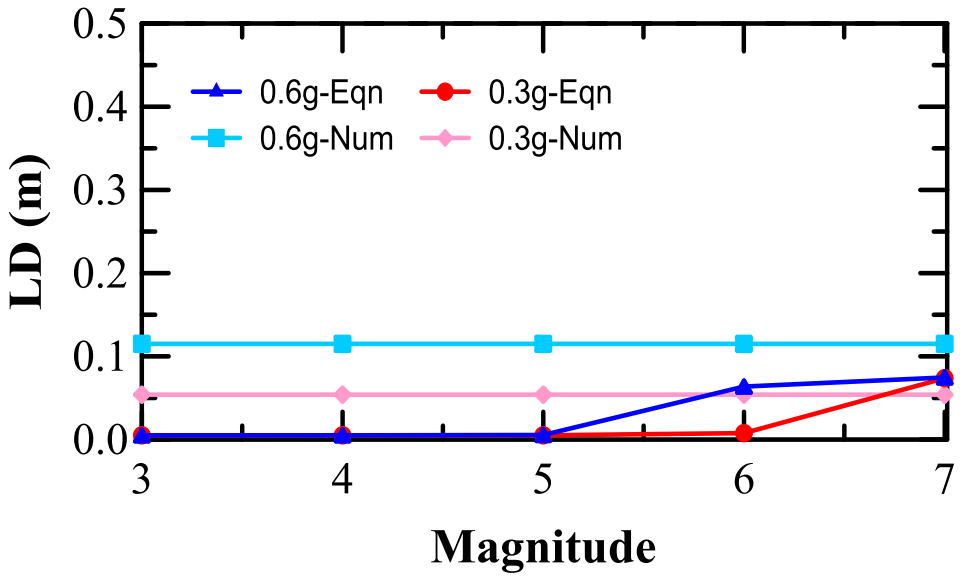


(a)

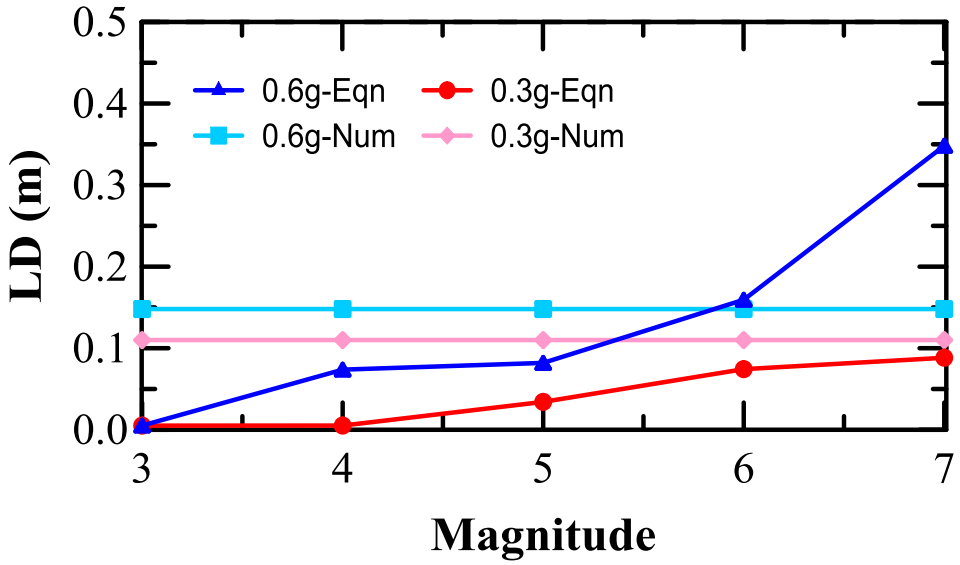


(b)

Figure 4.16: Lateral displacement (LD) estimated using numerical (Num) and semi-empirical (Eqn) methods for DCT 18 after applying (a) Salt Plains earthquake, and (b) Dexter earthquake

The lateral displacement at the ground surface was higher for DCD 11, as compared to DCT 18 (Figures 4.10 and 4.11). The 1.83m-thick liquefied $L_4$ layer of DCD 11 accumulated greater lateral deformation as compared to the 0.61m-thick $L_3$ layer of DCT 18. Hence, for any

given earthquake scenario, the lateral displacement computed using numerical and semi-empirical approaches increases with an increase in the thickness of the liquefiable layer.

Existing literature suggests that liquefaction-induced lateral displacement value less than 0.3 m can be considered as small (Holzer et al. 2005). In this case study, the predicted lateral displacements were smaller than 0.3 m for most of the sections and earthquake scenarios. A lateral displacement of 0.38 m was computed at DCD 11 for the Dexter earthquake at magnitudes greater than 6. To date, the strongest earthquake in Texas had a magnitude of 3.6 during the Azle earthquake of Nov 20, 2013. It may be assumed that the occurrence of a future earthquake event with a magnitude greater than 6 is highly unlikely in Texas. Thus, the EM dam can be considered to be safe and have no issues associated with liquefaction-induced lateral displacement during earthquakes that may transpire in the future.

## 4.4 Summary and Conclusions

The objective of this study was to predict liquefaction-induced lateral displacement for the Eagle Mountain dam, located in Fort Worth, Texas, USA, using numerical and semi-empirical methods and assess the chances of damage caused by liquefaction of foundation layers of the dam. The following major conclusions can be drawn:

- Two locations that had considerable amounts of silty sand to sandy material in the foundation of the EM dam. Selected layers at DCD 11 and DCT 18, may experience an increase in pore water pressure and liquefaction during future earthquakes similar to the hypothetical earthquakes considered in this study.
- In general, the estimated lateral displacements were higher for earthquakes with higher positive/negative average accelerations. Such earthquakes induce larger accelerations and shear stresses in the soil layers, resulting in higher horizontal movements during liquefaction.

- The estimated lateral displacement increased with an increase in the thickness of the liquefiable layers. Hence, for the same earthquake excitation applied at the base of two sections, the lateral displacement will be higher for the section with a thicker deposit that is susceptible to liquefaction.
- The lateral displacements estimated from the numerical and semi-empirical approaches were similar for earthquakes with magnitudes greater than 6. Small to moderate lateral displacements (<0.3 m) were estimated for most of the sections and earthquake scenarios considered in this study. The maximum lateral displacement of 0.38 m was computed for earthquake magnitudes greater than 6. However, such strong earthquakes typically do not occur in Texas. The EM dam can be considered to be safe and have no issues associated with liquefaction-induced lateral displacement.

# References


Arulanandan, K., and Scott, R.F. 1993. Project VELACS - control test results. Journal of Geotechnical Engineering,: 1276–1292.

Bardet, J. 1999. Liquefaction-induced Ground Deformation and Failure.

Bardet, J.P. 2003. Advances in analysis of soil liquefaction during earthquake. International Handbook of Earthquake and Engineering Seismology.

Bartlett, S.F., and Youd, T.L. 1992. Empirical analysis of horizontal ground displacement generated by liquefaction-induced lateral spreads.

Boulanger, R.W., and Ziotopoulou, K. 2015. Pm4Sand (Version 3): a Sand Plasticity Model for Earthquake Engineering.

Caballero, S. R., Bheemasetti, T. V., Puppala, A. J., Verreault, L., & Koterba, D. 2017a. Three-Dimensional Visualization Model of the Eagle Mountain Dam Using Cone Penetration Test Data Based on Geostatistics. In Geotechnical Frontiers 2017 (pp. 623-630).

Caballero, S.R. 2017b. A comprehensive resilience framework for the seismic evaluation of hydraulic fill dams in north Texas. The University of Texas at Arlington.

Chakraborty, S., Banerjee, A., Das, J.T., Mosadegh, L., and Puppala, A.J. 2018a. Impact of Variation of Small Strain Shear Modulus on Seismic Slope Stability Analysis of a Levee: A Sensitivity Analysis. Ifcee 2018,: 302–313. doi:10.1061/9780784481608.029.

Chakraborty, S., Das, J.T., Puppala, A.J., and Banerjee, A. 2018b. Natural frequency of earthen dams at different induced strain levels. Engineering Geology, **248**(August 2018): 330–345. Elsevier. doi:10.1016/j.enggeo.2018.12.008.

Franke, K.W., and Kramer, S.L. 2014. Procedure for the Empirical Evaluation of Lateral Spread Displacement Hazard Curves. Journal of Geotechnical and Geoenvironmental Engineering, **140**(January): 110–120. doi:10.1061/(ASCE)GT.1943-5606.0000969.

Gu, W., Morgenstern, N., and Robertson, P. 1993. Progressive failure of Lower San Fernando Dam. J Geotech Eng,.

Gu, W., Morgenstern, N., and Robertson, P. 1994. Postearthquake deformation analysis of Wildlife site. J Geotech Eng,.

Hamada, M., Towhata, I., Yasuda, S., and Isoyama, R. 1987. Study of Permanent Ground Displacement Induced by Seismic Liquefaction. Computers and Geotechnics,.

Hegazy, Y., and Mayne, P. 1995. Statistical correlations between VS and cone penetration data for different soil types. *In* Proc., International Symposium on Cone Penetration Testing, CPT ’95, Linkoping.

Holzer, T.L., Noce, T.E., Bennett, M.J., John C. Tinsley, I., and Rosenberg, L.I. 2005. Liquefaction at Oceano, California, during the 2003 San Simeon Earthquake. Bulletin of the

Seismological Society of America, **95**(6): 2396–2411. doi:10.1785/0120050078.

Javadi, A.A., Rezania, M., Mousavi, and Nezhad, M. 2006. Evaluation of liquefaction induced lateral displacements using genetic programming. Computers and Geotechnics, **33**: 222–233.

Kagawa, T., Abe, A., Ogawa, N., and Minowa, C. 1997. Shaking-table tests on a real-size pile foundation in liquefying sand. *In* Proceedings of SMIRT 14th Connference.

Khoshnevisan, S., Juang, H., Zhou, Y., and Gong, W. 2015. Probabilistic assessment of liquefaction-induced lateral spreads using CPT — Focusing on the 2010 – 2011 Canterbury earthquake sequence. Engineering Geology, **192**: 113–128. Elsevier B.V. doi:10.1016/j.enggeo.2015.04.001.

Kuhlemeyer, R.L., and Lysmer, J. 1973. Finite Element Method Accuracy for Wave Propagation Problems. Journal of the Soil Mechanics and Foundations Division, **99**(5): 421–427. ASCE.

Kulhawy, F.H., and Mayne, P.H. 1990. Manual on estimating soil properties for foundation design, Report EL-6800 Electric Power Research Institute, EPRI.

Liu, F. 2008. Data discovery on liquefaction-induced lateral ground deformations. University of southern California.

Marcuson, W.F. 1978. Definition of terms related to liquefaction. Journal of Geotechnical Engineering Division, **104(9)**: 1197–1200.

Mayne, P. 2006. In situ test calibrations for evaluating soil parameters. *In* Characterization and Engineering Properties of Natural Soils II.

Mejia, L.H., and Dawson, E.M. 2006. Earthquake deconvolution for FLAC. *In* 4th International FLAC Symposium on Numerical Modeling in Geomechanics. pp. 4–10.

Montoya-Noguera, S., and Lopez-Caballero, F. 2016. Effect of coupling excess pore pressure and deformation on nonlinear seismic soil response. Acta Geotechnica,.

Newmark, N.M. 1965. Effects of Earthquakes on Dams and Embankments. Géotechnique, **15**(2): 139–160. doi:10.1680/geot.1965.15.2.139.

Petersen, M.D., Mueller, C.S., Moschetti, M.P., Hoover, S.M., Shumway, A.M., McNamara, D.E., Williams, R.A., Llenos, A.L., Ellsworth, W.L., Michael, A.J., and others. 2017. 2017 one-year seismic-hazard forecast for the Central and Eastern United States from induced and natural earthquakes. Seismological Research Letters, **88**(3): 772–783. Seismological Society of America.

Puppala, A. J., Congress, S. S., Bheemasetti, T. V., & Caballero, S. R. 2018a. Visualization of civil infrastructure emphasizing geomaterial characterization and performance. Journal of Materials in Civil Engineering, 30(10), 04018236.

Puppala, A. J., Congress, S. S., Bheemasetti, T. V., & Caballero, S. 2018b. Geotechnical data visualization and modeling of civil infrastructure projects. In GeoShanghai International Conference (pp. 1-12). Springer, Singapore.

Rauch, A.F. 1997. EPOLLS: An empirical method for predicting surface displacement due to

liquefaction-induced lateral spreading in earthquakes.

Robertson, P.K. 1990. Soil classification using the cone penetration test. Canadian Geotechnical Journal,.

Robertson, P.K. 2009. Interpretation of cone penetration tests – a unified approach. Canadian Geotechnical Journal,.

Robertson, P.K., and Cabal, K.L. 2015. Guide to cone penetration testing for geotechnical engineering. *In* 6th Editio. Gregg Drilling and Testing Inc.

Robertson, P.K., Campanella, R.G., Gillespie, D., and Greig, J. 1986. Use of Piezometer Cone Data. *In* Use of In Situ Tests in Geotechnical Engineering, Specialty Publication, SM 92. pp. 1263–1280.

Robinson, K., Cubrinovski, M., and Bradley, B.A. 2013. Sensitivity of predicted liquefactioninduced lateral displacements from the 2010 Darfield and 2011 Christchurch earthquakes. *In* NZSEE Conference.

Towhata, I. 2005. Development of geotechnical earthquake engineering in Japan. *In* Proceedings 16th International Conference on Soil Mechanics and Geotechnical Engineering. pp. 251–291.

Towhata, I., Tokida, K., Tamari, Y., Matsumoto, H., and Ymamda, K. 1991. Prediction of Permanent Lateral Displacement of Liquefied Ground by Means of Variational Principle. *In* Proceedings, 3rd Japan-U.S. Workshop on Earthquake Resistant Design of Lifeline Facilities and Countermeasures for Soil Liquefaction.

Yasuda, S., Nagase, H., Kiku, H., and Uchida, Y. 1992. The mechanism and simplified procedure for analysis of permanent ground displacement due to liquefaction. Soil Foundat,.

Youd, T., Hansen, C., and Bartlett, S. 2002. Revised multilinear regression equations for prediction of lateral spread displacement. J Geotech Geoenviron Eng,.

Youd, T., and Perkins, D. 1987. Mapping of liquefaction severity index. J Geotech Eng, **113(11)**.

Youd, T.L. 1993. Liquefaction-Induced Lateral Spread Displacement. U.S. Navy, NCEL Technical Note,.

Youd, T.L. 1995. Liquefaction-induced lateral ground displacement. University of Missouri--Rolla, California.

Zhang, G., Robertson, P.K., Asce, M., and Brachman, R.W.I. 2004. Estimating Liquefaction-Induced Lateral Displacements Using the Standard Penetration Test or Cone Penetration Test. **130**(August): 861–871.

# Chapter 5:

# Conclusions and Recommendations

## 5.1 Conclusions

In this study, the applicability of numerical modeling for seismic response analyses of earthen dams and limitations that could occur due to the selection of the type of modeling and approaches for analyses were studied and discussed. Real and hypothetical earthen dams were modeled using commercially available 2D and 3D FEM-based software packages. Major findings can be named as:

- The 2D analysis results for the Eagle Mountain dam, located in Fort Worth, Texas, USA, were showing that a single-valued, first natural frequency of the entire dam, is not applicable for a heterogeneous earthen dam. Also, a uniform, laterally deformed mode shape that typically is expected for long homogeneous dams, is not observed for heterogeneous earthen dams. Eigenvalue analysis was unable to show the natural frequency of the structure in the 3D model. However, the sum of sines method was recognized to be the most applicable method for estimating the natural frequencies. Hence, for future studies, the sum of sines method is recommended to be used for any 2D or 3D models of heterogeneous earthen dams for the natural frequency determinations (Chapter 2).

- The 2D and 3D natural frequencies were similar for the analysis with the limited number of CPTu available. However, they were significantly different when ample information was available. Also, the earthquake-induced accelerations, forces, and shear stresses computed from a 2D analysis were found to be lower than those computed from a 3D analysis, irrespective of the frequency contents of the earthquake excitations. This indicates

that the 2D analysis underestimates the earthquake-induced forces and shear stresses, and may overlook the potential for stability issues. Hence, for situations, where extensive CPTu data is available it is recommended that 3D analysis to be used (Chapter 2).

- The effect of different methods of analysis in the case of high-level earthquake occurrence was also studied in this research. The analyses were performed on a hypothetical dam to recognize the differences in the pore water pressure ratio and associated deformations of a zoned earthen dam, using the equivalent linear analysis and non-linear analysis, considering three criteria: (i) level of earthquake shaking (PGA) (ii) frequency content of the applied earthquake, and (iii) relative density of the sand shells of the dam. The results suggest that it is more convenient to use the relatively simple equivalent linear analysis method when dams with dense sand shells experience earthquakes with low intensity of excitation, without chances of near-resonance condition. Under such scenarios, the results obtained from these two methods are similar. This part was performed on a hypothetical dam, further studies are required where actual post-earthquake deformation and pore water pressure data of real earthen dams are available for comparative studies with the numerical analyses results (Chapter 3).

- Simulation were performed to predict liquefaction-induced lateral displacement for two locations on the foundation of the EM dam which were recognized to have the potential for liquefaction. The lateral displacements estimated from the numerical and semi-empirical approaches were similar for earthquakes with magnitudes greater than 6. The maximum lateral displacement of 0.4m was computed for an earthquake magnitude 7. Such strong earthquakes are typically not expected to occur in Texas. Therefore, the EM dam

can be considered to be safe against damages caused by liquefaction-induced lateral displacement (Chapter 4).

## 5.2 Recommendations

- In this study, comparison of 2D and 3D analyses were performed on an earthen dam located at a region with low seismicity. Hence, the analyses were performed considering linear behavior of the soil. In future, non-linear 3D analysis can be performed to study the response of long earthen dams during strong earthquakes.
- Comparison of equivalent linear and non-linear approaches in this study were performed on a hypothetical dam. Performing similar study on a real dam located at high seismicity region, where real earthquake response data are available, could potentially provide information required to validate the findings of this research study.
- Data available from case studies pertaining to the response of real dams during earthquakes, along with findings of numerical simulations similar to those presented in this research study, could be used for developing ready-to-use guidelines for practicing engineers. These guidelines could be used to select appropriate methods of analysis based on the available field data.

# Appendix A:

## Cost Estimation Analyses of Finite Element Based Software Packages in Used

The main focus of this study is on numerical modeling. As mentioned by previous researchers, numerical models are relatively quick as compared to physical models. Unlike physical models, they can be performed in a few hours instead of months. Also, problems can be investigated over a wide range of scenarios in numerical models. In this work, most of the analyses are performed using finite element based software packages (ABAQUS, PLAXIS, and Geostudio). The governing motion equation for dynamic response of a system in finite element formulation is mentioned as:

$$[M]\{a"\} + [D]\{a'\} + [K]\{a\} = \{F\}$$

Where $[M]$ is a mass matrix, $[D]$ is the damping matrix, $[K]$ is the stiffness matrix and $[F]$ is a vector of loads.

In this research, dynamic studies of linear problems in ABAQUS are performed for 3D analyses of a long earthen dam. Eigenvalue problems are normally used in these types of analyses to check the responses of the desired model. Eigenvalue problems occur naturally in the vibration analysis of mechanical structures with many degrees of freedom. The solution to the eigenvalue problem gives the natural frequencies and modes of a system. The eigenvalues are the natural frequencies of vibration, and the eigenvectors are the shapes of these vibrational modes.

The eigenvalue problem is defined as:

$$(-\omega^2 M^{MN} + K^{MN})\varphi^N = 0$$

Where $M^{MN}$is the mass matrix, $K^{MN}$ is the stiffness matrix, $\varphi^{N}$is the eigenvector and $M$ and $N$ are degrees of freedom. The model created in this study is a long earthen dam since the analysis cost in ABAQUS increases linearly with the size of the model, it was almost taking around 24 hours for the 3D models' run to be completed for a time duration of 20.46s.

Some of the 2D modeling in this study were performed in Geostudio using SEEP/W, QUAKE/W, and SIGMA/W. The main keys in seismic response calculation consideration in this part are mentioned as inertial forces during excitation, pore water pressure generation and soil shear strength reduction. The analyses in Geostudio took approximately 1 to 2 hours for each model of each scenario. All three modulus of SEEP/W, QUAKE/W, and SIGMA/W were included in each model to complete equivalent linear dynamic analyses.

Non-linear analyses in this study were performed using PLAXIS. The analyses for each model took 5 to 6 hours where the start of calculation was from the initial phase to calculate initial stresses in the model before the start of excitation. In the second phase, the dynamic calculation type was selected and the seismic signal was applied at the base of models. At the end of analyses for each of the named finite element based software packages, graphs of different parameters such as acceleration, shear stresses, pore water pressure and so on, were plotted on the desired nodes along the body of the dam to interpret the seismic behavior and deformation of the dam under different circumstances.

# Appendix B:

## Obtained Permission to Reuse Contents of an Accepted Article

Permission to use the contents of manuscript ID **0280_0408_000325**, titled"**Comparison of Earthquake-Induced Pore Water Pressure and Deformations in Earthen Dams Using Non-Linear and Equivalent Linear Analyses**", which has been accepted for publication in Geo-Congress 2020, ASCE Geotechnical Special Publication.



Requesting permission of re-use of paper id_0280_0408_000325 (accepted for publication as ASCE GSP for Geo-Congress 2020

Mosadegh, Leila
Sun 01-Dec-19 10:38 PM
To: permissions@asce.org <permissions@asce.org>

**0280_0408_000325**
Hello,
I am Leila Mosadegh, PhD in Civil Engineering. at university of Texas at Arlington. I need to re-use the content of paper id_**0280_0408_000325, titled "Comparison of Earthquake-Induced Pore Water Pressure and Deformations in Earthen Dams Using Non-Linear and Equivalent Linear Analyses"** for my own doctoral dissertation and another publication in journal. I am the primary author of this paper, which was based on the findings of a part of my PhD research work, and I need to include it in my article-based dissertation and another publication. I would like to request permission for its re-use, although the GSP paper has not published online yet. Please let me know if anything else needs to be done on my part.
Thank you.
Regards,

**Leila Mosadegh**, *Graduate Research Assistant*
Department of Civil Engineering
University of Texas at Arlington
Nedderman Hall, Room 232

## RE: Requesting permission of re-use of paper id_0280_0408_000325 (accepted for publication as ASCE GSP for Geo-Congress 2020

PERMISSIONS <permissions@asce.org>
Mon 02-Dec-19 8:27 AM
To: Mosadegh, Leila <leila.mosadegh@mavs.uta.edu>

Dear Ms. Mosadegh,
Thank you for your inquiry. As an original author of an ASCE journal article or proceedings paper, you are permitted to reuse your own content (including figures and tables) for another ASCE or non-ASCE publication, provided it does not account for more than 25% of the new work.

A full credit line must be added to the material being reprinted. For reuse in non-ASCE publications, add the words "With permission from ASCE" to your source citation. For Intranet posting, add the following additional notice: "This material may be downloaded for personal use only. Any other use requires prior permission of the American Society of Civil Engineers. This material may be found at [URL/link of abstract in the ASCE Library or Civil Engineering Database]."

Each license is unique, covering only the terms and conditions specified in it. Even if you have obtained a license for certain ASCE copyrighted content, you will need to obtain another license if you plan to reuse that content outside the terms of the existing license. For example: If you already have a license to reuse a figure in a journal, you still need a new license to use the same figure in a magazine. You need a separate license for each edition.

For more information on how an author may reuse their own material, please view:
http://ascelibrary.org/page/informationforasceauthorsreusingyourownmaterial

Sincerely,

Leslie Connelly
Manager, Publications Marketing
American Society of Civil Engineers
1801 Alexander Bell Drive
Reston, VA 20191

# Biographical Information:

Leila Mosadegh received a Bachelor of Science in Physics from Damghan University of Basic Sciences, Damghan, Iran, in 2009. She received a Master of Science in Geophysics, with specialization in Earthquake Seismology, from the University of Tehran, Tehran, Iran, in 2014. Her Master research focused on probabilistic seismic hazard assessment using Monte Carlo simulations in north region of Iran.

Leila joined the doctoral program with the Department of Civil Engineering at the University of Texas at Arlington (UTA) in 2015. Leila worked under supervision of Dr. Anand Puppala to perform seismic response and deformation analyses of earthen dams. Leila's main research interest is geotechnical earthquake engineering focusing on dynamic analysis of earthen dams.